NTNU
Norwegian University of
Science and Technology

Faculty of Engineering
Science and Technology
Department of Hydraulic and
Environmental Engineering

Effects of anthropogenic activities on snow distribution, and melt in an urban environment

By

Bernt Viggo Matheussen

A Dissertation submitted to
the Faculty of Engineering Science and Technology,
the Norwegian University of Science and Technology,
in partial fulfilment of the requirements for the degree
Doctor Engineer

Trondheim, Norway, February 2004

Abstract

In many parts of the world snow melt runoff influence discharge from combined sewer overflows (CSO) and flooding in urban drainage systems. Despite this, urban snow hydrology is a field that has received little attention from the urban drainage community. The objectives of this research were to better understand urban snow hydrology and through field work and hydrological modelling quantify effects of anthropogenic activities (AA) on snow distribution, and melt in an urban environment. This means in principle how the presence (design geometry) and operation of roads and buildings influence the snow distribution and melt in urban areas. The Risvollan urban catchment (20 ha) located in Trondheim, Norway, was used as a study area. A literature review of urban snow hydrology was also carried out.

A gridded urban hydrology model (GUHM) was developed as part of the study. The principal idea of the GUHM is to subdivide an urban catchment into orthogonal equal area grid cells. The snow routine in the GUHM is based on an energy balance approach, which together with a soil-runoff routine is used to calculate a time series of rain, snow water equivalent (SWE), snow melt, and runoff, for each grid cell. In GUHM, processes such as snow clearing of roads, locally low albedos, heat/shadowing from buildings, and effects of slope and aspect are included in the model structure.

A technique for observing time series of snow covered area (SCA) for an urban catchment is presented. The method is based on image processing and neural network technology to calculate SCA from a time series of images taken from a tall building in the Risvollan catchment. It was shown that SCA on roads and roofs in general becomes more rapidly snow free during melt periods compared to the park areas of the Risvollan catchment. This can be explained by snow clearing of roads, snowdrift from roofs and high snow melt rates on roofs and roads. The high melt rates was attributed to locally low albedos in vicinity to roads, rooftop snow packs exposure to wind and solar radiation, in addition to anthropogenic heat release from the roofs themselves.

Field observations of SWE were carried out in the Risvollan catchment and it was shown that areal mean SWE located on/or nearby roads and buildings were significantly lower during mid and end of the winter, than in park areas. This can be attributed to higher melt rates caused by AA.

A time series of SCA and SWE was obtained through field work for the period from 2000 to 2003 in the Risvollan catchment.

The GUHM was applied and calibrated for the Risvollan catchment for a three year period. Two seasons were used as validation period. Comparison between the simulated and observed SWE, SCA and runoff data showed that the GUHM was able to simulate snow accumulation and melt for whole seasons with short time resolution (1 hour) satisfactory.

The GUHM was used to quantify effects of AA on snow distribution and melt for six different land use scenarios in the Risvollan catchment for the period June 1998 to June 2003. The modelling results showed that when the area coverage of buildings and roads increased, the SCA and SWE more rapidly decreased during melt periods. Because of this more runoff will be produced in the early winter season (Jan-March) compared to if the catchment had been covered with only sparsely vegetated areas. The simulation results showed that when the impervious surface covers of a catchment increase, the peak and volume runoff will also increase, as expected.

Both the field observations and the hydrological model study carried out in this work showed that AA lowers SCA and SWE more rapidly in an urban environment compared to more untouched terrain. The reasons for this are redistribution of snow, and strong snow melt rates on roads, roofs, and in snow deposit areas. Low albedos and anthropogenic heat release are the main reasons for the enhanced snow melt rates.

Acknowledgements

The research presented in this thesis was carried out in the period from Feb. 2000 to Feb. 2004 at the Norwegian University of Science and Technology (NTNU), Department of Hydraulic and Environmental Engineering in Trondheim, Norway. During these years I have also taken classes and participated in teaching at graduate level, equivalent of 2 years work. This project was mainly funded by NTNU, but the Norwegian Research Council supported funding for part of the field work.

I would specially like to express my sincere gratitude to my supervisor Associate Professor Sveinn T. Thorolfsson, at NTNU, for his endless support and for keeping me focused on the topic. I am also thankful to Associate Professor Thorolfsson for introducing me to the field of urban drainage in cold climate, of which he is one of the pioneers. He is the main reason for why Risvollan urban hydrological station was established in 1986, and has together with the municipality of Trondheim and the Norwegian Water and Energy Directorate (NVE) ensured collection of high quality data for use in analysis of urban drainage systems in cold climates. Without Risvollan, this thesis had never been written. I am also grateful to Associate Professor Thorolfsson for putting me in contact with Professor Dennis P. Lettenmaier at University of Washington, Seattle, USA, which gave me a good start for the doctor of engineering study that was to come.

In the period from Jan. 1997 to Jul. 1998 I worked as a visiting scientist at the University of Washington, Department of Civil and Environmental Engineering. I am very thankful to Professor Dennis P. Lettenmaier for giving me the opportunity to work in his research group and learn so much about computer science and hydrological modelling. I would also like to thank Pascal Storck for taking care of me when I first arrived in the U.S., and Greg M. O′Donnell for being such a patient colleague and a good friend during my stay in Seattle.

I would like to thank all my colleagues and friends at the Department of Hydraulic and Environmental Engineering, NTNU for the time we have had together.

At last I would like to thank my family for all the support that I have received during the years, and my heart full thanks to Laura, for encouragement and support during the years we have had in Trondheim.

List of Publications

Parts of this thesis have previously appeared as:

(1)

Matheussen, B.V. & S.T. Thorolfsson (2003)
Estimation of snow covered area for an urban catchment using image processing and neural networks
Journal of Water Science and Technology, **48(9)**
[Urban Drainage in Cold Climate]

(2)

Matheussen, B.V. & S.T. Thorolfsson (2003)
Estimation of snow covered area for an urban catchment using image processing and neural networks
In proceedings of 1st Int. Conf. on Urban Drainage and Highway Runoff in Cold Climate. 25-27 March, Riksgränsen, Sweden. IWA, IAHR, AIRH, Luleå Univ. of Techn. pp 315-326

(3)

Matheussen, B.V. & S.T. Thorolfsson (2003)
Calibration of a gridded urban hydrological model using observed values of snow water equivalent and snow covered area
In proceedings of 1st Int. Conf. on Urban Drainage and Highway Runoff in Cold Climate. 25-27 March, Riksgränsen, Sweden. IWA, IAHR, AIRH, Luleå Univ. of Techn. pp 339-350

(4)

Matheussen, B.V. & S.T. Thorolfsson (2002)
Estimation of snow covered area using web-camera - A sensor in urban snow hydrology
In proceedings of XXII Nordic Hydrological Conference
4-7 August, Røros, Norway. Vol II. pp 711-720
NHP Report no. 47, ISBN 82-7598-053-4

(5)

Matheussen, B.V. & S.T. Thorolfsson (2001)
Snow surveys in Risvollan, Norway
In proceedings of Urban Drainage Modelling
Specialty Symposium of the World Water and Environmental Resources Congress. Eds. R.W. Brashear & C. Maksimovic.
Orlando, Florida, USA 20-24 May, pp 89-99, ASCE, EWRI
ISBN 0-7844-0583-2

List of Abbreviations

AA	Anthropogenic activity
ANN	Artificial neural network
CFD	Computational fluid dynamics
CSO	Combined sewer overflow
DEM	Digital elevation model
EOS	Earth observing system
ET	Evapotranspiration
FAR	Floor area ratio
FRC	Fast responce component
GIS	Geographic information system
GUHM	Gridded urban hydrological model
ISC	Impervious surface cover
LCT	Land cover type
LCR	Lot coverage ratio
MODIS	Moderate resolution imaging spectroradiometer
NASA	National aeronautics and space administration
PD	Population density

Pop	Population
SCA	Snow covered area
SAR	Synthetic aperture radar
SRC	Slow responce component
SWE	Snow water equivalent
TIN	Triangular irregular network
UHI	Urban heat island

Contents

List of Figures

List of Tables

Chapter 1

Introduction

1.1 Background and motivation

In many cities in the world snowfall can be a significant part of the annual precipitation. Urban drainage systems built in these environments must therefore be able to function properly during snow melt conditions. In the Norwegian (European) standard for hydraulic design and environmental considerations for drain and sewer systems outside buildings (NS-EN752-4 1998), it is assumed that short duration summer rainfall produces the highest runoff peaks for which urban drainage systems are designed. This assumption is probably valid for most southern and central European cities where there is little or no snow during the winter. However, urban drainage networks based on current design practice may not be able to cope with runoff volumes produced during the winter. Nilssen & Bjørgum (2001) found that seven out of twelve major urban floods since 1978, in the city of Trondheim, Norway (cold maritime climate), happened during the winter period (Nov-Apr). Of the two largest floods, which had an estimated return period of around 50 years (1997 and 2000), one was a rainfall only event and the last was caused by rainfall in combination with snowmelt. In addition to this, several authors have indicated that in cold climates, e.g. in Sweden, Canada and northern USA, spring snow melt in combination with rainfall can produce annual peak flows equivalent or larger than rainfall generated runoff for urbanized catchments (Marsalek 1991, Bengtsson & Westerström 1992, Oberts 1994).

The runoff conditions during snow melt events are usually different

compared to a summer rainfall-runoff event. This is largely caused by changes in the runoff contributing area, reduced infiltration due to soil saturation or frozen soils, and release of extra water from melting snow packs (Marsalek 1991). The snow melt runoff can be sustained for several weeks during the spring and influence the urban drainage systems in many ways. For example Thorolfsson & Brandt (1996), found that flooding and combined sewer overflow (CSO) discharge in urban cold climate areas are heavily influenced by spring snow melt. It has also been reported that snow melt runoff and rain-on-snow events produce some of the highest pollutant loadings and most difficult management challenges in cold climate regions (Oberts 2003). Hernebring (1996) found that in northern Sweden infiltration of snow melt generated runoff into the wastewater systems can be significant. This leads to decreased water temperature causing operational problems at wastewater treatment plants.

Given the results of these studies, one can ask why snow melt considerations are not included in the Norwegian or the European standards for storm drainage design. One apparent reason is that most of the urban hydrological runoff models that are in use today have been developed mainly for the purpose of analysing rainfall runoff regimes (Maksimovic & Thorolfsson 1990, Maksimovic 2000). Therefore snow melt has not been considered during design of urban drainage systems. It is also known that snow melt calculations in urban environments are difficult (Huber & Dickinson 1992), largely due to lack of relevant and reliable hydrological data for the winter period (Buttle et al. 1990), and that methods for incorporating snow melt in urban drainage design have not been properly tested. It is also known that within the urban drainage research community there has been little focus on studying the effects of snow melt runoff quantity and quality in urban environments. Several researchers support this view (Oberts 1990, Bengtsson & Semádeni-Davies 2000, Marsalek et al. 2003). During the last 30 years substantial research has been conducted on snow hydrology for rural areas, for literature reviews see Dozier (1987), Bales & Harrington (1995) and Marsh (1999), but as indicated by Semádeni-Davies (1999*a*), there are processes in operation in the urban environment, which influence the snow distribution and melt, that are not present in rural areas. The main differences can be seen in the way various forms of anthropogenic activities influence the urban snow pack, e.g. humans clear roads and walkways for snow and thereby changes the snow distribution,

buildings are heated from the inside and easily melt the snow on the roofs, localized low albedos near roads and snow deposits increase melt rates, and outlet of anthropogenic heat alters the urban climate and thus the available energy for snow melt, etc. These processes are also highly variable in both space and time.

Current operational urban hydrological models have been criticised for using simplistic snow melt routines, not suited to simulate snow melt at the temporal and spatial scales necessary for urban environments (Semádeni-Davies & Bengtsson 2000, Semádeni-Davies 2000). Because of the diurnal cycle in snow melt runoff, and that the runoff responses seen in urban areas are rapid, a time step of 24 hours, often used in urban hydrological analysis, e.g. (Hernebring et al. 1997), will result in averaging of runoff peaks and is therefore not suitable for CSO discharge and flooding analysis of urban drainage systems (Bengtsson 1984, Matheussen & Thorolfsson 1999, Bengtsson & Singh 2000). Marsalek (1991) and Maksimovic (2000) emphasize the need for further development of urban snow melt calculations and that the models must be validated against high quality datasets. The above-mentioned problems motivate studies of snow accumulation, distribution, melt and runoff in the urban environment. Through an increased understanding of these processes better tools for urban planning, design, and management can be developed.

1.2 Question and objectives

The following question is addressed in this thesis:

> What are the effects of anthropogenic activities on snow distribution, and melt in an urban environment?

In this thesis anthropogenic activity (AA) is defined as all human activity that influences the hydrology, and specially the snow distribution and melt, in urban environments. Some examples of the most dominant AAs in urban areas are presented below.

The construction and presence of infrastructure, e.g. roads, is one AA that has a strong influence on the hydrology of an urban catchment. In cities, usually the road cover is of asphalt or some other impervious material which is known to increase volume, and peak runoff, and lower ground

water recharge, (Kang et al. 1998, Beighley & Moglen 2002), and others. Construction and presence (design geometry) of buildings are also an important AA that influences the hydrology of a catchment. Building size, height and type of surface materials are all factors that influence the urban energy balance, e.g. inside heating leads to melting of snow on rooftops, and increased emission of long wave radiation adds extra energy to nearby snow packs. The roofs are also impervious and force an increase in runoff from these surface types. After the infrastructure (roads, buildings) has been constructed, it is used and maintained by humans. These activities influence both the urban energy budget (Oke 1988) and snow distribution in several ways. Local heat emissions, such as domestic heating and ven-

Table 1.1: Examples of parameters used to quantify AA

AA	**Unit**
Lot coverage ratio (LCR)	$[m^2/m^2]$
Road/parkinglot coverage ratio (RCR)	$[m^2/m^2]$
Floor area ratio (FAR)	$[m^2/m^2]$
Annual daily traffic load (ADT)	$[vehicles/day]$
Population density (PD)	$[Population/m^2]$
Impermeable surface coverage (ISC).	$[m^2/m^2]$
Average building height	$[m]$
Domestic electricity consumption	$[kWh/(day\ m^2)]$
Industrial energy consumption.	$[kWh/(day\ m^2)]$
Use of anti-slippery and de-icing chemicals.	$[kg/m^2\ ]$
Area of roads cleared for snow	$[m^2/m^2]$
Snow transport to regional snow deposits.	$[kg,\ date\ and\ time]$

tilation systems, fuel combustion in cars, industrial energy consumption are sources of heat that will influence the melting of urban snow packs, with varying degree. Industry can also affect the hydrology in nearby areas trough outlet of dust particles in the atmosphere, that later will be deposited on urban snow packs and lower the albedo. Another AA that can be considered to be of a more operational character is road and walkway snow clearing. Together with use of de-icing and anti-slippery materials, such as sand and gravel, this AA affect snow covered area, snow water

Table 1.2: Floor area ratio (FAR) and impervious surface cover (ISC)

City/Area	**FAR (%)**	**ISC (%)**
Central Tokyo	155	83
Manhatten Island		77
Midtown Manhatten	875	
Midtown Trondheim	210	87
Risvollan, Trondheim	26	26

equivalent, and snow melt rates in an urban catchment.

Anthropogenic activities have strong spatial variability and can for a given catchment be quantified through several parameters. Some of them are listed in Table 1.1. In downtown areas the parameters in Table 1.1 will typically be larger than in suburban areas, thus downtown areas have higher influence from AA than suburban areas. Table 1.2 presents floor area ratio (FAR) and impervious surface cover (ISC) for four different areas in the world (TokyoMap 2004, Schilling et al. 1998). The FAR data for Midtown and Risvollan in Trondheim, were calculated assuming that all buildings had three, and two roof levels, respectively. Midtown Manhatten (New York, USA) has the largest FAR value of 875 %, which is much higher compared to Trondheim (Midtown) or the Risvollan area. This indicates large spatial variability in AA between cities and countries. AA can also be said to have temporal variability since for example, new buildings and roads are constantly being built and domestic heating is largest during the winter period.

An urban environment can be defined as an area where the influences from AAs are above a chosen threshold. Trondheim municipality (Trondheim 2002) defines a populated area as an area where 200 or more people live, and the average distance between the houses does not exceed 200 meters. Another definition could be for example that the ISC would be above, say 5 %, before an area or catchment could be defined as urban.

Based on the problems described in the introduction section and the question raised, the following objectives were identified for this research:

1. To increase understanding of urban snow hydrology.
2. To develop an urban hydrological model, specially designed for urban snow melt calculations, and test it on a point, and catchment scale.
3. Observe time series of SCA and SWE for a chosen study area, for the purpose of quantifying the effects of AA on snow distribution, and melt, and use these data to calibrate and validate the urban hydrological model developed under objective (2).
4. Use the developed urban hydrological model to quantify the effects of anthropogenic activities on snow distribution, and melt within a selected study area.

1.3 Organization of thesis

This thesis is organized as follows:

In chapter 2 a literature review of urban snow hydrology is presented followed by a description of a new urban hydrological model presented in chapter 3. Chapter 4 presents the study area (Risvollan catchment in Trondheim, Norway), and available meteorological data, used in this research. In chapter 5 the method and results from observations of SCA in the study area are presented. Chapter 6 describes the methodology and results from the field observations of SWE. Chapter 7 presents results from point and catchment scale testing of the developed urban hydrological model. Chapter 8 presents results from the analysis where the urban hydrological model was used to quantify the effects of AA on snow distribution, and melt in the study area. The last two chapters contain a summary, main conclusions, and proposals for future work.

Chapter 2

Urban snow hydrology

This chapter discusses urban snow hydrology and includes a review of literature which shows how AA is affecting the urban snow pack properties, distribution and energy balance. Examples of snow measurements techniques and urban runoff mechanisms are also presented. At the end urban snow melt models are reviewed and a discussion and some conclusions are given. Water quality aspects are only included to a limited extent.

2.1 Effects of anthropogenic activities on urban snow

Considerable work have been carried out on snow accumulation, melt and runoff processes for rural environments. Dozier (1987) and Bales & Harrington (1995) reviewed the research literature for rural snow hydrology before 1987 and 1994, respectively. Marsh (1999) reviewed the literature on snow cover formation, and melt. It was found that considerable advances have been accomplished in the understanding of blowing snow, sublimation, canopy interception, modelling and observations of snow pack energy and distribution, and internal processes, during the last 20 years. None of the literature cited by Marsh (1999), addressed urban snow processes specifically. Semádeni-Davies & Matheussen (2003) reviewed the literature of urban snow hydrology in the period 1990-2003. It was found that only a few researchers in Sweden, Norway, and Canada had worked with identifying differences between rural and urban snow hydrology. The various contributions from these and other researchers will be included later in this

section.

The key difference between urban and rural snow packs is that in urban areas AA affects the snow properties, distribution, and melt, through processes not present in rural environments. Literature demonstrating such effects is presented below.

2.1.1 Impact of roads on urban snow

One important factor to consider when assessing impacts of roads, traffic, and snow clearing procedures on urban snow packs, is albedo. Snow albedo may be defined as the integrated reflectance of light over the short wavelength spectrum (0.3 to 3 μm), and is known to depend on grain size, density, sun angle, surface roughness, liquid water content, etc (Gray & Male 1982). Winther (1993*b*) refer to work by Lillesand & Kiefer (1987) and shows that the albedo also varies with wavelength and that the amount of energy contained in the short wave radiation spectrum is largest in the visible range (0.4 to 0.7μm). In the visible wavelengths, pure ice is weakly absorptive and snow albedo is insensitive to grain size, allowing impurities in the snow to become the important determiners of snow albedo (Melloh et al. 2001). This can be attributed to that litter and larger particles have a low albedo compared to the snow and heats more rapidly in response to shortwave radiation. The litter then heats the snow pack through conduction and increase melt rates (Melloh et al. 2001). Due to changes in climatic conditions and solar position, albedo has both a diurnal and seasonal variation, where fresh fallen snow shows the highest values (0.8-0.95) (Winther 1993*a*) declining down to $\sim$0.4 or lower at the late spring melt season.

Urban snow often contains a large amount of impurities coming from airborne pollutions, roadway and roadside deposits, and various urban waste products (Marsalek et al. 2003). Some of these impurities can be easily seen, such as the deposition of vehicle petroleum products, and roadway surface deteriorated materials, etc, on and nearby roads. In addition to this, snow clearing procedures in combination with use of anti-slippery materials, such as sand and gravel, makes the snow on roads and in roadside snow deposits very dirty. Viklander (1999) studied substances in urban snow in different parts of Luleå city, Sweden. The concentrations of for instance, suspended solids were shown to increase with traffic density. These impurities will

lower the albedo of snow packs located on or near the roads (deposits). Bengtsson & Westerström (1992) observed snow albedo in different types of snow cover in downtown Luleå, Sweden, during April 1980. The daily average albedo of snow packs located near streets were in general 0.2 lower than in untouched snow packs leading to an increase in daily melt rates at about 10 mm. Semádeni-Davies (1999*b*) studied albedo of urban snow packs in the city of Luleå during April 1998. Undisturbed urban snow was found to have similar albedo values as nearby rural snow (0.5-0.6), while the albedo of snow piles had values around 0.3-0.5. Sundin (1998) registered albedo of snow deposits in Luleå city in Sweden during spring of 1992 and found that it varied between 0.2 and 0.5 in early melt season (March, early April), decreasing to about 0.1 in late spring (Late April, May). Ho & Valeo (2003) measured snow albedo within four urban snow cover types in Calgary (Canada) during the 2001 to 2002 winter season. The findings revealed that the albedo of urban snow packs had large spatial and temporal variability that were dependent on the types of urban snow cover. For all cover types the initial albedos had values in range 0.8-0.9, but showed a rapid decay when the melt period started. At the end of the melt period, Ho & Valeo (2003) reported that albedo of snow piles, and on road shoulders could be as low as 0.1-0.3, while albedos of snow in open areas (untouched snow) were measured to values of around 0.5-0.7. Conway et al. (1996) spread soot and ash on a snow pack and registered albedo decrease, and snow melt increase of about 30 % and 50 % respectively compared to untouched snow, which are comparable to the albedo conditions in snow packs on roads and in snow deposits during melt situations.

Figure 2.1 and 2.2 shows the snow conditions for a road in the Risvollan catchment in Trondheim, Norway for 20th February 2002 and 23rd of March 2002, respectively. Figure 2.1 indicates high snow albedos (visible spectrum) on the road, in the snow deposits next to the road, and in the park/garden areas. The picture is taken after snowfall the previous days and it can be assumed that the snow albedo is in the range of 0.8 to 0.9 for all surface covers. From Figure 2.2 it can be seen that the snow in the roadside deposits is very dirty compared to the snow in the garden areas. This indicates a lower albedo in the snow roadside deposits compared to in the garden areas (untouched). It should be noted that the albedo of roadside deposits will depend on traffic density, e.g. piles in low density housing areas can be fairly clean (Semádeni-Davies 1999*a*).

Fig. 2.1: Picture from Risvollan in Trondheim 20 February 2002

Fig. 2.2: Picture from Risvollan in Trondheim 23 March 2002

Snow clearing of roads and parking lots is an AA that influences the snow distribution of an urban catchment. Through snow clearing the natural variability of the snow pack is further enhanced. After snow clearing, the snow cover on the roads will be very low, typically only a few centimetres of compacted snow or ice. When the air temperature rises above freezing the little snow that is left on the road will easily melt due to low albedo caused by mixing of snow/ice with dust and particles from vehicles or road materials. The underlying surface, which is usually very dark, will also be easily heated by solar radiation and can heat the snow through conduction. Use of de-icing chemicals such as salts can also make the snow melt more rapidly, even during freezing conditions. These processes will make the snow on the roads disappear relatively rapid compared to undisturbed snow (parks). In catchments with a high percentage of road cover the SCA can therefore be expected to be more rapidly lowered compared to in rural areas. This has also been reported by other researchers (Bengtsson 1981, Westerström 1984, Westerström 1986, Buttle & Xu 1988, Buttle 1990, Bengtsson & Westerström 1992). Figure 2.2 illustrates the effects of snow ploughing and early melt on the roads. The road is completely snow free and the piles are dirty.

Snow deposits are usually found nearby roads and parking lots, but in city centres space limiting factors can result in snow being transported out of the city areas/centres. The melting of snow deposits is complicated by several factors. By piling the surface characteristics, shape and exposure to the atmosphere changes compared to a horizontal snow cover. Depending on the geometry of the piles the overall surface roughness can change and might therefore intensify turbulent mixing in the boundary layer (Sundin 1998), compared to flat snow packs. Although piles in general have low albedo, it is possible, as thawing proceeds, that an insulating crust can be formed by surface particles and litter (Semádeni-Davies 1999*a*). This process in addition to the extra snow received from nearby areas can make the snow in piles to remain long after the snow has disappeared in other parts of a catchment.

From Figure 2.2 and 2.1 and the literature cited, there are indications that the presence of roads, traffic and winter maintenance will enhance the natural variability of urban snow packs. The combination of snow ploughing, locally low albedos and use of de-icing chemicals will make the snow disappear more rapidly on roads compared to other land cover types.

Depending on the traffic density, albedo of snow packs located nearby roads (deposits) will in general be lower than in e.g. park garden areas of an urban area. The snowmelt rates in such cover types can therefore be expected to be higher than in areas more remotely located from roads. Despite this, snow piles can remain in a catchment long after snow in other areas has melted due to the extra snow received from roads via snow ploughing.

2.1.2 Impact of buildings on urban snow

The presence and geometry of buildings and their operation are important AAs that influence both the snow distribution and melt in urban areas. An individual building, consisting of wall and roof facets, each with a different time-varying exposure to solar radiation, long wave radiation exchange, ventilation, and heat conduction can alter the surface energy balance for a snow pack adjacent to, or on top of a building. Figure 2.3 presents a picture from the Risvollan catchment in Trondheim (Ch 4) at the 11th of January 2002. The picture shows that most of the roofs and roads are snow free, but there is still much snow left in the parks and garden areas. This indicates that there are processes in operation that consistently either removes or melts the snow located on roofs and/or roads, which can be explained by AA.

Figure 2.4 presents an illustration of the various energy components that are present on rooftops and in the vicinity of buildings. The modification of the net total radiation around buildings are characterized by the creation of irradiative components such as reflected solar radiation and long wave radiation between the various surfaces (Noilhan 1981). Due to inside heating, absorption of shortwave radiation, and a high emissivity, the building walls can emit a large portion of long wave radiation to nearby snow packs (Todhunter et al. 1992). Snow packs located in the vicinity of the walls will therefore be more exposed to long wave radiation compared to snow packs located more remotely. Multiple reflections of shortwave radiation between the snow packs and walls may also increase the available energy for snow melt (Semádeni-Davies et al. 2001), although such reflections can be disturbed by shadow effects from nearby terrain or buildings.

Fig. 2.3: Picture from a part of the Risvollan catchment in Trondheim, Norway, 11 Jan 2002

Bengtsson & Westerström (1992) measured long wave radiation close to two-storey houses and in an open area. It was found that the two-storey houses influenced the long wave energy budget up to 10 metres away. The mean increased net long wave radiation, averaged over 10 metres from a building, was 10 W/m^2, compared to an open area, which corresponds to an increased melt of 2.6 mm/day. Xu & Buttle (1987) measured spatial and temporal patterns of net radiation around buildings during snow melt. The fluxes were compared to those for an open area. In general the net

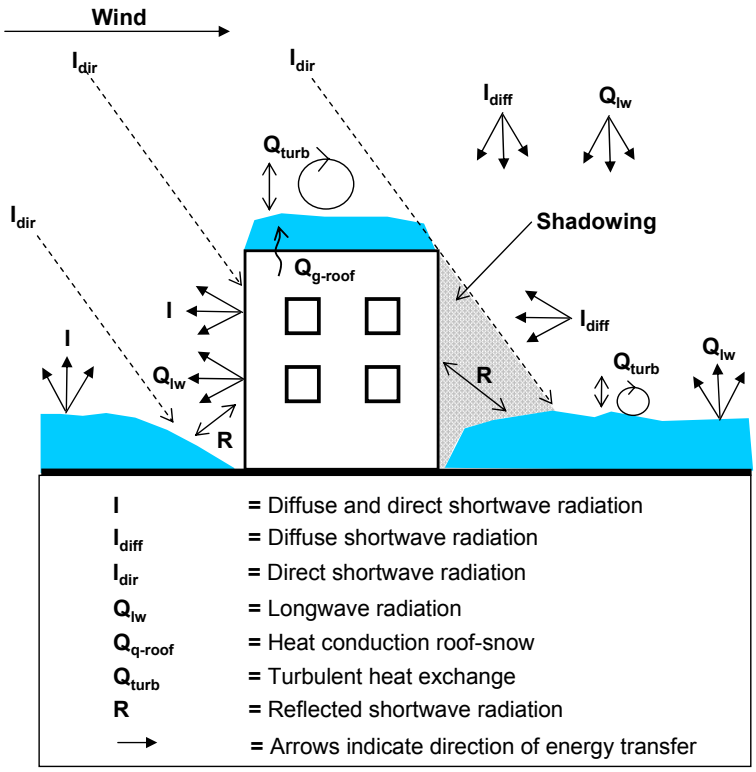

Fig. 2.4: Energy budget components for snow packs located on rooftops or in the vicinity of buildings (modified after Semádeni-Davies, 1999a and Todhunter et al.,1992)

radiation flux was found to decrease with distance from the houses, but shadow effects (Fig. 2.4), and orientation (North-South, East-West) of the houses also had an impact. The field observations showed net radiation totals over suburban snow packs, on cloudy days, to be up to 435 % of open terrain snow pack values. On more sunny days the net radiation for open sites showed larger values than the ones found nearby houses. This was attributed to shadowing of the sensors. Their findings suggested that daily snow melt may begin earlier in built-up areas than at nearby open areas.

Buttle (1986) and Westerström (1986) reported that most of the snow on

roofs melted more rapidly during spring conditions compared to the snow in other surface types. If the snow on roofs disappear more rapidly than snow in undisturbed areas, there have to be processes in operation that removes the accumulated snow. Several explanations to this exist. Wind speeds tend to be higher on the roofs than on the ground (dependent on building height, geometry and vicinity to other buildings). This can lead to snow drift from the roofs and into nearby areas (Tsuchiya et al. 2002, Bang et al. 1994), and will make the initially accumulated SWE to be lower compared to in for example park/garden areas. On the other hand, depending on the building configuration, roofs can also trap snow, which would make the initial SWE larger than, say in nearby areas. It should be noted that snow drift is not only present in the urban environment but can be seen in all parts of a terrain experiencing snow fall during the winter time, (Winstral & Marks 2002, Thordarson 2002), and many others. Due to higher wind speeds on roofs the turbulent heat fluxes might also be higher during melt periods, compared to in more sheltered areas such as in parks and yards. This will make the snow melt to be more intense. In addition to this the snow on the roofs are more exposed to solar radiation than snow in park areas (Buttle 1990, Buttle & Xu 1988), thus more energy is available for melt. Depending on the insulation the heating of the inside of a building contributes to melt the snow on the roofs through heat conduction (Q_{g-roof},Fig. 2.4). Hanssen et al. (1992) suggest values in the range 0.2-0.4 W/m^2K for roof heat transmission coefficients. With a difference between indoor and outdoor temperature of 25 K, the roof heat transmission, with a value of 0.4 W/m^2K, would be 10 W/m^2 resulting in an extra daily melt (ripe snow pack) of 2.6 mm. Byggforsk (1998) suggests heat transmission values for old wooden sloped roofs to be in the range of 0.6 to 1.3 W/m^2K, depending on the insulation. If all this energy is transformed into snow melt it would give 8.4 mm pr day (1.3 W/m^2K), given the same assumptions as mentioned earlier. Even though these energy fluxes are small, they can produce a significant melt if they are contained over several weeks. Because of this the SWE on roofs can be expected to be lowered as a result of heat from the roofs themselves. Buildings with sloped and slick roofs often experience that the snow slides of the building and onto the ground. This effect would result in reduced SCA compared to in untouched areas. In cities the insulation, surface colour, thermal properties, geometry, and inside heating will vary from house to house. It is therefore difficult to make

general assumptions on the effects of buildings on the snow distribution, and melt in urban environments.

2.1.3 Urban energy balance

The urban environment is a heterogeneous mixture of buildings, roads, parking lots, sidewalks, open areas, and sparse vegetation. Studies have shown that when cities grow in size, there will be a change in the boundary layer climate and energy balance, and the urban heat island (UHI) effect will start to show (Arnfield 2003). The reason for the change in surface energy balance, which in many cases leads to an increase in the local air temperature in the cities, can be attributed to several factors, such as anthropogenic heat release from heating of houses and fuel combustion. Due to the urban canyon geometry radiation can also be trapped between buildings and transformed into heat. Oke (1988) reports that during the winter season the differences in the urban energy balance between urban areas and its surrounding countryside are more clear than during the summer time. This may be attributed to various anthropogenic activities, such as, the removal of snow from the streets (low SCA), and the increased importance of snow free vertical walls in the low sun season, which contributes to lower the effective albedo. This was also investigated by (Kidder & Wu 1987) who studied differences in albedo, during snow covered conditions, for the St Louis area (USA) and found that the albedo over the city was in general 16 % lower than the nearby countryside with an estimated 3 K degree differences in equivalent blackbody skin temperature (urban-rural). It was also reported a 10 % to 30 % lower SCA for the city compared to the countryside. It should be mentioned that rural terrain also can have substantial albedo variations due to vegetation.

The magnitude of the urban heat island will differ locally within a city and between the cities themselves. Ruffieux (1995) modelled the winter surface energy budget of Denver, Colorado in the USA, using a distributed model with 10 meters grid cell resolution. The results showed that anthropogenic heat and heat emitted by buildings could reach values of 60 W/m^2 during the night and higher during the day. Local shadowing also had strong impact on the urban energy budget. Steinecke (1999) studied the distribution of air temperature and wind speed in the city of Reykjavik, Iceland, during the period from Nov 1991 to Sept 1992. It was found that

Reykjavik had a weak heat island effect where the anthropogenic heat releases were estimated to be around 35 W/m^2. Ichinose et al. (1999) studied the impact of anthropogenic heat on the urban climate in Tokyo, Japan. It was found that the anthropogenic heat flux from the household sector in the suburbs reached about 30 W/m^2, while in the city centre of Tokyo the anthropogenic heat flux exceeded 400 W/m^2, during winter time.

Due to complex wind patterns around building geometries and the outlet of anthropogenic heat, the turbulent heat fluxes can be strongly disturbed in urban areas. Because of the anthropogenic heat release the stability of the atmospheric boundary layer, which can suppress or increase the exchange of turbulent heat above a snow surface (Anderson 1976, Storck 2000), will be disturbed. Conventional flux-profile relationships and Monin-Obukhov similarity theory (Anderson 1976), might therefore not be valid (Oke 1988). With the extreme spatial heterogeneity of urban surface characteristics it is also unlikely that the spatial variability in turbulent heat exchange can be estimated from a few point measurements of wind speed and relative humidity, although methods from the field of computational fluid dynamics (CFD) might provide methods for estimation of spatially interpolated and distributed wind speed data for urban environments (Bang et al. 1994, Thordarson 2002). Such techniques could also be used to calculate wind fields and thus, turbulent heat fluxes, for urban snow packs, although the computational expense of such applications, for a large urban area would be enormous.

The magnitude of the UHI, and its impact on urban snow melt processes, will depend on the degree of AA for a given city/catchment. In Table 1.2 differences in FAR and ISC for four different areas in the world was shown. In for example the Risvollan catchment in Trondheim the FAR and ISC values are much lower compared to the three other areas/cities, and it is likely that the air temperature will not have increased significantly as a result of anthropogenic heat release, although there are other AAs influencing the urban snow pack, e.g. snow clearing and locally low albedos.

2.1.4 Snow measurement techniques

There are several reasons for why it is interesting to measure snow cover data in a catchment. Firstly, field observations of both SWE and SCA

can give a better understanding of the processes influencing melt rates and snow distribution. In this work, this is mainly how AAs are affecting the snow distribution, and melt, in an urban environment. Secondly, within the field of hydrological modelling there is a need for verification of the models performances against catchment representative measurements of SWE and SCA. Such data could also be used to update the state variables, e.g. simulated SWE and SCA, within a hydrological model (Turpin et al. 1999).

One common method to measure SWE in a point is to use a scale, weight, tube and spade. The tube is penetrated into the snow until it reaches the ground-snow interface and the weight of the snow, together with the snow volume inside the tube, is used to calculate the density. This information, together with snow depth gives the SWE. Snow pillows and weighing pans (weighing lysimeters) can also be used to measure SWE in a point, having the advantage of recording continuously data through the winter season. In addition to these methods, sonar (depth), gamma ray attenuation (density) and microwave radiation (density), can be used to estimate the SWE in a point (Pomeroy & Gray 1995).

For surface based areal measurements of SWE there are in principle two different strategies. One of them is the use of snow courses which involves measuring depth and vertically integrated density at regular intervals along selected lines (Pomeroy & Gray 1995). The location and length of the snow courses should be chosen so it covers variability in the snow pack caused by regional ($>$ a few km) differences in elevation and precipitation, and at the local scale (50 m to a few km) effects of wind (redistribution). The distance between each point is determined depending on the site conditions and uniformity of the snow cover at the micro scale ($<$ 50 m) (Killingtveit & Sœltun 1995). The SWE in each point can be measured using a snow tube, weight and scale, but such a method can be time consuming, especially if many long snow courses are used. Another technique, which is useful for covering large areas, is use of a snowmobile mounted georadar combined with a global positioning system (Marchand et al. 2001). Together with density measurements, this method can produce SWE data for large areas in a relatively short period of time, but can be limited by terrain constraints.

Another approach to observe SWE is to use stratified sampling. Random samples, of depth and density, are taken within pre-selected land cover classes and are used to calculate the average SWE within each class. The catchment is subdivided into different classes depending on terrain, eleva-

tion, land use and vegetation data (Pomeroy & Gray 1995). The catchment SWE can then be calculated as an area scaled value of the SWE in the respective land cover classes.

The reports of snow surveys carried out in urban environments are scarce in the snow hydrology literature, but a few examples exist. McMurter (1976) used a combination of stratified sampling and snow courses to observe SWE within three different land use zones (rural, construction and urban) in a 183 ha large catchment in Peterborough Ontario during the winter of 1973 to 1974. The sampling technique used in the rural area consisted of 8 snow courses each of them going in different compass directions. In the construction zone a stratified snow surveying method was used. The area was divided into 5 sub-areas based on the elevation differences and a grid was overlaid each of them. Measurement points were then selected randomly within each sub-area. In the urban area, which consisted of 273 house lots, 68 eight of them were randomly selected and SWE samples were taken in the front and back yards. Buttle & Xu (1988) also measured SWE in the same catchment as McMurter (1976) using a similar method. None of the authors report that they measured SWE on roofs, which can be questioned since the urban catchments can contain large areas of these surfaces.

Snow covered area can be mapped in several ways. Davies et al. (1995) prepared daily snow cover maps for a small area (1.8 ha) using manual techniques. The procedure involved travelling around the area to reference points sketching the snow/no-snow boundary on a map. For small catchments this procedure seems to be economic and time efficient, and could maybe be used in urban areas. According to Tait et al. (2000) some investigators have used interpolation techniques to project snow cover information obtained at climate stations (snow pillows) to a larger area. If such a method should be used to map snow cover in small catchments (local to micro scale), a large number of snow pillows would be needed, which would increase the cost substantially

Snow cover (SCA and SWE) can also be detected and monitored with a variety of remote sensing techniques. Remote sensing is the process of inferring surface parameters from measurements of the upwelling electromagnetic radiation from the land surface. This radiation is both reflected and emitted by the land surface (Schmugge et al. 2002). Both air and space born sensors can be used. The most important satellites for snow cover

studies are the NOAA, Landsat and SPOT series of satellites (Killingtveit & Sœltun 1995). The various satellites have different instrumentation and measure energy/radiation in many different wavelengths. The application of these data, to determine SCA, can be limited by clouds, mountainous terrain, vegetation and atmospheric haze (Pomeroy & Gray 1995). There is also a trade of between repeat cycling time and spatial resolution of the data. For example the Landsat Thematic Mapper data has a spatial resolution of 30 metre, but the cycle time is 16 days, while the Earth Observing System (EOS) Moderate Resolution Imaging Spectroradiometer (MODIS) instruments on NASAs EOS satellites provide daily global snow cover data with a spatial resolution of 500 metre Hall et al. (2002). Daily geographical data with spatial resolution of 250 metre is also available from the MODIS datasets (Schmugge et al. 2002).

Air borne sensors have also been used to map snow cover. One advantage with such a technique is that the resolution of the data will improve significantly since the distance between the earth and the sensors are much lower compared to space born sensors. An example of this is the work by Fily et al. (1995) who used a synthetic aperture radar (SAR) mounted on an aircraft to map snow cover for a small area in the French Alps. The spatial resolution of the SAR images were 1.5x1.0 metre. This method is useful for studies of snow cover in small catchments, but requires access and the finances to rent and instrument an airplane. If continuous observations (daily cycles), over a long period of time (years), is to be carried out, the expenses for such an application would become very large.

Another technique which also can be considered to be remote sensing is use of a camera mounted on the ground, but on a location far above a lower lying catchment. This technique was used by Tappeiner et al. (2001) who reported estimates of snow-covered area using images taken with an automatic camera from a hill slope for a 2 km^2 catchment in Italy. The brightness information in each pixel was used to decide whether there was snow on the ground. Each image had a spatial resolution of approximately 1x1 metres. With such a technology the temporal resolution of the images could be in minutes.

The outputs from many remote sensing techniques are images representing reflected or emitted energy in different wavelengths covering the area of interest. These images have to be post processed, interpreted, and converted into images of for example SCA. One method to do this is the use

of artificial neural networks (ANN). Artificial neural networks consist of a set of computational nodes (or cells) and a set of one-way data connections joining each node (Gallant 1993). They have proved to be excellent computational tools that can compute a mapping from one non-linear multivariate input space to another (Govindaraju 2000*b*, Govindaraju 2000*a*). An example of their use has been presented by (Simpson & McIntire 2001) who used a feed-forward ANN, trained with the back propagation algorithm to estimate areal extent of snow cover from a variety of remote sensing data (see also Islam & Kothari (2000)).

It has been shown that there exist a wide range of different methods and techniques that can be used to observe SWE and SCA at the earth surface. One can ask which one of the techniques, manual, remote sensing, etc, that is cheapest, most practical and provide the best results for measurements of SWE and SCA in urban environments? To answer this question it is important to decide what the data will be used for and at what temporal and spatial resolution the data should be sampled at. Due to snow ploughing of the streets, snow sliding and or rapid melt on roofs in addition to complex snow drift patterns around building geometries, the urban snow pack is extreme heterogeneous in its distribution. Within a distance of a few meters the snow depths can change from zero to many meters (roads, piles), and several land cover types can be mixed together (roofs, roads, park, etc). So if the SWE data where to be used to assess differences in SWE between several land cover types (roofs, roads, piles, etc) the spatial resolution had to be very high (<10m). In coastal maritime climates as for example in Trondheim, snow melt can start at any point during the winter time. Within a few days the ground can go from fully snow covered to almost snow free conditions, thus observations of SWE and SCA should preferably have a high temporal resolution (one day or lower). Due to these factors most space born sensors are unsuited for use in urban maritime cold climates, since the repeat cycles are low, when the resolution is high, and visa versa. This view was also commented by Bengtsson & Singh (2000) and Semádeni-Davies (1999*a*). If there are limited finances in a project, the use of air borne sensors might also be disregarded as a tool for use in urban snow surveying. It can therefore be argued that the best way to observe SCA and SWE in an urban environment is to use ground based techniques.

In the earlier sections it was argued that processes influencing snow distribution, and melt in the urban environment are location dependent.

Roads, roofs, deposits, park/garden, and snow packs located nearby building walls are all exposed to processes that vary between the land cover types. An urban snow survey should if possible include measurements within all these land cover types. The snow measurement equipment should preferably be of light weight since piles can be large and cumbersome to measure, in addition to that roofs often can only be accessed through use of a ladder, which place some weight constraints on the equipment.

2.2 Urban runoff mechanisms

Urban drainage networks are designed for the purpose of transporting storm and sanitary water out of a catchment and thereby protecting the urban environment against flooding and environmental risks. The pipe network together with removal of vegetation and introduction of impervious surfaces will change the runoff conditions in a catchment, resulting in an increase in the peak storm discharge and total runoff volume, while the time of concentration, groundwater recharge, and base flow will decrease (Kang et al. 1998, Weng 2001, Beighley & Moglen 2002). Buttle & Xu (1988) did a comparison of runoff response from the suburban and rural part of a 97 ha catchment in Canada. It was reported that the suburban area reacted more rapidly to rain-on-snow inputs and generated larger flow response ratios than the rural part. It was also noted that the quick flow yield from the rural part increased at the end of the melt season. This can be explained by high loads of melt water saturating the soil (low infiltration capacity) and therefore increases the contributing runoff area (Westerström 1986). Milina et al. (1999) studied effects of urbanization on runoff using a hydrological model simulating pre- and post-development runoff conditions. The results for one 96 ha large catchment in Norway, which had a planned increase in impervious surface area from 5 % to 26 %, showed that runoff volumes would be 2-3 times larger post development for all types of runoff events. The effects of urbanization on runoff for three seasons (summer, fall and spring) were studied by Taylor (1977) for a small catchment in Ontario, Canada. It was found that urban direct runoff volumes exceeded rural volumes by factors of 1.2, 2.3 and 7.5 for summer rainstorms, fall rainstorms, and snow melt and rain on snow events, respectively. The peak discharges showed a similar pattern, and are comparable to the results

found by Milina et al. (1999).

In winter time, the runoff conditions change compared to rainfall runoff events. Frozen soil may lower the infiltration capacity of the soil in the pervious surface covers and thereby contribute to a larger runoff area. Many of the paved surfaces are free from snow, thus during snow melt only, the paved areas do not contribute to runoff (Bengtsson & Westerström 1992). This effect might lower the runoff from urbanized areas during snow melt situations only, even if the snow melt intensity is locally enhanced by low albedo and anthropogenic heat. On the other hand soils in urban areas are often compacted and runoff from impervious surfaces is more likely to occur (Semádeni-Davies 1999*a*).

Due to time constraints in this research it was decided not to review soil-runoff, infiltration, frozen soils and pipe flow hydraulics in any detail.

2.3 Urban snow melt modeling

Hydrological models are mathematical equations that relate input to output, e.g. the transformation of precipitation to runoff. The models can be classified according to the way they treat the randomness and space and time variability of hydrologic phenomena (Chow et al. 1988). A deterministic model does not consider randomness and a given input always produces the same output, while a stochastic model produce different output for each time it is run. Within urban hydrology, many of the models that have been developed are deterministic, e.g SWMM ((Huber & Dickinson 1992) and MOUSE RDII (DHI 2000)).

Hydrological models can be said to be lumped or distributed according to how they handle heterogeneity and variability of the hydrological processes they intend to model (Refsgaard 1996). A lumped model treats all processes as averaged over a catchment area, whilst a distributed or gridded model considers the hydrological processes taking place at various points in space. Killingtveit et al. (1994) demonstrated use of a semi-distributed hydrological model where a catchment was divided into a number of sub-areas with reasonable homogeneous hydrological characteristics. The complexity of hydrological models vary from simple black-box type models to physically based distributed models (DeVries & Hromadka 1992). The demand for input data usually follows the increasing degree of complexity of hydrological

models.

Estimating watershed runoff in areas with seasonal snow cover requires that a snow melt algorithm be part of the modelling system. During the last 20 years, advances in computational power have made possible development of complex point/lumped, as well as distributed snow melt models. The complexity in deterministic point snow melt models varies from relatively simple degree-day models (Killingtveit & Sœltun 1995) to physically based multi-layered energy balance models (Jordan 1991). Sand (1990) tested 16 different point snow melt models with different degrees of complexity and found that an energy balance based model showed the best performance when simulating snow melt in a point. Melloh (1999) made a synopsis and comparison of 10 operational and research snow melt models that are in use in the U.S. today. Modelled processes, such as: snow interception by canopy, snow pack temperature, albedo, cold content, water retention, flow through snow, etc, and data requirements were used to compare the different models. Some of the findings were that, even though the complexity of the snow melt models has increased, the available input data to the models have not developed in equal pace. Since digital terrain and land cover data are now available, it was argued that these data should be used in snow melt modelling. Bales & Harrington (1995) reviewed literature within snow hydrology and argued amongst many things, that remote sensing technologies could fill the data needs that are required by physically based hydrological snow melt models.

One type of models that have been used in several urban snow melt applications is the family of degree day based conceptually lumped or semi distributed models. The advantage of these types of models is that they require relatively small amounts of input data, air temperature and precipitation. They can also be executed relatively rapid on personal computers. The US Environmental Protection Agency (EPA) Storm Water Management Model (SWMM) is one such model that has been widely used within the urban drainage community, although the applications for cold climates are very limited. The SWMM model is a mathematical model for simulation of urban runoff quantity and quality in storm and combined sewers (Huber & Dickinson 1992). SWMM has a surface and subsurface hydrology component which are capable of simulating both rainfall and snow melt runoff. Usually SWMM is applied as a semi-distributed model, i.e. the catchment is divided into several sub-catchments each draining to an inlet. Snowmelt

calculations in SWMM can be run as either continuous or event based simulations. Only the continuous simulation mode will be commented on here. Each sub-catchment is divided into three impervious (A1, A3, A4) and one pervious area (A2). Snow distribution is simulated in the following way. Area A1 is impervious with depression storage. When the SWE in area A1, exceeds a user specified threshold the snow is split into five fractions; it is redistributed into the snow covered impervious or pervious areas (A2, A3 or A4), it is removed from the catchment, can be melted immediately, or be transported to pervious areas in another sub-catchment. This functionality is meant to account for snow removal/ploughing practices in the catchment. The snow covered parts of the sub-catchment are subject to areal depletion curves. SWMM calculates snow melt in two ways depending whether there is rainfall or not. If there is rain greater than 0.1 mm (depending on the air temperature), a simplified energy balance model is used to calculate snow melt. It is assumed that solar radiation and net long wave radiation are zero, and that the snow pack is isothermal at zero degrees. SWMM then uses monthly wind speed values together with air temperature and precipitation to calculate snow melt with a simplified energy balance model, effectively, being almost the same as a degree-day model. If there is no rainfall a degree-day model is used to calculate snow melt. A simplified cold content calculation is used to delay start of snow melt when the air temperature rises above freezing. No mass is released from the snow pack before the maximum free water holding capacity ($W_{liq,max}$) of the snow is exceeded. For details on runoff, evaporation and infiltration computations, see (Huber & Dickinson 1992). Semádeni-Davies (1999*a*) did an extensive literature search to find results where SWMM had been used for wintry conditions, but no references were found. Brunvold (2000) used the SWMM model to simulate runoff, snow melt included, from an urban catchment (Risvollan, 20 ha) in Trondheim, Norway. A daily time step was used and the results were promising. The model was calibrated by comparing simulated and observed runoff only. Simulated SWE was not compared with available observed SWE data.

MOUSE RDII (DHI 2000) is a proprietary urban runoff model which can include snow melt simulations. It is normally applied as a semi-distributed model to a catchment. The MOUSE system consists of a surface hydrology model (RDII) which generates hydrographs used as input to the pipe flow model. MOUSE RDII splits an urban sub-catchment into a pervious and

impervious part. Runoff from each part is called Slow Response Component (SRC) and Fast Response Component (FRC), respectively. The snow pack is uniformly distributed in both the FRC and SRC areas, and snow melt is calculated with the degree-day equation. Water is only released from the snow pack after the threshold ($W_{liq,max}$) in the snow (set to 8% of total SWE) is exceeded. If there are cold periods within the melting season the liquid water can refreeze, and the liquid water holding capacity has to be refilled again before any mass release from the snow pack takes place. These processes are meant to simulate a change in cold content during fluctuations between warm and cold periods. No redistribution of snow from roads, etc to nearby areas is simulated. Only precipitation and air temperature are used to drive the snow melt simulations. Gustafsson (1995) reported results from applications of the Mouse-Nam concept, which is an earlier version of MOUSE RDII, to 36 urban catchments in Sweden. In all the simulations, a 24 hour time step was used. No comparison of simulated and observed snow cover was carried out. The degree-day factors had a range of 2-7 mm/(deg-day), with a mean around 4 mm/(deg-day). The various applications were calibrated against observation of runoff at the downstream end (mostly at treatment plants), for each catchment. The results indicated that the Mouse-Nam is capable of simulating daily runoff from catchment areas with a 24 hour time resolution. Hernebring et al. (1994) used the Mouse-Nam concept to simulate daily snow melt runoff and infiltration to sewer systems for several urban catchments in Sweden. The simulated SWE was compared with a time series of snow depth point measurements that was transformed to SWE assuming a density of 0.3 mm. The simulated and observed SWE showed the same trends, and runoff was simulated to a certain degree with success. A discussion on how representative the point measurements of SWE were, relative to the true basin SWE, was not given. Sætern (2002) used MOUSE RDII to simulate runoff from two urban catchments (20 ha, 550 ha) in Trondheim, Norway. For the smallest catchment (Risvollan) the winter season of 2000-2001 was simulated with a time step of 1 hour. The R^2 calculated from observed and simulated runoff for the Risvollan catchment, gave a value of 0.86. No comparison of simulated and observed SWE was done although data were available. For the larger catchment (550 ha) a 2.5 year time series was simulated, however the R^2 value of 0.36 indicated a poor fit between observed and simulated runoff. Hernebring et al. (1994) recommended that the snow model in Mouse-Nam could benefit

from dividing the urban area into sub-surfaces (roofs, streets, woodlands, etc) having different snow melt rates. Hernebring et al. (1997) used the MouseNam concept to simulate snow melt and runoff from a small urban catchment in northern Sweden (Porsöberget catchment, 13 ha, Luleå), using an hourly time step. Only the main melt period of about 1 month was simulated for the years 1983-1985. The initial value of SWE was based on field observations. The simulated and observed SWE agreed relatively well, but simulated and observed runoff showed poor correlation. It was argued that air temperature was not adequate as input data for hourly simulations of snow melt. Simulation of snow clearing procedures should also be taken into account when simulating snow melt from urban areas. These processes are not accounted for in the Mouse-Nam model.

Westerström (1984) used a degree-day approach to simulate snow melt from an urban area (13 ha) in northern Sweden. For the snow melt period (28 days in spring of 1983), simulated and observed SWE was found to match satisfactory. It was concluded that the degree-day method can be used to simulate daily snow melt runoff from an urban area. Thorolfsson & Killingtveit (1991) carried out an event based (16 hours) runoff simulation for an urban watershed (6.85 km^2) in Trondheim, Norway, using the lumped conceptual HBV model cited as Bergström (1976). The snow melt simulations were based on the degree-day model and indicated that runoff for one day could be simulated with the HBV model. The initial condition of SWE was set arbitrarily, not based on field measurements. Similar simulations where carried out by Oveland (1995) who used a lumped conceptual model, developed in the PINE system (Rinde 1998), to simulate runoff from the Risvollan (20 ha) and Fredlybekken (550 ha) catchment for the time period from January 1995 to December 1995. The snow melt model was based on a degree day approach with a 24 hour time step. Individual events were simulated with shorter time steps. The results showed best performance in the summer period, but the results from the winter period were also promising.

Within the literature of urban hydrology there are also examples of how energy balance models have been used to simulate snow melt runoff. For example, Valeo & Ho (2003) developed two versions of an urban snow melt model (USM) based on the lumped snow distribution formulation in SWMM. A full and a simplified energy balance model were used to simulate snow melt for an urban catchment (25 ha) in Calgary, Canada. The full

energy balance (USM1) was fed with precipitation, air temperature, wind speed, incoming shortwave and long wave radiation, relative humidity, and vapour pressure data. The simplified version (USM2) used only precipitation, air temperature, and solar radiation as input data, excluding the calculation of turbulent heat fluxes and advection from rain. Change in cold content was not included in the model. Both USM1 and USM2 used albedo decay curves depending on land cover type and the snow pack could be redistributed in much the same way as in SWMM. Both USM1 and USM2 used calibrated aerial depletion curves when calculating net snow melt. The liquid water in the snow pack had to exceed a certain threshold ($W_{liq,max}$) before any mass release from the snow pack took place. Both models (USM1 and USM2) and the original SWMM model were tested against data for a snow melt period of 22 days. The results showed that the simulated runoff from USM1 and USM2 agreed quite well with observed runoff. Testing of the original SWMM model did not show such good results. Comparison of simulated and observed SWE and SCA was not carried out.

Semádeni-Davies (1998) used an energy balance based snow model to simulate urban snow melt runoff for a 8.25 km^2 in the city of Luleå, Sweden. Three types of snow cover (undisturbed, compact/dirty, piled) and two surface permeabilities were included in the simulations. The winter season of 1992-1993 was simulated. Hourly data was used to drive the energy balance, but the time series for a whole season was incomplete so effectively snow melt was only calculated for the spring melt period. Several mid-winter melt periods were not simulated correctly. The simulated SWE in the different snow cover types was not compared with field measurements. Only runoff observations were used to calibrate the snow model. Bartosova & Novotny (1999) simulated spring runoff quantity and quality for a 50 km^2 urban catchment in Milwauke, Wisconsin, U.S. The model used an energy balance approach to simulate snow melt within four different surface covers. For a period of two months in the spring of 1997, simulated runoff and water quality parameters showed a poor correlation with observed data. Another example of energy balance based urban snow melt models is the work by Matheussen (1996) who continued the work by Oveland (1995) and used both a degree day model and an energy balance approach to simulate snow melt runoff from the Risvollan catchment in Norway. Matheussen (1996) also used the PINE system (Rinde 1998)). The catchment was divided into a triangular irregular network (TIN) and the average slope and aspect of

each triangle was used to correct the effective short wave radiation. Runoff from both pervious and impervious surfaces was included in the simulation. Matheussen (1996) was not able to get the energy balance based snow melt and runoff simulations to outperform the degree day based model snow melt runoff model. It was argued that this was attributed to the lack of understanding of how AA influences snow distribution and melt in the urban environment.

Most of the models sited above uses the degree day approach to calculate snow melt intensity. The models are in general applied as semi distributed or lumped models and snow distribution is simulated with areal depletion curves and/or allows for redistribution of snow to simulate the effects of snow clearing procedures. The majority of the models were applied with a 24 hour time step, although some shorter events where simulated with higher resolution (1 hour). It has been argued by several researchers that a time step of 24 hours is too long for flooding and CSO analysis of urban drainage systems (Zhu & Schilling 1994, Matheussen & Thorolfsson 1999, Semádeni-Davies 1999*a*, Bengtsson & Singh 2000). The reason for this is that a time series of runoff with a time step of 24 hours will have lower peak values than a time series with 1 hour time resolution. Therefore CSO discharge and flooding analysis should not be carried out with 24 hour time step data. This view was also pointed out by Bengtsson (1984), who argued that the degree day model is inadequate for use in snow melt simulations with a time step shorter than day. This view seems to have not been shared by the modellers using the degree day model to simulate snow melt runoff in urban areas with a time step of 24 hours.

Hernebring (1996) claimed that with a verified urban hydrological model it is possible to run long term simulations (years) of an urban drainage system to estimate dimensioning snow melt volumes. Assessment of measures taken to reduce flooding and CSO discharge could also be carried out with such a model. One can ask why the simulations with 1 hour time step cited in this chapter, e.g. (Valeo & Ho 2003), were only carried out for snow melt events (1 month or shorter). From an operational point of view, it can be argued that the goal of urban hydrological model development must be to find model structures that are capable of simulating long time series (several years) with short time resolution ($\leq$1h). With such models more accurate estimates of peak values and CSO discharge could be made. Thus simulating short time periods of spring snow melt does not contribute sig-

nificantly to solve this problem. In regions where mid-winter melt periods can occur, it is of equal importance to simulate the accumulation season as it is to simulate the melt season adequately. This is because simulated snow melt runoff is dependent of the state variables of SWE and SCA in a model (Turpin et al. 1999). Therefore whole seasons should be simulated. One likely reason for the event based modelling approaches is that there is a lack of available urban hydrological and meteorological data with adequate length (whole seasons) to conduct continuous simulations with short time resolution. Another problem with event based modelling is that the initial conditions of both soil moisture levels, SWE and SCA have to be set in the first time step of the simulation. This requires field observation of these parameters, which in most situations are not available. If whole seasons are simulated this problem is avoided. If the initial values are set arbitrarily or by calibration, it is likely that the hydrologic memory of the model influences the simulated results, and the models ability to transform precipitation into snow and runoff can be questioned.

Semádeni-Davies (2000) refer to work by Hillel (1987), Beven (1993) and others, and emphasize that the performance of hydrological models should not be judged solely on catchment wide hydrographs. The validity of each internal module, such as the snow model, should be demonstrated. None of the urban hydrological snow melt models, reviewed in this section, e.g. (Hernebring 1996, Westerström 1984, Semádeni-Davies 2000), have been tested and validated against catchment representative measurements of SWE and SCA. Moreover, to carry out such a test of the snow models, independently of the runoff simulations, there is a need for field observations of SWE and SCA that can be used for calibration and validation of urban snow melt models.

Except for the ability to simulate effects of snow clearing procedures, none of the urban snow melt models cited in this section implements a physical description of the processes occurring around roads and buildings. Such a model would be desirable if snowmelt runoff should be simulated correctly at the spatial (< 10 m) and temporal (< 1h) scales appropriate for use in urban environments. A gridded or distributed urban snow melt model which incorporate such effects have not yet been properly tested against catchment representative observations of SCA, SWE and runoff in an urban environment.

2.4 Conclusions

The albedo of snow packs located near or on roads tend to have a rapid decay and in general lower albedos than untouched snow packs. The low albedos, typically found in piled snow or snow packs nearby roads, increases snow melt intensity. The natural variability of urban snow packs are enhanced by snow clearing procedures occurring on roads and parking lots. Because of the total influence of AA on urban snow distribution and melt there are indications that both SCA and SWE will be more rapidly lowered in urban environments compared to areas not influenced by AA.

Due to the large variability of urban snow packs within relatively short distances (<10m) it was argued that remote sensing techniques do not provide sufficient temporal and spatial resolution for measurements of SWE and SCA in the urban environment. Ground based techniques that cover roofs, roads, snow deposits, and park/garden areas should be taken into consideration when designing urban snow surveys.

It was argued that an urban hydrological model specially designed for urban snow melt calculations should model the effects of roads, and buildings and should be tested against catchment representative measurements of SWE and SCA in addition to runoff. The model should be tested for whole seasons with short time resolution (<1h). Such a model and testing against catchment representative observations of SCA, SWE and runoff has not yet been carried out in an urban hydrological setting.

Chapter 3

Gridded urban hydrological model

Gridded Urban Hydrological Model (GUHM) is a model, specially designed to deal with urban snowmelt processes. The model was developed as part of this research. This chapter provides a documentation of the GUHM model structure and the input data needed to run it.

3.1 Modelling objectives

In chapter 2 it was argued that most of the urban hydrological models in use today, are using simplified model structures not taking into consideration the effects of AA on urban snow melt processes, to a satisfactory degree. One of the objectives in this research was therefore to develop an urban hydrological model specially designed for urban snow melt calculations. This means in principle to develop a model that tries to simulate how the presence (physical geometry) and operation of roads and buildings influence the snow distribution and melt in an urban environment. Chapter 2 documented several effects of AA on snow distribution and melt that should be considered in such a context. It was therefore decided that the model should try to include processes and effects of

- Snow clearing procedures
- Slope, aspect and shadowing
- Albedo of urban snow packs
- Roof heat conduction

- Altered long wave radiation budgets in vicinity to building walls.
- Exposure of roof snow packs to wind

as realistic as possible. In addition to this the general principles of conservation of mass and energy should also be followed and equations for calculation of evapotranspiration and soil-runoff also had to be implemented.

One difficult question within design of hydrological models is to decide at what temporal and spatial scales the model should operate at. In chapter 2 it was argued that a too coarse temporal resolution (24 hours) will lower peak flows and can therefore not be used in CSO discharge and flooding analysis in an urban hydrological setting. Matheussen & Thorolfsson (1999) recommended that a time resolution of 1 hour or lower should be used in urban snow melt models. This was based on an analysis of winter (Nov-Apr) storm water data from the Risvollan catchment (20 ha) in Trondheim Norway. Time series with different time resolutions, ranging from 2 minutes to 24 hours, was used to calculate discharge from an artificial overflow. The results from the time series with 1 hour time resolution agreed relatively well with the 2 minutes time resolution data, while the coarser resolutions gave wrongly estimated discharge volumes from the artificial overflow. Based on this a time resolution of 1 hour or lower was recommended for use in urban snow melt models. One objective for the model developed in this research was therefore that it should operate at a temporal resolution of 1 hour or less.

The decision on using a model time step of 1 hour has several implications. First of all the snow melt intensity cannot necessarily be calculated with the simple degree day model. The degree-day model calculates mean daily snow melt as a linear function of the mean air temperature and does not simulate diurnal cycles satisfactorily (Bengtsson 1984). For short term forecasts a physically based approach is therefore recommended (Gray & Prowse 1992), thus, in this research it was decided to use an energy balance approach to calculate snow melt intensity. One advantage with this method is that effects of e.g. low snow albedo, slope, aspect and shadow effects of the terrain can be taken into consideration in the model, in addition to modified energy fluxes in vicinity of houses. The major drawback of using an energy balance model to calculate snow melt is that it requires extensive input data, precipitation, air temperature, short wave radiation, relative humidity and wind speed, to run.

In chapter 2 it was argued that within a few metres the urban environment may contain several land cover types (roads, roofs, etc), mixed together. If processes such as low albedos, slope, aspect, shadow effects and relocation of snow from roads to nearby terrain, should be modelled in an urban hydrological the spatial resolution must therefore be high. Because of this a gridded (distributed) model with grid cells of a few metres might be favourable compared to a lumped or semi distributed model. It was therefore decided that a gridded model should be developed in this research. The output from the model should be time series or spatial plots of snow covered area (SCA) and snow water equivalent (SWE), snow melt intensity and runoff. It was also an objective that the model should be as general as possible so it could be used also in other parts of the world with cold climates.

Due to time constraints some limitations had to be set. Algorithms simulating effects of snow drift was not included, mainly because of the extreme complexity of these processes, the need for computational power and lack of field data to verify such algorithms in urban areas.

3.2 General working method

The principal idea of the GUHM is to subdivide an urban catchment into equal area orthogonal grid cells. Figure 3.1 shows a schematic of how this is done. The size of the grid cells (spatial resolution) is set by the user. Within each grid cell the following method is used: Meteorological data from nearby stations is assigned to each grid cell. Then a physically based energy balance snowmelt routine is used to calculate time series of rain and snowmelt (R+M), and SWE, etc. At the end a soil-runoff routine is used to calculate runoff using the input time series from the snow routine. The lower part of figure 3.1 shows a flow chart of how this is done. At runtime GUHM loads all necessary input data, then it loops through all grid cells calculating snowmelt and runoff, and at the end catchment runoff for each time step is simply the sum of runoff from all cells (Eq. 3.1). Currently, GUHM has no pipe flow module, but can be coupled with existing public domain or proprietary pipe flow models such as SWMM (Huber & Dickinson 1992) or MOUSE (DHI 2000).

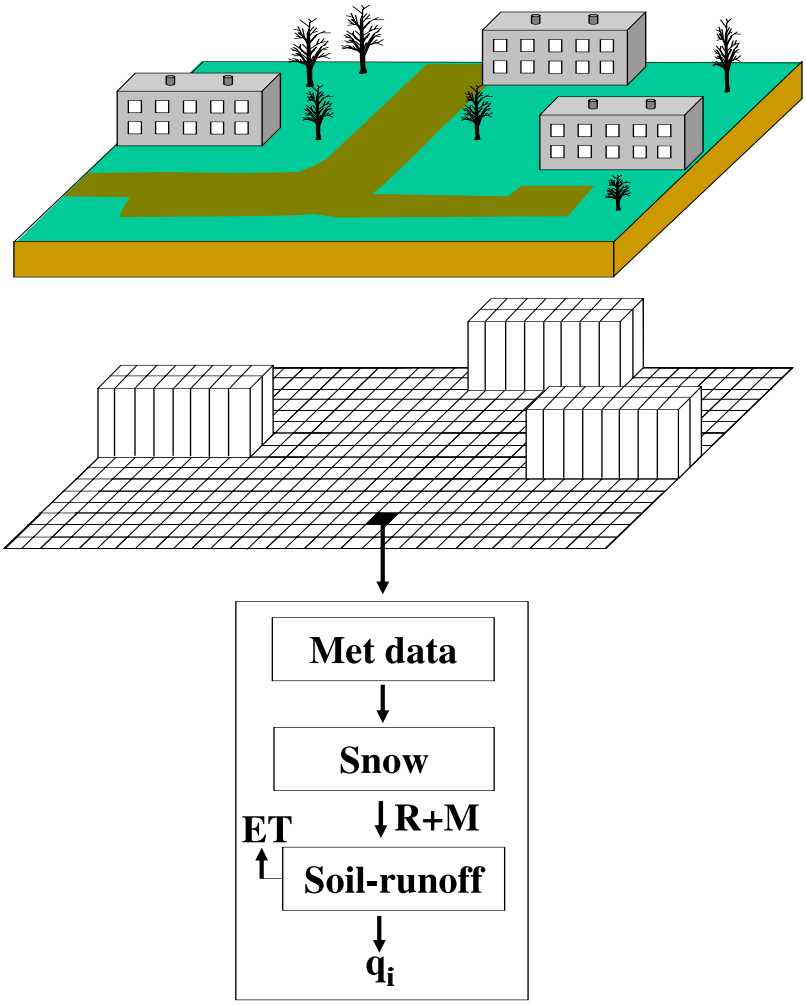

Fig. 3.1: Schematic of GUHM

$$Q_t = \sum_{i=1}^{i=gridcells} q_i \tag{3.1}$$

3.3 GUHM snow routine

Within each grid cell in GUHM, snow accumulation and melt is calculated using a snow energy balance model (Eq. 3.2). Some of the equations are the same as in the work by Storck et al. (1998) and Storck (2000), and have also been used in other work, e.g. Matheussen et al. (2000). It should be noted that there are several existing hydrological models that also uses various energy balance approaches, e.g. (Anderson 1976, Jordan 1991, Tarboton & Luce 1996, Bruland & Killingtveit 2002) and many others.

In equation 3.2, c_s is specific heat of ice, ρ_w is density of water, W is the water equivalent of the snow pack in metres (m), T_s, is the temperature of the snow pack, Q_{sw} is net shortwave radiation flux, Q_{lw} is net longwave radiation flux, Q_s is sensible heat flux, Q_e is latent heat flux, Q_p is heat from rain and snow, Q_m is the energy flux given to the pack due to liquid water refreezing or taken from the pack during melt and Q_g is ground heat flux. All energy fluxes into the snow pack is defined as positive and expressed as W/m^2. The solution of equation 3.2 is accomplished via a forward finite difference scheme over the model time step shown in equation 3.3 (Storck 2000).

$$\rho_w c_s \frac{dWT_s}{dt} = Q_{sw} + Q_{lw} + Q_s + Q_e + Q_p + Q_m + Q_g \tag{3.2}$$

$$W^{t+\Delta t} T_s^{t+\Delta t} - W^t T_s^t = \frac{\Delta t}{\rho_w c_s}(Q_{sw} + Q_{lw} + Q_s + Q_e + Q_p + Q_m + Q_g) \tag{3.3}$$

3.3.1 Shortwave radiation

In equation 3.3 the net shortwave radiation flux is calculated using equation 3.4. A is the snow surface albedo. I_x is the observed incoming shortwave radiation corrected for slope, aspect and if the grid cell is in shadow or not,

depending on time of day and year.

$$Q_{sw} = I_x(1 - A) \tag{3.4}$$

A digital elevation model (DEM), including buildings, is used to calculate if a grid cell is in shadow or not. This is done with the following method. First the solar angle and azimuth relative to the grid cell is calculated using the algorithms supported by RReDC (2000) (C source code downloaded from the internet). The equations are based on the work off Michalsky (1988*b*), Michalsky (1988*a*), Zimmerman (1981), and Iqbal (1983). Then the solar angle in the solar azimuth direction is compared with the height of the grid cells adjacent, and in the solar azimuth direction, to the grid cell considered. If there are any grid cells crossing the direct beam from the sun, then the grid cell is considered to be in the shadow. This is carried out for each model time step and for each grid cell. Solar radiation is split into a direct and a diffuse component following (Skartveit & Olseth 1987). If a grid cell is not in the shadow from other cells, the direct component of the solar radiation is modified for slope and aspect after methods described by (Vignola & McDaniels 1988). Section 3.6 provides more information on the shadowing calculations.

$$A = a_1(a_2)^{(sa)^{(a_3)}} \tag{3.5}$$

Equation 3.5 (Storck 2000) shows how albedo is calculated as a function of time since last snow fall (snow age (sa), in days). The user has to specify the parameters (a_1, a_2, a_3) used in the albedo decay function (Eq. 3.5). One of the benefits of using such an albedo formulation is that the albedo will change when new snow falls on old snow. For every new snowfall the albedo will be reset to its initial value a_1. The user has the option to specify an albedo curve for the accumulation season (no liquid water present in the snow), and one for the melt period (liquid water present in the snow).

3.3.2 Longwave radiation

Net longwave radiation (Q_{lw}) is calculated with equation 3.6. T_a is air temperature in the grid cell and T_s is the snow surface temperature. σ is the Stefan-Boltzmann constant and e is vapor pressure in the air, in millibars (Bras 1990). I_g is observed shortwave radiation and I_{xx} is extraterrestrial shortwave radiation.

$$
\begin{aligned}
Q_{lw} &= K\sigma(0.740 + 0.0049e)T_a^4 - \sigma T_s^4 && (3.6)\\
N^2 &= \frac{1.0 - I_g/I_{xx}}{0.65} && I_g > 0\\
N^2 &= 1.25 && I_g \leq 0\\
K &= 1 + 0.17N^2
\end{aligned}
$$

3.3.3 Latent and sensible heat

Calculation of sensible heat flux into or out of the snow surface is given by Equation 3.7. ρ_a is air density, c_p is specific heat of air and $r_{a,s}$ is the aerodynamic resistance between the snow surface and the near surface reference height, typically the instrument height at which the meteorological data are sampled (Eq. 3.12, 3.13).

$$Q_s = \frac{\rho_a c_p (T_a - T_s)}{r_{a,s}} \tag{3.7}$$

$$Q_e = \frac{\lambda_i \rho_a \left[\frac{0.622}{P_a}\right] [e(T_a) - e_s(T_s)]}{r_{a,s}} \tag{3.8}$$

Calculation of latent heat is given by equation 3.8. λ_i is latent heat of vaporization when liquid water is present in the snow and the latent heat of sublimation in the absence of liquid water. P_a is the atmospheric pressure. e and e_s are the vapour and saturation vapour pressure, respectively.

During snow melt, warm air is typically cooled right above the snow surface. If wind is present cold air can be transported upwards, by turbulent eddies from the snow surface, but since the air is cooler than the ambient air the cold air tends to sink down to the snow pack again. This mechanism suppresses turbulent exchange of energy (stable atmospheric conditions). If an air parcel right above the snow surface is colder than the snow surface turbulent fluxes are enhanced since the cool air will be warmed up by the snow and rise. This enhances turbulent energy exchange

(unstable atmospheric conditions). The calculation of turbulent heat fluxes is therefore complicated by the stability of the atmospheric boundary layer (Anderson 1976, Storck 2000).

Aerodynamic resistance is given by equation 3.9, were z and z_0 are near surface reference height (usually instrument height above ground) and snow surface roughness, respectively. k is the von Karman constant, usually set to 0.4 and U_z is the wind speed at the reference height. g is gravity. Ri_b is the bulk Richardsons number, which is a dimensionless ratio relating the buoyant and mechanical forces acting on a parcel of air (Storck 2000). Ri_{ul} is the upper limit of Ri_b developed by Storck (2000) to compensate for underestimation of latent and sensible heat fluxes during common melt conditions. Aerodynamic resistance is corrected for stable and unstable conditions with equation 3.12 and 3.13, giving $r_{a,s}$.

$$r_a = \frac{ln\left[\frac{z}{z_0}\right]^2}{k^2 U_z} \tag{3.9}$$

$$Ri_b = \frac{gz(T_a - T_s)}{\frac{(T_a+T_s)}{2}{U_z}^2} \tag{3.10}$$

$$Ri_{ul} = \frac{T_a}{\frac{(T_a+T_s)}{2}(ln\left[\frac{z}{z_0}\right] + 5)} \tag{3.11}$$

Stable conditions

$$r_{a,s} = \frac{r_a}{(1 - \frac{Ri_b}{Ri_{cr}})^2} \qquad 0 \leq Ri_b \leq Ri_{ul} \tag{3.12}$$

Unstable conditions

$$r_{a,s} = \frac{r_a}{(1 - 16Ri_b)^{0.5}} \qquad Ri_b < 0 \tag{3.13}$$

In urban areas, the idea of calculating turbulent heat fluxes, with stability corrections is highly uncertain. Complex building geometry and heat from several anthropogenic sources, such as fuel combustion, domestic heating, etc., changes the wind and temperature fields and strongly influences the turbulent eddies and the stability of the atmosphere. Due to time constraints it was chosen to use this method despite the uncertainty associated with it. The users of GUHM have the option to specify a different snow surface roughness for each LCT. Section 3.5 presents more on this.

3.3.4 Advective energy

Energy from rain and snow is given by:

$$Q_p = \frac{\rho_w c_w T_a P_r + \rho_w c_s T_a P_s}{\Delta t} \tag{3.14}$$

where c_w is specific heat of liquid water and c_s is specific heat of ice and ρ_w is density of water. The rain water is added to the liquid water content in the snow and can refreeze and release latent heat of fusion. Precipitation (P) is partitioned into snowfall (P_{snow}) and rainfall (P_{rain}) with equation 3.15. T_{max} and T_{min} are threshold temperatures separating rain and snow (user specified). Precipitation is corrected for precipitation gauge under catch with equation 3.16 and 3.17, where PC_{rain} and PC_{snow} are user specified input parameters.

$$\begin{aligned} P_{snow} &= P, & T_a \leq T_{min} \\ P_{snow} &= \frac{T_{max} - T_a}{T_{max} - T_{min}} P, & T_{min} < T_a < T_{max} \\ P_{snow} &= 0, & T_a \geq T_{max} \\ P_{rain} &= P - P_{snow} \end{aligned} \tag{3.15}$$

$$P_s = P_{snow}\, PC_{snow} \tag{3.16}$$

$$P_r = P_{rain}\, PC_{rain} \tag{3.17}$$

3.3.5 Net energy and mass balance

When the snow pack exchanges energy with the atmosphere the snow pack can be cooled down or heated, liquid water can be partially or totally refrozen, or melt can be produced. For a given time step this is controlled by the net energy available for the snow pack. The net energy (Q_{net}) is given by equation 3.18.

$$Q_{net} = (Q_{sw} + Q_{lw} + Q_s + Q_e + Q_p + Q_g)\Delta t \tag{3.18}$$

If Q_{net} is negative, energy is being lost by the pack. Liquid water (if present) is then partially or totally refrozen. If Q_{net} is sufficiently negative to refreeze all liquid water, then the pack may cool. If Q_{net} is positive, then the excess energy available after heating the snow pack to zero degrees, produces snow melt. Equation 3.19 and 3.20 illustrates this.

$$Q_m \Delta t = min(-Q_{net}, \rho_w \lambda_f W_{liq}), \quad Q_{net} < 0 \tag{3.19}$$

$$Q_m \Delta t = -(Q_{net} + c_s W_{ice} T_s^t), \quad Q_{net} \geq 0 \tag{3.20}$$

The mass balance of the snow pack is calculated using the following equations:

$$\begin{aligned} \Delta W_{liq} &= P_r + \frac{Q_e}{\rho_w \lambda_v} - \frac{Q_m}{\rho_w \lambda_f} \\ \Delta W_{ice} &= P_s + \frac{Q_e}{\rho_w \lambda_s} + \frac{Q_m}{\rho_w \lambda_f} \end{aligned} \tag{3.21}$$

, where λ_v is latent heat of vaporization, and λ_s is latent heat of sublimation. Q_e exchanges water with the liquid phase if liquid water is present, and exchanges water with the ice phase in the absence of liquid water. If W_{liq} exceeds the maximum free water holding capacity ($W_{liq,max}$) of the snow pack, then excess ($W_{liq} - W_{liq,max}$) is drained trough a linear reservoir and into snow pack outflow. The outflow of snowmelt from the linear reservoir is controlled by K_{snow} which can be altered during calibration. The linear reservoir represents the dynamics of liquid water percolating through the snow pack (Sand 1990).

Equations 3.2 - 3.21 are solved with an iterative method. Given initial snow surface temperature and water equivalent, additional snowfall is added to the snow pack and its temperature is adjusted accordingly. The snow routine then calculates Q_{net}. If Q_{net} is positive the snow pack is first heated to zero degrees and the rest of the positive energy is transformed into melt. If Q_{net} is negative, liquid water is refrozen, if there is still negative energy the snow temperature is iteratively lowered, and Q_{net} is recalculated, until the energy balance is satisfied. The model assumes uniform temperature in the snow pack, i.e. one layer and isothermal conditions. This is debatable

since the top layer of the snow can have a different temperature then the base, i.e. a vertical temperature gradient within the snow pack. The snow routine produces a time series of rain, melt and SWE which is used as input to the soil-runoff routine described in the following sections.

3.4 Soil-runoff routine

The soil-runoff routine in GUHM is a modified version of the soil routine in the HBV model (Bergström & Forsman 1973), see also Killingtveit & Sœltun (1995). Figure 3.2 shows the schematics of how the soil-runoff routine works in GUHM. It consists conceptually of three zones, the soil zone (SM), upper (UZ) and lower zone (LZ). Net precipitation (R+M, rain plus melt) from the snow routine is split in two as dUZ and dSM according to equation 3.22. dSM is water added to the soil layer (SM) and dUZ is runoff transported to UZ. The maximum water content in the soil zone is controlled by the field capacity (FC in equation 3.22).

$$\begin{aligned} deficit &= FC - SM \\ dUZ &= R + M - deficit \qquad R + M > deficit \\ dUZ &= (R + M)(\frac{SM}{FC})^{\beta} \qquad R + M \leq deficit \\ dSM &= (R + M) - dUZ \end{aligned} \tag{3.22}$$

Water is removed from the soil layer only through what is called actual evapotranspiration (ET). The purpose of this is to simulate how nature removes water from the soil through evaporation and transpiration. If the water content in the soil layer exceeds a user specified threshold value (LP), the actual ET equals the potential ET. If the soil moisture is below the threshold (LP) actual ET is scaled with the factor SM/FC. This forces actual ET to decrease as the soil layer dries. Calculation of potential ET is shown in later sections. The UZ consist of a linear reservoir with three outlets (see Fig. 3.2). In addition water can flow to the lower zone through

what is called percolation (q_{perc}). The lower zone (LZ) consists of a linear reservoir with two outlets. The lower zone represents slow response runoff.

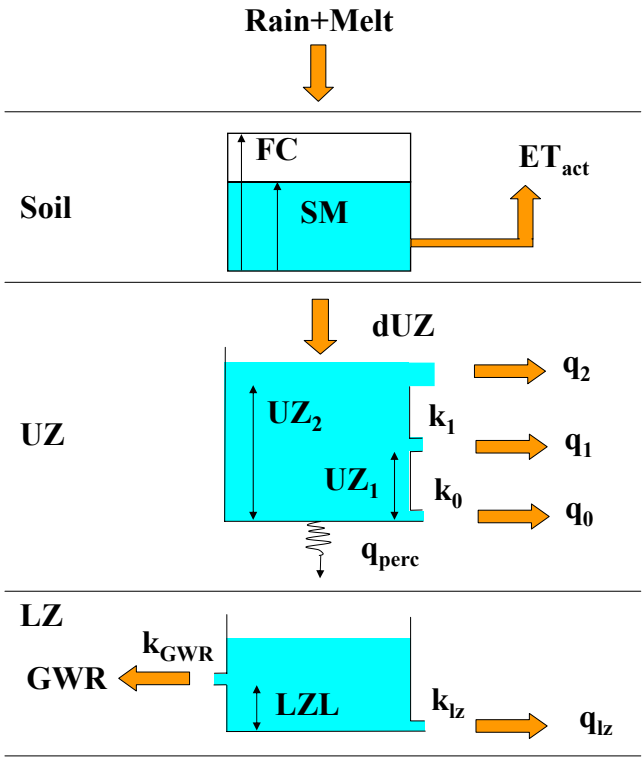

Fig. 3.2: GUHM Soil-runoff routine

In an urban hydrological model the water balance is controlled by several factors such as precipitation gage correction factors, estimation of catchment area, calculation of actual ET, etc. Runoff measured at a gauging station, in the subsurface pipe network, might not be an accurate estimate of the total water volume leaving a catchment. Some water contributes to recharge groundwater and never enters the pipe network. This effect is implemented in GUHM and is the water going out of the LZ as GWR, controlled by k_{GWR} and LZL. This feature is only used in LCT park.

The runoff from one grid cell is calculated with equation 3.23.

$$q_i = q_0 + q_1 + q_2 + q_{lz} \tag{3.23}$$

Calculation of potential ET (ET_{pot}, Eq. 3.24) is done with the Penman-Monteith equation (Shuttleworth 1993). In equation 3.24 R_n is net radiation added to the water surface. This is the sum of shortwave (solar radiation) and longwave radiation, the latter calculated with equation 3.6, replacing T_s with T_a. Λ is calculated using equation 3.25, where T_a is air temperature. γ is the phsycrometer constant, r_s is surface (stomatal) resistance. c_p is specific heat of moist air. Calculation of aerodynamic resistance r_a^P is given by equation 3.27, where z and z_w are instrument reference height and aerodynamic roughness, respectively. D is vapour pressure deficit and U_z is windspeed. The reason for using the Penman-Monteith equation was that potential ET can be estimated for vegetated surfaces and/or from free water surfaces (setting r_s to zero). The current version of GUHM does not allow for different calculation of potential ET depending on surface cover, but this will be implemented at a later stage. In the current version of the model the user can specify the r_s value. If it is set to zero, potential ET is calculated as being the potential evaporation from a free water surface.

$$ET_{pot} = \frac{1}{\lambda_v}\left[\frac{\Lambda R_n + \rho_a c_p D/r_a^p}{\Lambda + \gamma(1 + r_s/r_a^p)}\right] \tag{3.24}$$

$$\Lambda = \frac{4098 e_s}{(237.3 + T_a)^2} \tag{3.25}$$

$$e_s = 0.6108 exp(\frac{17.27 T_a}{237.3 + T_a}) \tag{3.26}$$

$$r_a^p = \frac{4.72[ln(z/z_w)]^2}{1 + 0.536 U_z} \tag{3.27}$$

3.5 Land cover specific features

In the GUHM, each grid cell is classified as one out of five possible land cover types (LCT). Grid cells of the same LCT are assumed to have the same hydrological homogenous characteristics. The five LCTs currently used in GUHM are road, roof, deposit, wall and park, illustrated in Figure

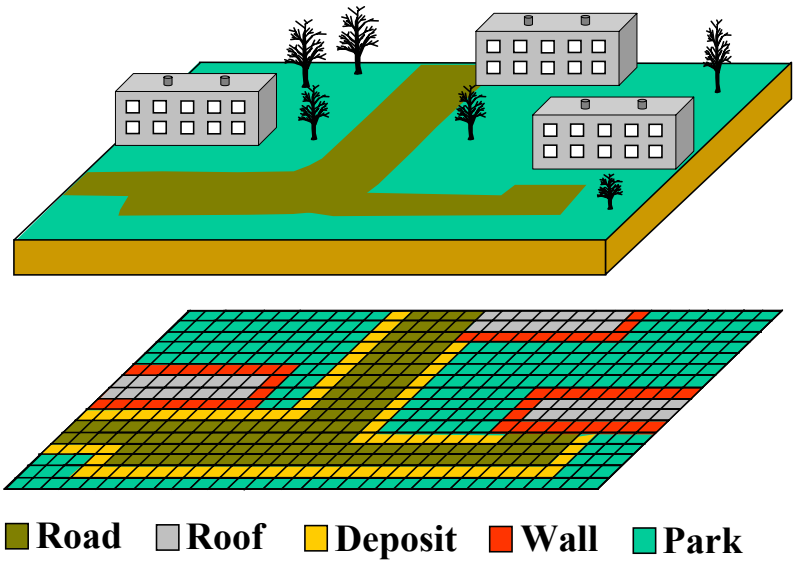

Fig. 3.3: Subdivision of an urban area into grid cells of different land cover types

3.3. Within each grid cell, the same snow and soil-runoff routine is used, but modified according to the dominating AA within each LCT. In LCT park it is assumed that no AA is present and the snow and soil-runoff routines are used as described in previous sections. Figure 3.4 illustrates how the snow routine is modified to account for AA influencing distribution and melt of the urban snow pack. The land cover specific features presented in this section was not used in the snow model developed by Storck (2000).

3.5.1 Land cover type roof

LCT roof represents building rooftops. Snow on rooftops is more exposed to sun and wind compared to the snow on the ground. Stronger wind speeds will enhance snow drift (lower accumulation) and increase the turbulent heat fluxes when the snow is melting. The complex wind flow field around buildings in the urban environment also complicates the snowmelt calculations. Within GUHM, the elevation difference between building rooftops and the terrain is assumed to be of the same height, specified by the user.

The wind speed is then corrected following a logarithmic wind profile adjusted for the difference between instrument height above ground and the height of the buildings. Inside heating of buildings contributes to an increased heat flux into the snow through heat conduction. The magnitude of this flux will differ from house to house depending on the insulation in the roofs. In GUHM the user must specify the magnitude of this flux named Q_{g-roof}. For grid cells of LCT roof, Q_g in equation 3.2 is set to the user specified energy flux Q_{g-roof}. In all other LCT heat from underlying surface is set to zero. In the soil-runoff routine the thickness of the soil layer (FC) should be set in the range 0-10 mm, user specified, to simulate the fact that most roofs are impervious and has a fast runoff response.

3.5.2 Land cover type road and deposit

In urban areas, after heavy snowfall, the roads are cleared, and the snow is moved to deposit areas, often within a few metres of the road. To model this effect the LCT road is only allowed to accumulate SWE up to a user specified threshold level (SWE_{max}), before it is relocated to the nearest grid cell of LCT deposit. This threshold should be based on snow removal practices in the area being modelled. For example Valeo & Ho (2003) used a value of 6.5 mm of SWE_{max} before the snow was relocated from roads. For this effect to be modelled with satisfactory results the grid cells should be sufficiently small. A grid cell size of 1-5 meters is recommended, to ensure that redistribution of snow from roads to nearby areas is simulated in a most realistic manner. Figure 3.4 illustrates the redistribution of snow from road to deposit grid cells.

LCTs road and deposit should be given steep albedo decay function that causes the albedo to drop rapidly to 0.2-0.4 during melt periods. This is to account for the low albedo caused by impurities in the snow as a result of e.g. traffic. From chapter 2, Bengtsson & Westerström (1992) and Semádeni-Davies (1999*a*) reported albedo of a downtown snow pile to be as low as 0.2, during melt periods.

LCT road is usually impervious and thin soil layers should be specified by the user. Deposit areas are considered to be impervious and should therefore have a thicker soil layer, typically 75-300 mm, according to Killingtveit & Sœltun (1995). The thickness of the soil layers are subject to calibration.

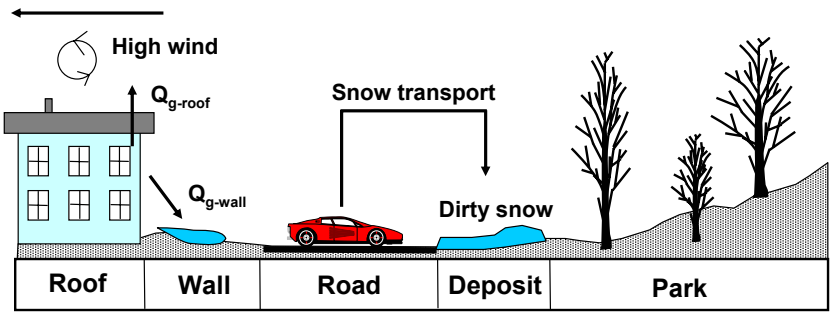

Fig. 3.4: GUHM land cover types (LCT)

3.5.3 Land cover type wall

When a building is heated from the inside or outside (inside heating, outside solar radiation), the outside wall surface temperature arise. This leads to increased emission of long wave radiation. In cities, buildings differ in colour, shape and location and the overall effect of increased wall temperature on snowmelt is difficult to estimate. The effective snow albedo can also be lowered in proximity to buildings since the shortwave radiation is reflected multiple times between the different surfaces which add an extra energy component to the snow pack. Grid cells of LCT wall are meant to account for these effects by adding an extra energy flux (Q_{g-wall}) to the snow pack. Grid cells of LCT wall are located adjacent to the roof grid cells. Since the magnitude of this heat flux cannot be estimated accurately on a spatial average, this heat flux is a user specified input to the model. For grid cells of LCT wall, Q_g in equation 3.2 is set to the user specified energy flux Q_{g-wall}.

3.6 GUHM input data

The GUHM model needs extensive input data. Each grid cell needs a time series of precipitation, air temperature, wind-speed, relative humidity and short wave radiation, usually taken from nearby stations. Three text files provide information about start date and time of the simulations, number of records to run, catchment, snow and soil model structure input parameters, etc. A grid of the catchment showing the five LCT must also be given as

input. As explained earlier GUHM redistributes snow from road cells to the nearest deposit cell. For each road cell GUHM must keep track of which deposit cell should receive the snow. This is done with two grids called closestX and closestY. These two files are pre-processed from a LCT grid, containing only grid cells of type road, roof, park and wall, with a program called ClosestCell. This program, written in C, was developed during the research. For each road grid cell, the closest grid cell of LCT park is converted into LCT deposit, and will receive snow from the road cell. This produces a final LCT grid which is used as input together with the ClosestX and ClosestY grids. These grids can also be manually changed to account for different snow clearing procedures.

Slope and aspect grids are also required input to GUHM and should be pre-processed using the following procedure. Three different digital elevation models (DEM) must be prepared. One is a DEM were only the terrain (buildings excluded) is included. This will be referred to as DEM-terrain. The second is a DEM where only the buildings in the catchment are included. This will be referred to as DEM-building. The last one is a DEM were both terrain and buildings are included (DEM-tb). First slope and aspect must be calculated separately for the DEM-terrain and DEM-building. Then the slope and aspect grids from the DEM-buildings is overlaid the slope and aspect grids from DEM-terrain. This makes the slope of grid cells adjacent to buildings to be flat.

DEM-tb is used to calculate if cells are in shadow or not. This is done by the following method. At first 24 sky directions is defined. For each grid cell and for each sky direction an angle called α_{shadow} is found. In Figure 3.5 this angle is shown and represents the lowest solar angle permitted, without putting the grid cell in shadow. To find this angle the height and distance of every grid cell in the sky direction is considered. This exercise is pre-processed in GUHM with a program called DEM-SHADOW, also developed as part of this research. The output from this program are 24 grids, one for each sky direction, with values of α_{shadow}. GUHM then uses the solar azimuth angle to define which sky direction that should be used when comparing the solar angle α with α_{shadow}. If α is smaller than α_{shadow}, then the grid cell is in the shadow for the current time step. These calculations are only carried out when the sun is above the horizon. Since the buildings are included in the DEM, shadowing effects will then be accounted for by GUHM. At runtime GUHM reads the 24 grids and

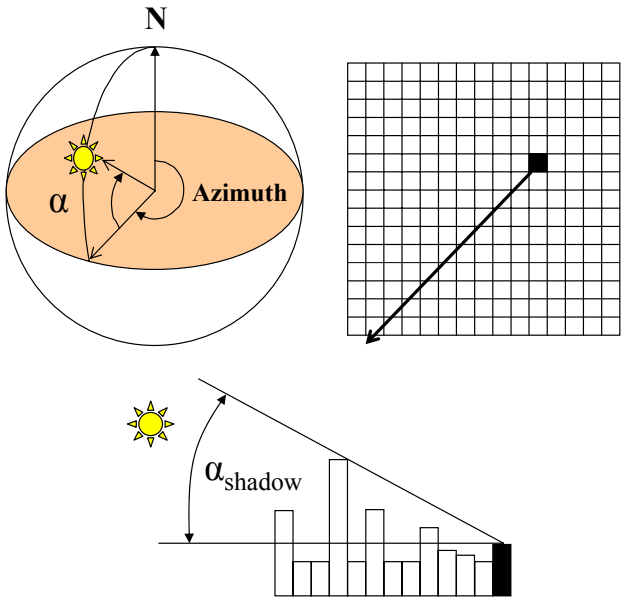

Fig. 3.5: Shadowing of grid cells

uses them to decide if cells are in the shadow. If a time step of 30 minutes is used in GUHM, 48 grids containing an α_{shadow} value must be prepared. The shadowing calculations presented in this section was not used by Storck (2000).

Chapter 4

Study area and available data

This chapter presents the study area used in this research. Documentation of two urban hydrological measuring stations and climate data, which will be used in later chapters are also presented.

4.1 Risvollan catchment

In this research, the Risvollan urban catchment was used as the study area (Fig. 4.1). The reason for using Risvollan was that it is located close to NTNU, is a relatively small catchment and high quality datasets of hydrological and meteorological parameters exists for the catchment. It is located about 4 km southeast of the centre of Trondheim city (Norway) and is a 20 ha residential area. It consists of 26 % impervious surfaces (13 % roofs and 13 % paved areas) and 74 % grass lawn and park areas. About 1500 people live in the catchment (Thorolfsson & Høgeli 1994). The majority of the buildings is residential and mainly consisting of two floors (FAR = 26 %, ISC = 26 %). The soil types in the Risvollan catchment are mostly silt-clay, but gravel and sand are used around some of the buildings and in children playgrounds. Within the grass lawn and park areas there are scattered groups of trees, mostly birch and fir. In the lower right corner of Figure 4.1, two red circles can be seen. These are locations of the hydrological stations, Risvollan and Voll, which will be described in later sections. Figure 4.2 presents the Risvollan catchment with roads, buildings and the separate storm and sanitary systems. Both systems drain towards the north western part of the catchment and collects runoff from both the

impervious and pervious surfaces of the catchment. The parts not covered with roads or buildings in Figure 4.2, are mostly park and garden areas.

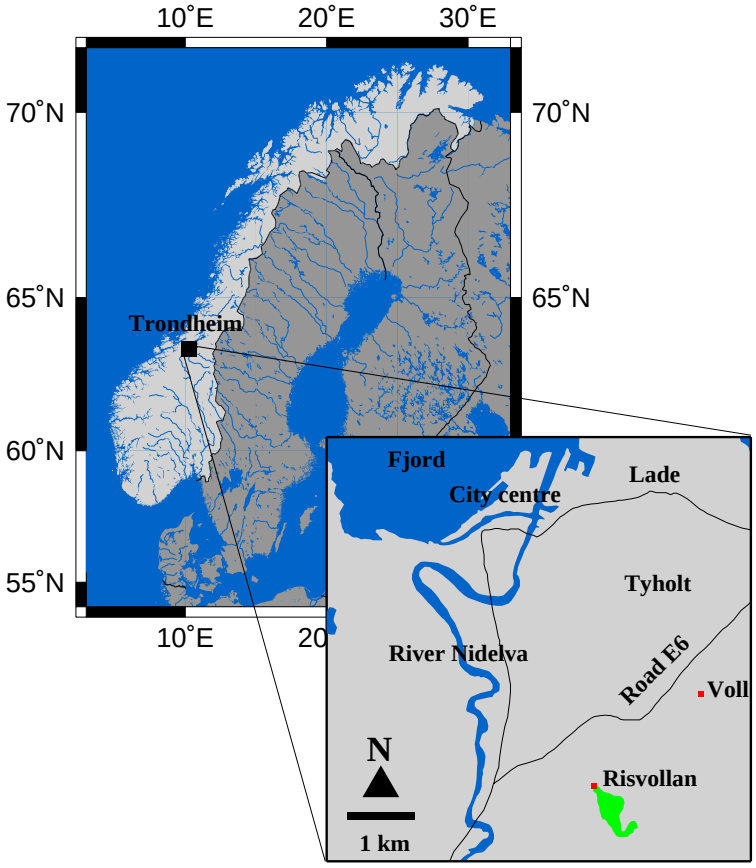

Fig. 4.1: Scandinavia, Norway, Trondheim, Risvollan

Figure 4.3 shows a digital elevation model (DEM) of the Risvollan catchment. The thick black line is the hydrological boundary of the catchment. Within the DEM shown in Figure 4.3 the building rooftop elevations are included. The lowest point in Risvollan is at the outlet of the storm and sanitary system at 84 metres. The highest point, at 143 metres, is on top of one of the buildings in the southern part. The average elevation in the DEM (buildings included) for the Risvollan catchment is 114 metres.

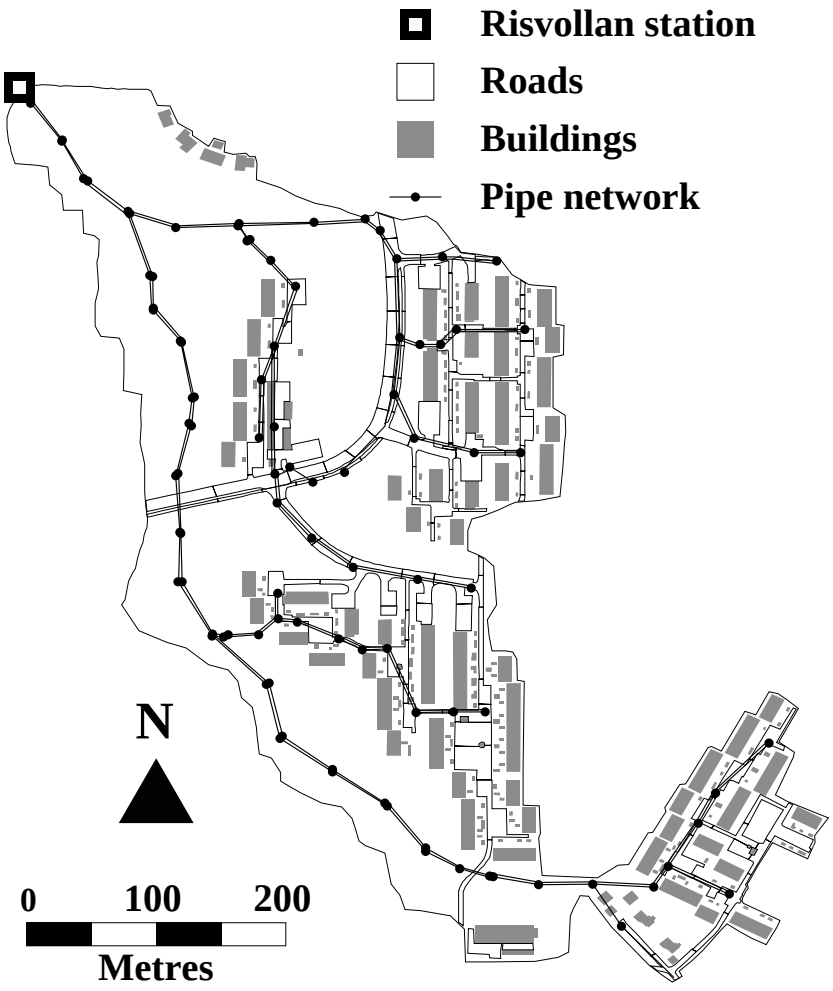

Fig. 4.2: Risvollan catchment

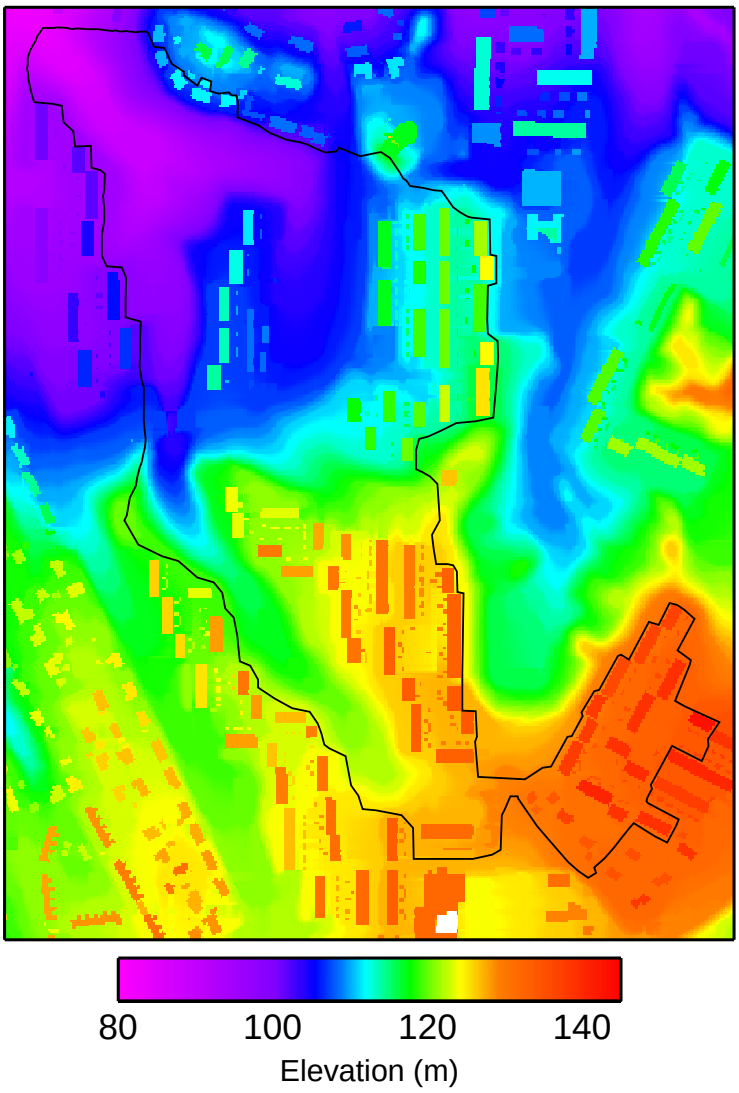

Fig. 4.3: Digital elevation model (DEM) of Risvollan catchment

4.2 Risvollan urban hydrological station

At the downstream end of Risvollan (upper left corner of Figure 4.2) the Risvollan urban meteorological and hydrological station, which will be referred to as Risvollan station, is situated. The Risvollan station was built in 1986 with the objective to collect high quality urban meteorological and hydrological data for research purposes. The station collects data with 2 minutes temporal resolution continuously year round. Precipitation is ob-

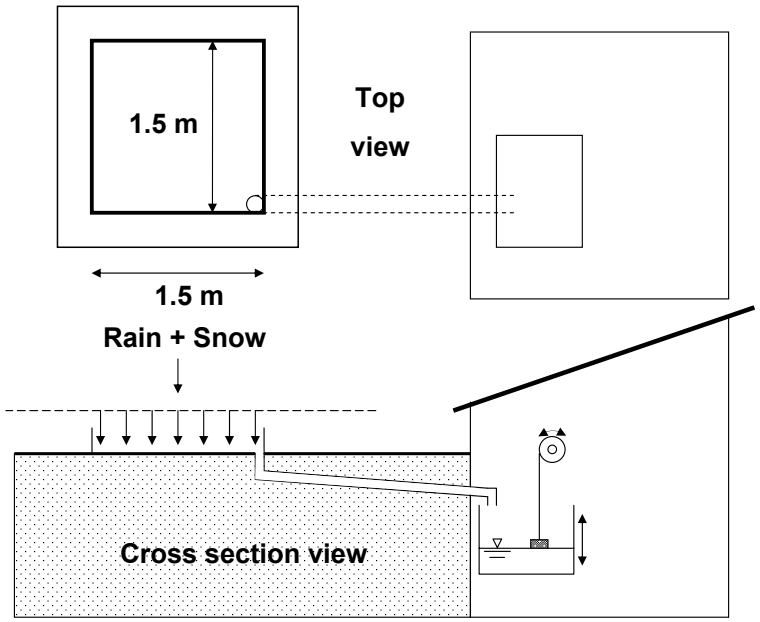

Fig. 4.4: Sketch of snow melt lysimeter at Risvollan station

served with three gages, but only data from the Lambrecth and FUESS instruments were used in this research. The lambrecth instrument is an unshielded heated tipping bucket precipitation gage and the FUESS instrument is an unshielded weighing precipitation gage, both placed two meters above ground. Below the rim of the FUESS gage there is a bucket collecting the precipitation. The instrument is emptied once a week, and oil

and anti-freeze are added in the bucket to reduce evaporation and freezing. Air temperature is observed 2 metres above ground with an Aanderaa 3145 sensor. In addition solar radiation (shortwave Aanderaa sensor 2770), wind velocity (Aanderaa sensor 2740), and relative humidity (Aanderaa sensor 2820) are also recorded at this height. Storm water runoff is recorded by observing the water level trough a 100 degrees triangular-notch, thin plated weir. The triangular- notch was designed according to the ISO 1438/1-1980(E) standard. The stage through the notch is recorded with a float placed in a stilling well. The float is connected to a potentiometer recording the change in water level. A snow melt lysimeter is also installed. It is placed on the ground and collects seepage water from rain and snow melt. Figure 4.4 shows a sketch of how the lysimeter functions. A 1.5 x 1.5 m tray collects the seepage water into a vessel. The change in water level in the vessel is recorded with a float connected to a stage recorder. More documentation and examples of use of the data collected at the Risvollan station can be found in Thorolfsson et al. (2003), Thorolfsson & Brandt (1996), Thorolfsson & Høgeli (1994), Thorolfsson & Sand (1991), Sand (1990), Risholt (2000) and Lei (1996).

4.3 Voll hydrological station

About 2.5 km north east of the Risvollan station (see Fig. 4.1) Voll meteorological station is situated. Several climate parameters are available at this station, but only solar radiation and wind speed measurements were used in this research. The solar radiation instrument is a Pyranometer Kipp & Zonen CM 6B at 2m elevation, and the wind speed is measured with a Vaisala, WAA15A at 10 m elevation (Dalsbø 2003). The station is situated in a large open field.

4.4 Hydrological data

Figure 4.5 displays monthly averages for hydrological and meteorological data from Risvollan and Voll stations from June 1999 to June 2003. In Figure 4.5 (a) precipitation and runoff is shown. The annual average precipitation at Risvollan was 881 mm and at Voll 729 mm. The data are not corrected for wind affecting the gage efficiency. The precipitation gage

at Voll is located in an open field and is therefore more exposed to wind. This might explain the differences in annual precipitation. It might also indicate that there is spatial variability in the precipitation patterns over Trondheim city. The month of April has the lowest precipitation with only 36 mm at Risvollan. The annual runoff from Risvollan is 564 mm. The runoff coefficient, the ratio of average runoff for average precipitation is therefore calculated to 0.64 for the Risvollan catchment. It can be seen that for the month April runoff is about twice as large as the precipitation, due to snowmelt in the catchment. January has the highest runoff with 111 mm precipitation and 79 mm of runoff.

Figure 4.5 (b) shows wind speed and air temperature recorded at Risvollan and Voll stations. The wind speed data from Voll are observed 10 metre above ground, in an open field, compared to 2 metre above ground in a vegetated depression area at Risvollan. This can explain the higher wind speeds seen at Voll station in Figure 4.5 (b). From Figure 4.5(b) it can also be seen that air temperature is lower at Risvollan than on Voll station during winter time. This can also have been caused by differences in location, vegetation and terrain for the two stations.

Figure 4.5 (c) presents relative humidity, and incoming shortwave radiation, observed at Risvollan and Voll stations. Relative humidity is stable in the range 60 to 80 % at both stations. The differences in solar radiation at the two stations can be explained by adjacent terrain, and height of instruments. Differences in instrument types and incorrect calibration are also plausible reasons for this.

4.5 Uncertainty in observed discharge

Sources of errors contributing to uncertainty in the measurements of discharge i.e. errors in discharge coefficient, error in measured geometry of the notch, measured water stage which also depends on the error in determination of gauge zero, and corrective terms for viscosity and surface tensions are presented in ISO1438 (1980). For triangular notches ISO1438 (1980) and Mosevoll et al. (1991) estimates the 95 % confidence interval for the observed discharge to be roughly +/- 2 % to 3 % if the specifications given in ISO1438 (1980) are followed during construction of the notch. Standard deviations and errors of width, height, etc of the notch is then in the range

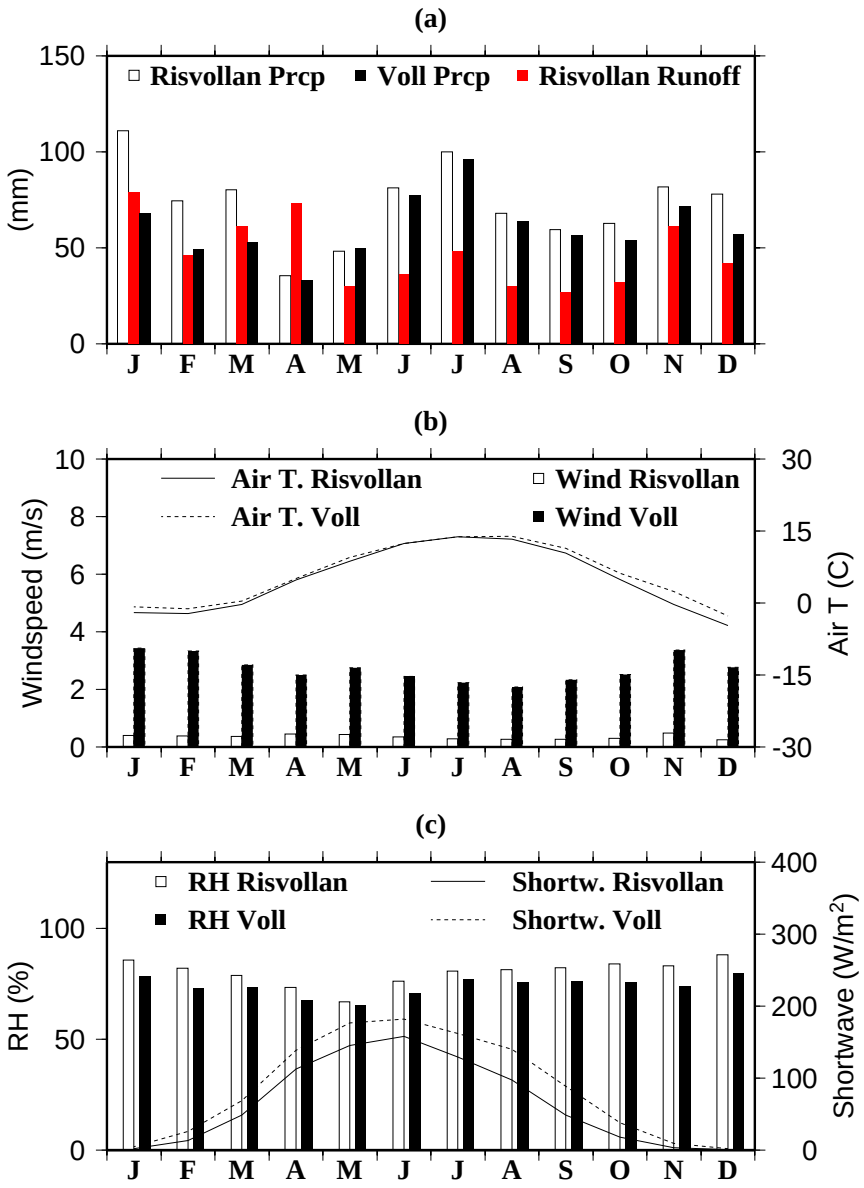

Fig. 4.5: Monthly averages of hydrological and meteorological data from Risvollan and Voll stations (June 1999 - June 2003)

0.05 to 0.5 mm. It should be noted that the uncertainty in the discharge is dependent on water stage. At high water stages, the uncertainty is less than at low levels. This means that the dry weather flow has a higher uncertainty related to it compared to wet weather flows. At Risvollan the error of the estimated stage is assumed to be around 1 mm when the potensiometer and the float recording the water stage are newly calibrated. This gives an uncertainty of about 3 % at a water stage of 100 mm.

When long time series (years) of hydrological data with short time resolution (minutes, hours) are put together there will be more sources of uncertainty than the ones mentioned in ISO1438 (1980). Most of them are a result of human error e.g. lack of calibration and updating of conversion formulas, data loggers erased for data before downloading, clocks adjusted wrongly, etc. This introduces uncertainty in the measurements of water stage. For some periods the digital recordings were not functioning at Risvollan station. For example at 13 July 2001 the station was flooded as a result of heavy rainfall. All electronic data logging units were out of operation for one week, but mechanical stage recorders were functioning. These data were scanned and digitalized to replace lost electronic data. The accuracy of the estimated water stage is believed not to be better than +/- 5 mm for such events. During large discharges, e.g. 10 June 2002, at the Risvollan station, observations showed that the flow conditions upstream the notch was very turbulent and near critical flow, which is not ideal for estimating discharge from water stage. This also introduces an extra uncertainty at high water stages. All these factors introduce uncertainty that under certain conditions can increase the uncertainty above the 1 mm (3 %) level. If the error in the water stage is 5 mm at a stage of 100 mm, then the 95 % confidence interval is about +/- 10 %. Similarly, if the error is 10 mm in 100 mm water stage the confidence interval is +/- 20 % (Mosevoll et al. 1991).

Chapter 5

Observations of snow covered area

In this chapter a technique developed for observing time series of SCA for an urban catchment is documented. The method is presented together with results and a discussion. At the end some conclusions from the work are drawn. The objectives of the SCA observations was to a) identify differences in SCA between three land cover types (road, roof and park), and b) use the observed time series of SCA to calibrate and validate the GUHM described in chapter 3

5.1 Method

In chapter 2 it was argued that remote sensing (space born) techniques for observing snow cover in an urban environment do not provide the desirable spatial and temporal resolution simultaneously. Air borne sensing would also be relatively expensive for use in urban environments. Because of this it was decided to use overview digital camera images of the Risvollan catchment to estimate SCA. If images are taken on a continuous basis, a time series of SCA can be developed and used to verify the performance of urban snowmelt models, in this case the GUHM. At the boundary of the Risvollan catchment there is a 45 metre tall building. In March 2001 a digital camera (AXIS 2120 Network Camera) was placed on top of it, such that the camera had maximum visibility over the catchment (see Fig. 5.1). The camera recorded images every fifteen minutes, with a width and height of 704 and 576 pixels. This corresponds to a vertical and horizontal image resolution of 300 pixels per inch. All images used the RGB (Red

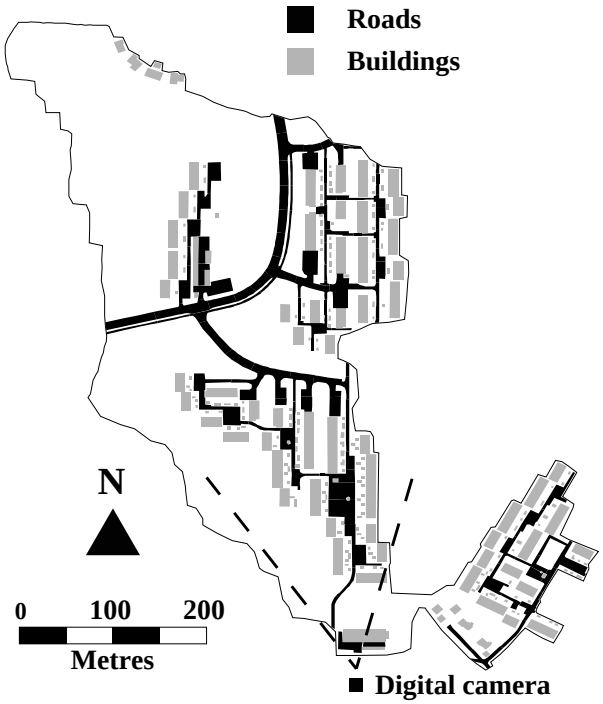

Fig. 5.1: Top view of digital camera placement in Risvollan catchment

Green Blue) three layers colour model. Each of the three layers had a range from 0 to 255 (quantities of light). The camera was stationary so that the angle of the images relative to the ground was constant. Figure 5.2 illustrates how the camera was placed on the roof of the building. The camera communicated with a computer that stored all the images for later use.

5.1.1 Calculation of snow covered area

Not all parts of the images from the digital camera were of interest with respect to snow-cover estimation. Sky, trees and building walls were of no interest when estimating SCA, hence only parts of the images that displayed ground were used. Three LCTs, roof, park, and road were identified in the

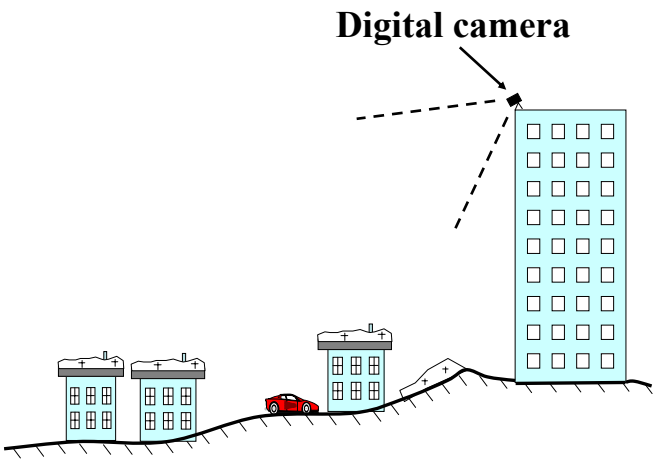

Fig. 5.2: Side view illustration of the digital camera placement

images. A mask grid file with the same width and height as the images was used to identify the pixels that were located inside the specific LCT categories of interest. Pixels that fell inside the specific LCT were given a 1 and the ones outside were given a 0. This coding controlled whether SCA for this pixel should be calculated or not.

Figure 5.3 displays an example of the images taken with the digital camera. The black coloured pixels within Figure 5.3 shows the areas of the three LCTs that were analysed for SCA. Although all LCTs were coloured black in Figure 5.3, three mask files (one for each LCT) were made to keep track of the different areas that were to be analysed for SCA. The three LCTs selected have different characteristics in terms of snow accumulation patterns and available energy for snowmelt (the results and discussion section presents more details on this). It was also desirable that all LCTs should have areas (pixels) with different horizontal distance to the digital camera. Areas that were strongly influenced by shadows were not considered in the analysis. In Figure 5.3, almost all parts of the ground are clear and visible. This was not the case for all images. In some, shadows and dirty snow made the contrast between the LCTs less distinct.

Many types of artificial neural networks (ANN) have been used within the field of hydrology. An introduction to the topic and applications can be found in Govindaraju (2000*b*) and Govindaraju (2000*a*). Figure 5.4 shows

Fig. 5.3: Example image from digital camera. Black areas were analysed for snow cover

the topology of the three layered feed forward ANN used in this research. The ANN was used to establish a relationship between pixel information (Red, Green, Blue) and snow or bare ground. After this the ANN was used to classify pixels as either fully snow covered or bare ground within the three LCTs. There are three nodes in the input layer, one for each colour in the pixels (Red, Green, Blue), six nodes in the hidden layer and one node in the output layer. The sigmoidal function was used as the activation function (Gallant 1993). The ANN is trained for a small set of pixels selected from each image and afterwards applied to all the pixels in the image that falls within the three LCTs shown in Figure 5.3.

5.1.2 Data sampling, training and validation of neural network

In this work, a supervised ANN, optimized with the back-propagation algorithm (Gallant 1993, Govindaraju 2000*b*, Islam & Kothari 2000), was used. This means that before the ANN can be used in any analysis, it has to be trained for a given dataset. The purpose of the training data is to establish a relationship between the RGB values in the pixels and the snow cover.

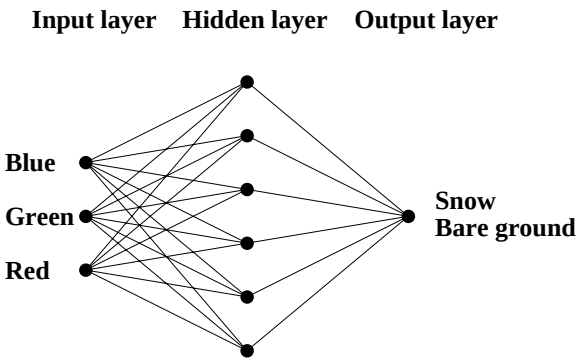

Fig. 5.4: Three layer feed forward artificial neural network used to map between pixel information and snow cover

A pixel was chosen to be either fully snow covered or have no snow in it. Sampling of the training data was done in the following way. For every image, an attempt was made to sample at least 10 pixels with snow and 10 pixels without snow. The pixels were sampled from all three LCT shown in Figure 5.3. In some images some of the LCTs were free of snow so sampling could not be done in a consistent way for all the images. For each of the pixels in the training data, the RGB values were recorded. Pixels with full snow cover were given a value of 1 if they had snow in them and 0 if not. All training data were sampled using an interactive Matlab program developed as part of this research. The program reads in one image at the time and displays it for the user. The user clicks on pixels with and without snow. The RGB values for each of the pixels are saved to a text file together with the snow value (one or zero). The data are then read by the ANN which is a C++ program, also developed as part of this research.

Validation of the results is an important part of hydrological model studies. This is also important when using ANN as classifiers. Validation can be seen as a performance test of the ANN and can be evaluated by subjecting the ANN to new input data not used in the training process. In this research, validation was done using training data from five images. Table 5.1 shows the dates, number of pixels (training sets), number of wrongly classified pixels (error), and number of iterations used to train the ANN. All five training datasets were split in two. One network was trained for each of the two datasets and validated against the other half of the data.

Table 5.1: Results from cross training of neural network

Date	Pix T1	Pix T2	Err 1	Err 2	Iter 1	Iter 2
16Mar01	31	30	0	0	101	68
04Apr01	36	35	0	0	1106	333
07Nov01	16	16	0	0	188	186
11Feb02	15	14	0	1	433	272
06Apr02	27	26	0	0	405	45

From Table 5.1 it can be seen that only one pixel was incorrectly classified. This was in the training data from the image dated 11 Feb 02. For this dataset, 15 points (pixels) with RGB and snow values were used to train the ANN. Only 272 iterations were needed before the network converged. This gave 1 incorrect classified cell out of 14 when the ANN was applied to the other half of the data not used in training. In all the other datasets all pixels were correctly classified. This indicates that even a small set of pixels is enough to train the ANN before it can be used to classify pixels as either snow or bare ground. At start of the training process the ANN was initialised with random values between minus one and one. All the RGB values were scaled with 255 so the input node values were in the range zero to one. The ANN was trained with momentum, learning rate and error tolerance set to 0.5, 0.9 and 0.1, respectively. When the ANN was applied to a dataset, a threshold value of 0.5 was used on the output node to decide if the pixel was snow covered or not.

5.2 Results

The digital camera was in operation from 10 March 2001 and recorded images every day until all the snow had melted in late April 2001. The camera was in operation for the entire 2001-2002 winter season, but due to several operational problems a continuous time series could not be constructed out of the images. The camera was placed in a heated protective box, but sometimes snow and ice covered the window in front of the camera lens, due to the time it took the heater to melt it. During heavy snowfall, the camera visibility was too low for SCA estimation. Some hardware and software

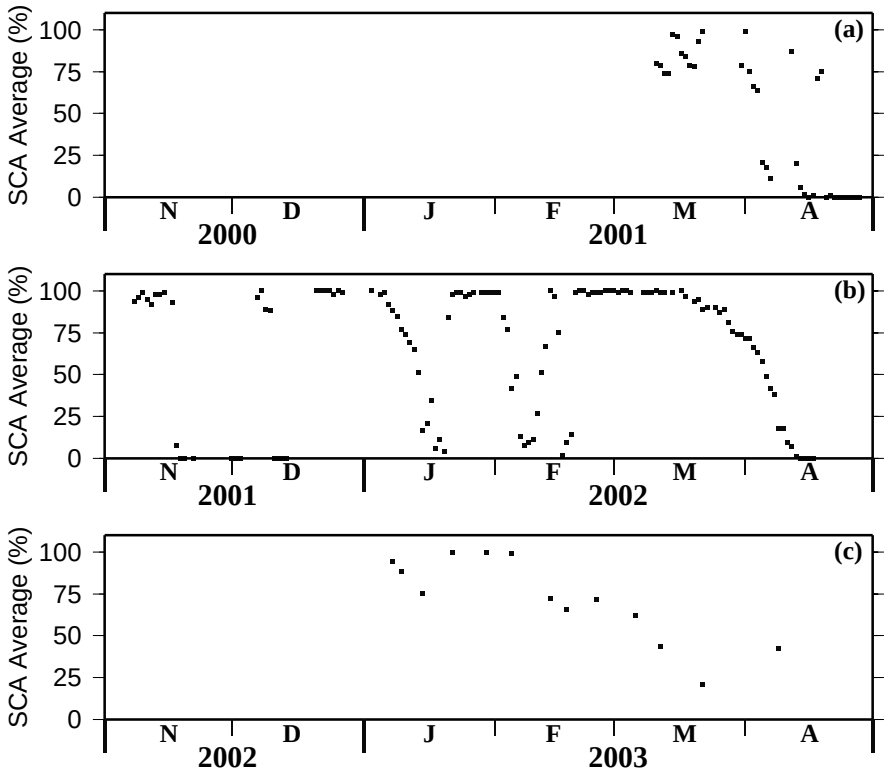

Fig. 5.5: Estimates of average SCA for Risvollan catchment

problems also resulted in loss of images. The camera was not in operation during the winter of 2002/2003. Instead a handheld digital camera was used to take images on a weekly basis. A total of 13 images were taken during the winter 2002/2003. A manual inspection of each image before calculation of SCA was done to ensure that each image had the right quality. A total of 178 images were selected from spring 2001 to spring 2003 and used to produce a time series of SCA for the Risvollan catchment. Only one image was selected from each day (at noon) due to data volumes and processing time.

Figure 5.5 presents results from using the ANN to analyse snow cover for the 178 images. Within the three LCTs, SCA was estimated as the fraction of white (snow) pixels to the total amount of pixels. In Figure

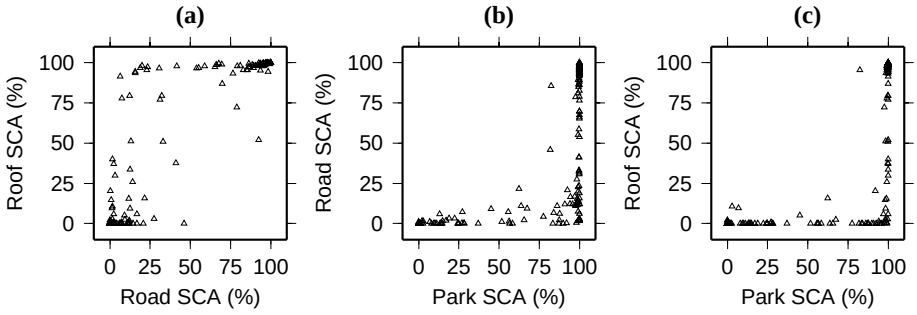

Fig. 5.6: Correlation of SCA between LCT Road, Roof and Park

5.5, the average SCA is shown as a percentage for the Risvollan catchment. All values in Figure 5.5 are calculated as an area-scaled average using SCA from the three cover types. It can be seen that the first snowfall in the autumn of 2002 came in beginning of November (Fig. 5.5 (b)). In the spring all snow was melted around 20 April in 2001 and 15 April in 2002 (Fig. 5.5 (a) and (b)). It can also be seen that there are several mid-winter melt periods during the winter of 2001-2002. During these periods the ground was snow free before new snow fell. This is typical for the climate in Trondheim where snowmelt can start at any time during the winter. In the winter 2002/2003 there was relatively little snowfall in the Risvollan catchment (Fig. 5.5 (c)). The roads and roofs were mostly snow free the whole winter season, resulting in that the average SCA in Figure 5.5 (c) is never at full snow cover.

Figure 5.6 shows the correlation of SCA between all the three LCTs (roof, roads and park). During partial snow cover SCA on roofs tend to be higher than on roads (Fig. 5.6 (a)). Park areas have in general more snow cover for most of the time than both roads and roofs (Fig. 5.6 (b) and (c)). The differences in SCA for these LCT types can be explained by AA. Wind speeds are higher on roofs and might cause less snow to accumulate during snowfall, due to snow drift. Since the wind speed is higher the magnitude of the turbulent heat fluxes are also higher and will lead to more available energy during melt. Conduction from the roofs themselves will also contribute with heat to the snow pack, in addition to that roofs are in general are more exposed to solar radiation compared to e.g. park areas. All these factors can explain the rapid melt and early snow free

conditions on the roofs. Roads are usually cleared for snow after heavy snowfall. This AA is probably the one that has most influence on the SCA in the urban environment. The snow on roads is more exposed to traffic and the albedo will be lower than in the park areas. Lower albedo and use of de-icing chemicals will give more rapid melt and the roads become rapidly snow free during melt situations. After the snow removal from roads there is often a thin ice or snow layer left on the road. Road cover such as asphalt has very low albedo (0.05-0.1) and will absorb almost all the solar radiation that it receives. This will increase the surface temperature of the road and provides energy through conduction to the overlying snow. During melt conditions air that flows over the snow free asphalt can also be heated and increase melt through sensible heat in nearby areas (Semádeni-Davies 1999*a*). This effect has also been reported for patchy snow covers in rural terrain (Liston 1995, Granger et al. 2002). Wind speeds are lower on park LCTs than on rooftops and may lead to more accumulation of snow. The lower wind speed will also result in less turbulent energy available during melt periods. Shadowing from buildings and trees also have influence on melt rates since there will be less solar radiation that hits the snow pack in the park LCT. Since AA is weak in the park LCT, the albedo will in general be higher than on roads. This will lower melt rates compared to roads.

5.2.1 Estimation of SCA from aerial photos

Aerial photos were taken on four days during the spring of 2002. For every flight 72 photos were taken from different angles above the catchment. All photos were inspected manually and closed polygons were drawn around the snow free areas on a digital map using a Geographical Information System (GIS). The total SCA for the whole catchment was then calculated. The SCA estimated from the aerial photos were used to verify the ANN methodology on these dates.

Figure 5.7 shows estimated SCA from the photos taken for two of the days (14th Mar 2002 and 5th Apr 2002). On the 14th Mar 2002 there is almost full snow cover in the Risvollan catchment. Only the main road is free for snow. Before this image was taken, the roads were probably cleared for snow and melt has removed the little snow cover that was left. On the 5th Apr 2002, the snow had almost completely melted in most part of the

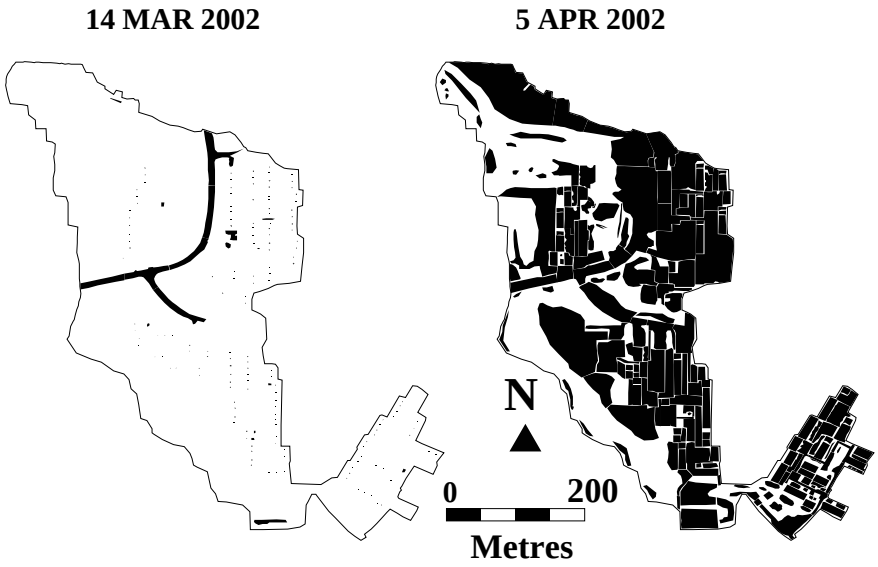

Fig. 5.7: Snow-covered areas estimated from aerial photos. Black colour indicates snow free areas and white areas with full snow cover

catchment. Park areas still had some snow cover.

5.2.2 Uncertainty in estimates of SCA

An error analysis of the calculated SCA was carried out. The domain of SCA is from zero to hundred % [0,100]. For all values of SCA there will be an upper limit and a lower limit error level. If SCA is estimated as 90 % the upper error cannot exceed 10 % but the lower error can be as large as 90 %. It can also be assumed that for a given date and time there will be one true SCA value for a given catchment. If it is assumed that the aerial photo estimated SCA has low uncertainty and is close to ground truth. The error of SCA estimated from the digital camera images can be estimated as the difference between the two sampling methods. This assumption could be verified by having different people estimating SCA from the aerial photos, although this was not done in this research. Another approach would be to view the two different estimates of SCA as independent and use the mean of the two as the estimated SCA value.

Table 5.2: Estimates of SCA (%) from aerial photos. Digital camera in parenthesis

Date	Road	Roof	Park	Average
09Jan02	11 (12)	44 (16)	96 (99)	80 (77)
11Jan02	8 (12)	4 (0)	80 (91)	62 (69)
14Mar02	78 (93)	99 (99)	97 (100)	97 (99)
05Apr02	5 (2)	3 (0)	51 (66)	40 (49)

Table 5.2 shows SCA (%) estimated from aerial photos and digital camera (in parenthesis) for four days during winter and spring of 2002. SCA for each individual LCT and the catchment average is estimated. The average SCA for the digital camera data was calculated as an area scaled average from the SCA in LTC roof, road and park. It can be seen that SCA agrees relatively well between the two methods, indicating a correlation between the two datasets (digital camera and aerial photo). On the 11th of Jan 2002 the snow in road and roof LCT are almost completely melted while in park the SCA is estimated to 80 % and 91 % using the aerial photos and digital camera methods. The snow is basically melted in the areas mostly influenced by AA (roads and roofs). From Table 5.2 it can be seen that the largest difference between the two methods tend to be when there is partial snow cover in the catchment. For example at the 9th of January 2002, the difference for LCT roof between the two methods is 28 %. One reason for this can be that the digital camera is placed south of the areas used for SCA estimation. The roof areas visible in each image are therefore more exposed to the sun than the roofs not visible in the images. The aerial photos cover the whole catchment and roofs that are in shadow of the sun are also taken into consideration. At low and high SCA values both methods seems to coincide relatively good. The average SCA for the whole catchment on 9th January 2002 had an error of -3 %. The highest recorded error value was 9 % between the two methods when the whole catchment was considered. This indicates that the methods work best when the whole catchment is considered.

5.3 Discussion

This research demonstrated how a digital camera can be used to estimate SCA for an urban area. The methodology was based on image analysis and the use of ANN. The calculation of SCA was influenced by the light conditions in the image. The brightness in the image was a function of the suns position and cloud cover when the image was taken. Shadowed areas could be interpreted as bare ground by the ANN. Dirty snow might also, depending on the light conditions, be counted as bare ground. In December and January there is little sunlight at latitudes around 63 degrees North. This made it difficult to get high quality images, especially on cloudy days. There might be possible solutions to the problems of shadowing and dirty snow that was not explored in this research. Increased contrast in the images might give better results when calculating SCA. Use of an infrared camera could also improve detection of snow cover, because during melting periods the bare ground will usually have surface temperatures above zero degrees Celsius, which can be detected from an infrared image. An infrared camera could also be used 24 hours a day.

In this research, image pixels were not allowed to have partial snow cover. On the boundary between snow and bare ground, there will be pixels that have partial snow cover. When many cells are analysed, it is believed that this error will have little influence on the results. Another solution would be to give pixels that had RGB values in a certain range only 50 % snow cover. It was also assumed that each pixel in the image covers the same size area projected to the horizontal level. This was not the case and introduces uncertainty in the estimation of SCA. This problem could be voided with geometric corrections of the individual pixel sizes compared to the ground area they cover. In this work pixels located at various distances from the camera were chosen in an attempt to even out the errors from not using geometric corrections. Fily et al. (1995) corrected SAR images using geometric and radiometric corrections together with a digital elevation model to get better estimates of SCA. When light travels from the ground and into the camera, it is intercepted by dust particles and snow in the air. This can change the RGB values in the images and lead to misclassification of pixels. Due to time constraints no corrections for these effects where done in this research.

If AA has any effect on the urban snow pack energy balance and dis-

tribution, the observed values of SCA should be lowest in the areas most heavily influenced by AA. The results of this research support this theory. Roads and roofs had in general lower SCA than the park LCT. These two LCTs must therefore be influenced by factors not present in LCT park, namely AA.

Aerial photos were used to verify the estimates of SCA from the digital camera. The results indicated strong correlation between the two methods. It should be noted that in both methods human interpretation of the images might have influenced the final results. One weakness in the verification process (use of aerial photos) is also that data from only four days were used. It may therefore be argued that the digital camera method could have been better verified. In addition to this it should be noted that the camera covered a relatively small part of the Risvollan catchment. The camera observed snow cover in only 9 %, 15 %, 5 % of LCT road, roof, park, respectively. This is a weakness in the digital camera methodology, but could be solved by using more cameras positioned at various locations in the catchment.

5.4 Conclusions

A technique for observing time series of SCA for an urban catchment was presented. The method was based on image processing using ANN technology to calculate SCA from a time series of digital images taken of the Risvollan catchment. The method was verified against SCA estimated from aerial photos, and proved to give good estimates of SCA. The largest difference in the aerial photo and digital camera estimated SCA was 9 % when the whole catchment was considered. Three different LCTs were investigated for snow cover. It was shown that SCA on roads and roofs were in general lower than in park areas of an urban catchment. This was explained by the difference in influence from AA. Snow clearing of roads, snowdrift from rooftops, low snow albedos on roads and release of heat from the roofs themselves all contributed to lowering the SCA more rapidly on roofs and roads compared to in the park LCT. The observed time series of SCA for the Risvollan urban catchment can be used for calibration and validation purposes of an urban hydrological model. From this it can be concluded that objective number 3 set in chapter 1 has partly been achieved.

Chapter 6

Observations of snow water equivalent

This chapter presents results from field observations of SWE in the Risvollan catchment. The objectives of collecting the SWE data were to identify differences in mean areal SWE between four land cover types (road, roof, deposit, park) and use these data during calibration and validation of the GUHM presented in chapter 3. The snow survey method and results are presented, followed by a discussion and some conclusions.

6.1 Method

It was decided to observe mean areal SWE for the Risvollan catchment by use of manual snow courses. In 1994, three snow courses were selected for the Risvollan catchment (Brandt & Torgersen 1994). One course contained areas were AA (snow piling, etc) was dominant. The two others were courses where the AA was less dominant (park areas). Amongst the location criteria for selection of the three snow courses were concavity/convexity and slope of terrain, and degree of urbanisation. Three courses of about 70 metres were selected. Each course included ten equally distanced points where SWE was observed. The three courses selected in 1994 are called the basic courses and can be seen in Figure 6.1 as course number 1, 2 and 3. Originally, Brandt & Torgersen (1994) selected six snow courses, but three of them were excluded since they went through private property.

In 2001 it was decided to extend the snow courses, established by Brandt & Torgersen (1994) with six additional snow courses. Figure 6.1 shows the location of these, as course number 4 to 9. Measurements on roofs were

also carried out. The measurement points on roofs are marked with a star in Figure 6.1. In course number 4 to 7 (see Fig. 6.1) the distance between

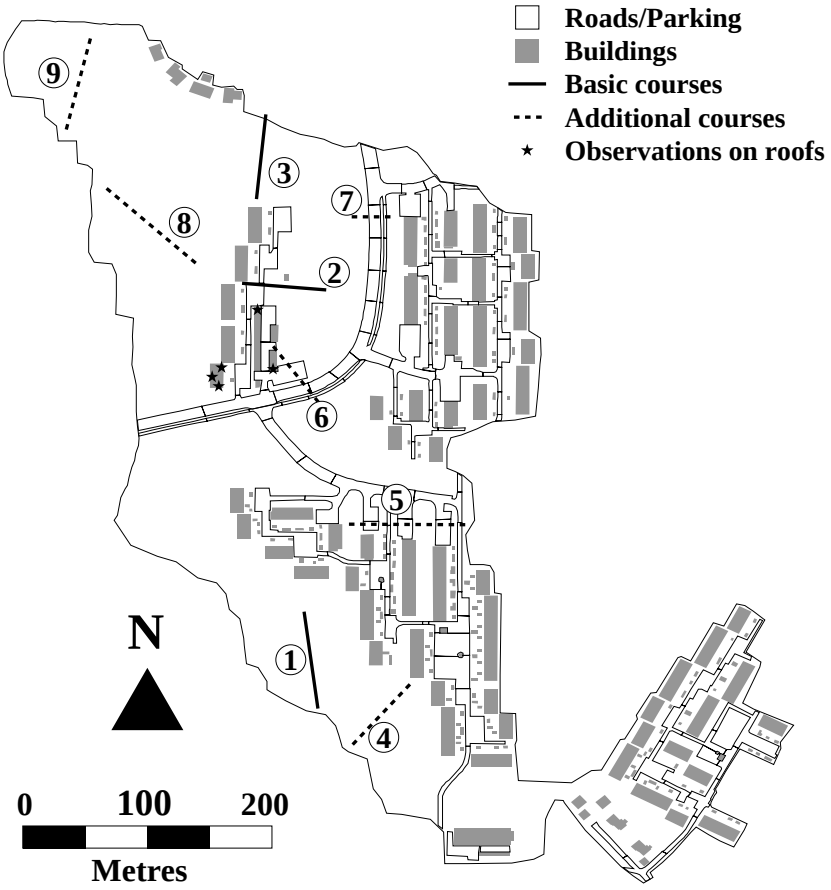

Fig. 6.1: Snow courses in Risvollan catchment

each measurement point was set to about 1 metre. In practice this distance varied for several reasons. Sometimes cars had parked in the snow course so measurements could not be carried out. In piles, the snow sometimes had strong ice layers making it impossible for the tube to penetrate the snow pack. A nearby point, within 1 metre, was then chosen. In snow courses 8 and 9, the distance between each measurement point was about ten metres. Density was measured only for every 4th measurement point. The locations

of the additional snow courses were chosen to go trough different LCTs and be easy accessible, for practical reasons.

On survey days, a detailed map showing the 9 snow courses was brought in the field. The exact location of each measurement point was noted. In each measurement point a snow tube, ruler, weight, and spade was used to estimate depth and density of the snow. At every survey day the following procedure was used to try to minimize the measurement errors. Before any point samples were taken the date, start time and inside diameter of snow tube was noted. Then the weight was calibrated against a two kg known weight. After this, the snow tube, clean of snow, was weighed. The weight reading of the clean tube was then noted. In every measurement the procedure shown in Table 6.1 was used.

Table 6.1: Procedure for depth and density measurements

1. Clean snow tube.
2. Penetrate snow tube into snow. Make sure its hitting the soil below.
3. Dig out the snow tube and make sure no snow is lost from the core.
4. Weigh the snow tube with snow in it and note the reading.
5. If there is ice slush or ice at the bottom, measure depth of ice and/or slush layer and note it. If ice is hard use screwdriver to dig down to soil layer.
6. Measure snow depth and note it.
7. Note the exact position of the measurement point on the detailed map.
8. Make sure the readings seem reasonable and check weight for snow.

6.2 Results

During the period from Jan 2000 to May 2003 a total of 20 snow surveys were carried out. The winters of 2000/2001 and 2002/2003 had relatively little snow so the numbers of days with snow surveys were limited. After all

the snow surveys were carried out, the SWE point samples were grouped into four categories depending on which LCT they were sampled from.

Table 6.2 presents mean aerial SWE within the four LCTs (road, roof, deposit and park) for all the days when a snow survey was carried out. The left most numbers in parenthesis is average scaled variability (standard deviation (SD) divided by the square root of the number of samples (n)) divided by the average SWE and multiplied by a hundred (Eq. 6.1). This will be referred to as ERR throughout the rest of this thesis. The right most number in parenthesis (Tab. 6.2) is the number of samples taken in the LCT.

$$ERR = \frac{SD \;\; 100}{\sqrt{n} \;\; \overline{SWE}} \tag{6.1}$$

From table 6.2 it can be seen that SWE data were sampled from all the 9 snow courses (Fig. 6.1) only on 7 days (21 Feb 02 - 27 Mar 02). On the other days SWE was sampled only in the basic courses (course 1 - 3 in Fig. 6.1). In the basic courses only one point out of the 30 could be classified as being in the LCT road. Three points were classified into LCT deposit. When the additional courses were included in the snow survey, a total of about 120 samples were taken. Sampling on roofs was limited to 5 samples since it was difficult to access them, and a permit from the building owner had to be obtained.

From Table 6.2 it can be seen that ERR in LCT deposit was large when the number of samples were only three. The ERR values were in the range of 17 to 75 %. When the number of samples were increased to around 30, the ERR was reduced to below 10 %. This indicates that taking only three samples in LCT deposit, as was done in the basic courses, will give large uncertainty in the estimates of mean SWE. For LCT park it can be seen from table 6.2 that the ERR was not noticeably reduced when the number of samples were increased from 26 to about 65. This indicates that it may be sufficient to take about 26 samples, or less, within the LCT park. It can also be seen that the ERR within LCT park was about 3 % lower, compared to the ERR in LCT deposit, for days when all the nine snow courses were sampled. One explanation to this can be that the AA has stronger influence in LCT deposit than in LCT park. Road clearing of snow will give larger variability in SWE within LCT deposit. The ERR within LCT road is somewhat larger than in LCT park. This can also be explained by the differences in influence of AA within the various LCTs.

Table 6.2: Average SWE (mm) within four LCTs in Risvollan. Average scaled standard error (%) and number of samples in parenthesis.

Date	Roof	Road	Deposit	Park
07Feb00	- (- 0)	10 (- 1)	102 (64 3)	49 (9 26)
15Feb00	- (- 0)	15 (- 1)	143 (55 3)	54 (8 26)
22Feb00	- (- 0)	30 (- 1)	111 (26 3)	99 (6 26)
29Feb00	- (- 0)	30 (- 1)	127 (52 3)	91 (8 26)
07Mar00	- (- 0)	40 (- 1)	175 (17 3)	133 (5 26)
14Mar00	- (- 0)	60 (- 1)	213 (31 3)	155 (4 26)
21Mar00	- (- 0)	40 (- 1)	182 (22 3)	143 (5 26)
28Mar00	- (- 0)	0 (- 1)	202 (22 3)	166 (5 26)
26Feb01	- (- 0)	15 (- 1)	86 (70 3)	30 (6 26)
22Mar01	- (- 0)	10 (- 1)	66 (38 3)	45 (5 26)
04Jan02	- (- 0)	2 (- 1)	97 (56 3)	37 (2 26)
10Jan02	- (- 0)	0 (- 1)	85 (75 3)	20 (9 26)
21Feb02	28 (12 3)	23 (14 25)	58 (10 33)	34 (3 68)
25Feb02	40 (11 6)	36 (14 26)	118 (7 34)	75 (4 66)
01Mar02	43 (13 5)	8 (39 24)	140 (8 26)	77 (6 66)
06Mar02	74 (11 5)	15 (12 25)	225 (6 30)	117 (3 65)
13Mar02	80 (8 5)	9 (24 21)	255 (7 31)	142 (4 65)
19Mar02	79 (8 5)	9 (26 22)	266 (6 29)	167 (3 63)
27Mar02	59 (10 5)	0 (0 23)	220 (9 24)	134 (4 27)
09Jan03	- (- 0)	49 (- 1)	130 (66 3)	54 (6 26)

From Table 6.2 it can also be seen that the ERR values in general are larger within the LCT road, roof and deposit, which implies that the variability of urban snow packs are enhanced by AA.

Figure 6.2 presents estimates of average SWE within four LCTs for February and March 2002. It can be seen that LCT road in general had lower SWE than the three other LCTs. LCT deposit had the largest SWE amongst all the LCTs. The reason for the differences in SWE for the four LCTs can be explained by the differences in accumulation, available energy for melt and the degree of influence from AA. Figure 6.2 shows that the differences in average SWE was minor in the beginning of the accumulation

season (Feb 2002) but increased during the season as spatial variability in energy and AA influenced snow melt and distribution. LCT road had the largest SWE at the beginning of the accumulation season, this was before the roads were cleared for snow or melt had not removed the ice layer on the roads.

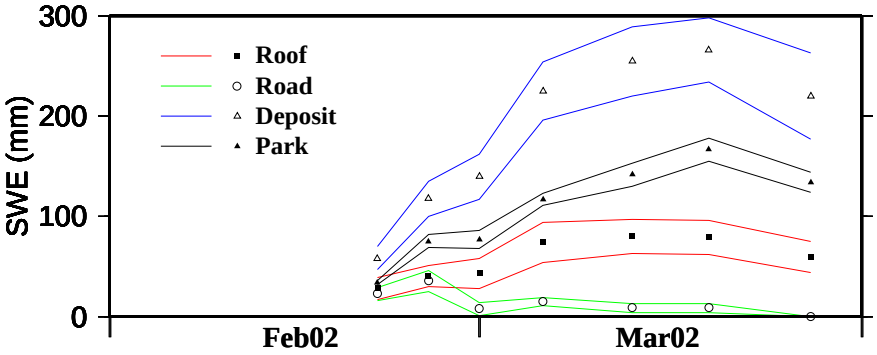

Fig. 6.2: Timeseries of SWE Feb and Mar 2002

If it is assumed that the SWE data are randomly selected and Gaussian distributed (unknown variance), the uncertainty in the mean aerial SWE can be estimated from Table 6.2, using a student t-distribution (Pomeroy & Gray 1995, Walpole et al. 1998). In Figure 6.2 the upper and lower limits of the 95 % confidence intervals for the average observed SWE for Feb and Mar 2002, are shown as solid lines. The two blue lines are the lower and upper confidence limits for LCT deposit, respectively. It can be seen that it is only in the first two samples that the confidence limits between the four LCTs overlap. In whole March 2002 none of the confidence intervals overlap which is a strong indication that the average SWE within the four LCTs were not the same. The reason for this can be explained by the degree of influence from AA in the various LCTs. Roads are cleared for snow and therefore have less SWE compared to the other LCTs. The albedo is also low resulting in more rapid melt caused by the increased energy received by solar radiation. The roofs have lower SWE due to snow drift and increased melt energy from the underlying roof, etc, as explained in chapter 2. Deposit areas receive snow from nearby road areas and therefore have a higher SWE. It can be seen from Figure 6.2 that it is within LCT deposit that the confidence limits have the largest range. The unevenly

distributed snow pack, caused by redistribution of snow, in addition to that the average SWE is largest in this LCT can be explanations for this. The average confidence limits for the roof, road, deposit, and park data shown in Figure 6.2, was +/- 28 %, 38 %, 16 %, and 8 % of the average SWE, on each sample day, respectively. This expresses a general uncertainty within the estimates of average SWE for each LCT.

In chapter 3, the LCT wall was defined as the areas lying within 2 metre of a building and that is not part of LCT roof, road or deposit areas. In Risvollan the pervious surface areas have been estimated to 74 %. Some of this area is used to pile snow in winter time and can be classified as LCT deposit. If LCT deposit and LCT wall is subtracted from the pervious surface area, LCT park covers only 64 % of the total catchment area. The urbanized part of Risvollan can then be calculated to 36 % and includes the LCTs roof (13 %), road (13 %), deposit (5 %), and wall (5 %). Chapter 7 present more on this. Based on this an area scaled mean of SWE can be calculated for the urbanized (LCT wall, deposit, road, roof) and rural (LCT park) areas, by letting LCT wall have the same SWE value as LCT park. On 13th March 2002, the mean SWE of the urbanized and rural parts of Risvollan were 91 and 142 mm, respectively, assuming that the SWE within the LCT wall was the same as in LCT park. For 27th March 2002 these values were 74 and 134 mm. So for the 13th and 27th of March 2002 the mean SWE within LCT road, roof, wall and deposit, was 36 % and 45 % lower than in LCT park. From this it can be concluded that AA in Risvollan, lowers the mid and end of winter mean SWE compared to if Risvollan had been covered with only untouched (park) areas. McMurter (1976) found similar patterns, showing that the end of winter mean SWE within the urban parts of a small catchment in Canada was substantially lower than in the rural/untouched parts. The results found in this chapter corresponds with the results reported by McMurter (1976).

Figure 6.3 presents a frequency plot of the SWE data sampled in LCT park (a), roof, road, deposit (b), and all four LCTs (c), for 25th February 2002. The bin width of the plot is 10 mm of SWE. It can be seen that the frequency of SWE samples lower than 20 mm and above 120 mm is larger in Figure 6.3 (b) compared to in (a). The most probable reason for this can be attributed to snow clearing procedures of roads. This will lower SWE on roads and increase SWE in piles. The same trends can be seen in Figure 6.3 (d), (e) and (f), where an even larger portion of the

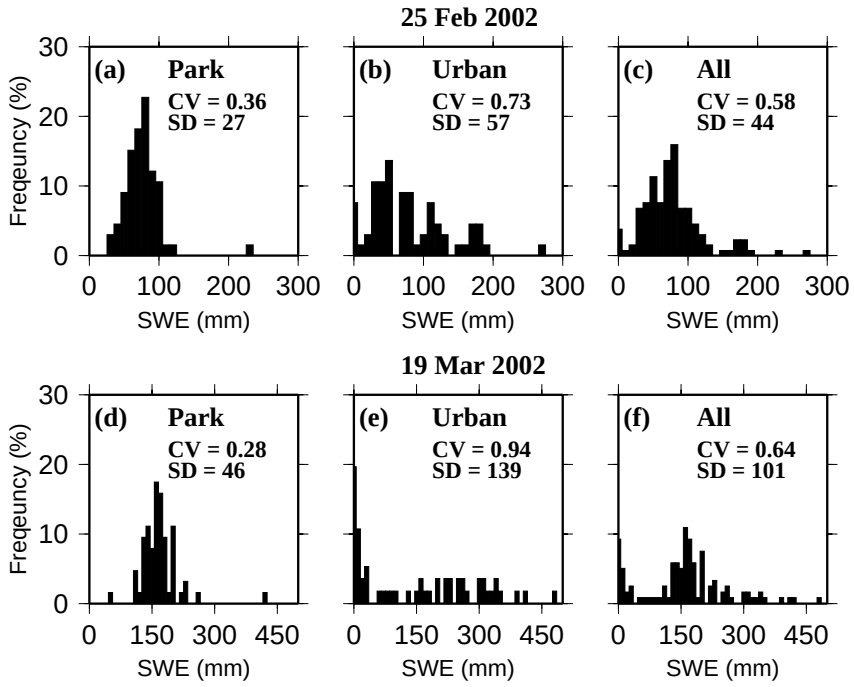

Fig. 6.3: Frequency distribution of SWE data from 25 Feb and 19 Mar 2002

samples are below 40 mm of SWE in the urban (LCT road, roof, deposit) compared to in LCT park. Strong melt rates on roofs in addition to lower accumulated SWE, due to snow drift, may be additional explanations for the differences seen in the snow distributions. In Figure 6.3 (c) and (f) the SWE distribution seems to be double peaked, with one peak around zero and one peak around 80 mm and 160 mm respectively. Compared to the snow distribution in LCT park which has only one peak, it seems like the AA causes a shift from one peaked to a two peaked distribution. Marchand & Killingtveit (2003) studied statistical properties of spatial snow cover in mountainous catchments in Norway. For some of the catchments a double peaked snow distribution, similar to what is seen in Figure 6.3 (c) and (f), was reported. Marchand & Killingtveit (2003) fitted several statistical distributions to the snow cover data and found that a mix of two log-normal distributions could be fitted to a double peaked snow distribution. Such a distribution could maybe also have been fitted to the data presented in

Figure 6.3 (c) and (f). Due to time constraints in this thesis work it was decided not to pursue this any further.

Figure 6.3 also presents the standard deviation (SD) and coefficient of variation (CV, SD divided by the mean) for the SWE samples. It can be seen that the variability in the SWE data sampled in LCT roof, road and deposits are larger than in LCT park. This was also seen in Table 6.2 where the ERR values was largest in these LCTs. From this it can be concluded that AA, (snow clearing, etc) increases the natural variability of urban snow packs.

6.3 Discussion

The confidence intervals drawn in the previous section is highly dependent on the variability of the SWE data sampled. The variability can be explained by several factors. First of all the weight and snow depth reading of the snow might not be correct. There might be ice on the ground which the snow tube will not penetrate. For these situations the observer has to estimate the thickness of the ice and try to estimate the SWE of the ice as correctly as possible. In wet snow there can be a slush layer near the ground that will be lost from the snow tube during measurements, of which the observer must manually account for. In snow deposits sand and gravel in the snow can make the observed SWE values larger than they should be. This causes the SWE in each measurement point to have an uncertainty which increases variability. During snow surveys all the samples are not taken at the same time. Depending upon the number of samples the survey can take many hours. If there is strong snowmelt on the survey day, the snow pack will change during the measurements and influence the variability. This effect may be important when doing measurements in shallow snow packs, say below 40 cm of depth.

In highly heterogeneous and exposed areas, differences in surface cover and terrain features may produce wide variations in accumulation patterns due to effects of surface roughness on air flow patterns and snow transport. As the winter proceeds into spring, spatial variability in available melt-energy results in further variability in the snow pack, e.g. south facing slopes have higher melt rates since they receive more solar radiation, etc. In urban areas both the snow accumulation pattern and the energy balance

is altered by AA. The influence of AA differs with location and region, and enhances the natural variability in the snow pack. Since AA is a dominant process in the urban environment its effect on the mean and variability of the SWE can therefore not be regarded as measurement error or bias in the data.

To avoid bias and increase how representative the SWE data are to the whole catchment, randomly selected measurement points can be used. From a practical point of view, this might create several difficulties. Roofs can be dangerous to access and a permit from the building owners must be obtained. This can easily exclude measurement points located on roofs, even they are randomly selected. Roads are trafficated and cars are parked and removed constantly. On the survey days a car might have parked in the points selected for sampling, thus, random selection of the location of the sample can be hard to carry out in these LCTs. In piles there can be several thick ice layers in the snow and it can be impossible to penetrate a tube into the snow. When such situation occurs, the observer has no choice but to move to another nearby location. From this it can be argued that random selection of where to carry out measurements of SWE is difficult in urban environments.

To run a T-test on the mean of the samples, assumptions of normality and randomized samples have to be made. The snow data presented in Table 6.2 does not necessary meet these requirements. First of all the locations of the snow courses were not chosen by random. The reasons for this were discussed earlier. Figure 6.4 shows a Gaussian probability plot of the SWE data sampled at 25ft of Feb 2002. None of the data perfectly fits a straight line and the assumption of Gaussian distributed data is weak. It can also be seen from figure 6.4 that the variance or skewness from the Gaussian distribution is larger for the LCTs deposit, road and roof compared to the park LCT. This can be explained by the difference in influence from AA which is lowest in the LCT park. It also seems like it is the SWE samples in LCT deposit that has the strongest deviation from the Gaussian distribution. This might be the result of the relocation of snow via snow clearing. The confidence intervals estimated earlier might not be correct since the data are only weakly Gaussian distributed and random sampling was not carried out.

Uncertainty in the estimates of average SWE is dependent on the factors mentioned previously, but there will also be an extra uncertainty com-

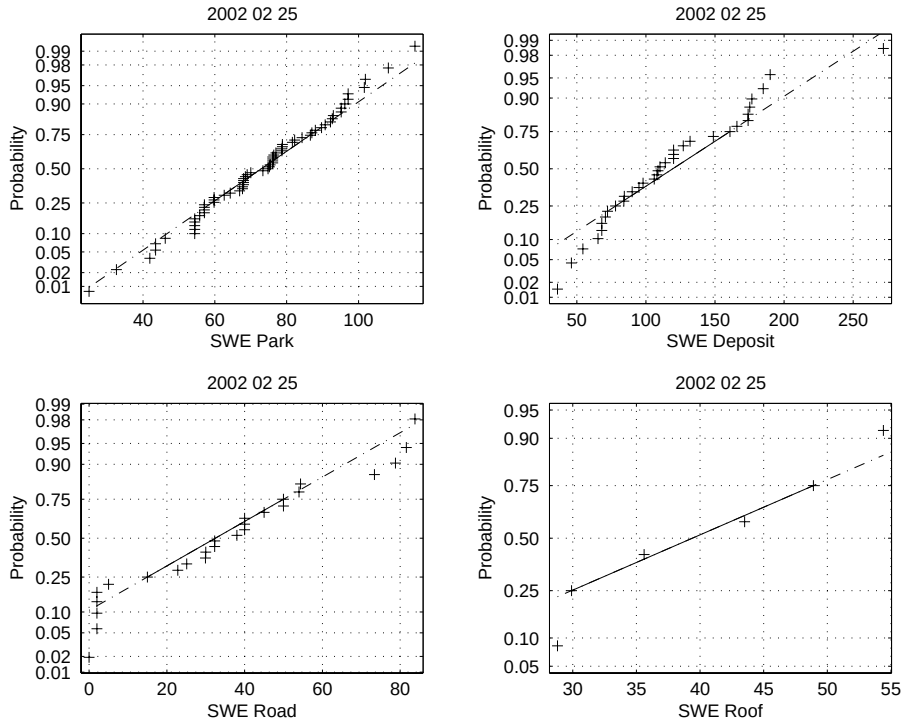

Fig. 6.4: Gaussplot of SWE data (25 Feb 2002)

ponent added from how representative the snow courses are for the snow distribution of the whole catchment or LCT. The snow courses were not selected randomly which can give basis for an over sampling of SWE data in for example North facing slopes in the LCT park. This will bias the estimates of mean SWE. It has not been done any attempts to estimate how much uncertainty this introduces in the SWE data.

Despite the discussion on uncertainty in the data, it is believed that the objectives of the SWE snow surveys were achieved. It was shown that there exist large differences in mean SWE between the four LCTs investigated (road, roof, deposits, park), which can be explained by the degree of which they are influenced by AA. The obtained SWE data can be used for calibration and validation of an urban hydrological model.

6.4 Conclusions

Observations of SWE were carried out in 9 different snow courses in the Risvollan catchment in Trondheim, Norway, from 2000 to 2003. The data were grouped into four different LCTs, road, roof, deposit and park. It was shown that the SWE within the LCT deposit had the highest values of SWE. Despite this, the areal mean SWE within the urbanized parts of Risvollan was 36 % and 45 % lower than in the LCT park at mid and end of the 2001/2002 winter season. From this it can be concluded that AA lowers the mean SWE more rapidly in the Risvollan catchment compared to if it had been covered with only park areas. Snow clearing of snow from roads and walkways, snowdrift from rooftops, in addition to high melt rates on roofs, roads and in deposit LCTs, are the plausible reasons for this. It was also shown that the variability of urban snow packs is enhanced and modified by AA. Based on the results presented in this chapter, and in chapter 5, objective number 3 set in chapter 1 can be said to have been accomplished. Effects of AA on SWE in an urban catchment have been documented and the observed SWE data can be used for calibration and validation of an urban hydrological model.

Chapter 7

Point and catchment scale testing of GUHM

In this chapter the calibration and results of testing the GUHM snow routine against data from the snow lysimeter at Risvollan are presented. Results from the application of the GUHM to the Risvollan catchment are also documented together with a discussion of the results.

7.1 Point testing of GUHM snow routine

The snow routine in the GUHM was tested against data from the snowmelt lysimeter (point measurements) at the Risvollan station. During the winters of 1994/1995 samples of SWE were carefully taken on the snow melt lysimeter by the operators at Risvollan station. Snow melt outflow from the snow pack was also recorded. This made it possible to calibrate the snow routine in the GUHM for this winter season, and quantify its performance against observations of snowmelt intensity and SWE. With this, the snow routine in the GUHM could be tested for a point, independently of the soil-runoff routine.

The snow routine in the GUHM is driven by precipitation, shortwave radiation, wind speed, relative humidity and air temperature. Input data sets for these parameters for the winter season 1994/1995 were prepared with a temporal resolution of 1 hour. During calibration the following parameters can be tuned; snow surface roughness (z_0), threshold temperatures separating snow and rain (T_{max},T_{min}), maximum free water holding capacity

of the snow ($W_{liq,max}$), coefficient of linear reservoir simulating percolation of melt water trough the snow (K_{snow}) and gauge catch correction factor for snow and rain (PC_{snow},PC_{rain}). Since the snow pack on the lysimeter at Risvollan is relatively undisturbed by human activity a decay function giving high albedo values was chosen, but it was decided not to calibrate on this. The parameters $a_1 = 0.92$, $a_2 = 0.85$, $a_3 = 0.46$, results in a snow albedo of 0.66 for a period of 10 days without snow. During the calibration only three parameters were tuned. These were z_0, $W_{liq,max}$, and T_{max}. To limit the number of calibration parameters, T_{min} was set equal to T_{max}, in all simulations.

Calibration was carried out in the following way. At first the range of each parameter was defined by a lower and upper boundary (Eq. 7.1). It was then decided to split the range, of each parameter, into 21 values starting from the lower boundary and proceeding up the upper boundary. This gave a total of $21^3 = 9261$ discrete points in the parameters space. The snow routine was then run for all possible combinations. The correlation coefficient R^2 was used as an objective function for each model run. Since snow melt is only released during melt periods R^2 was calculated only for the main melt period. In the season 1994/1995 this period was from 10 April to 8 May. During the 1994/1995 winter season the operator at Risvollan station took 15 samples of SWE on the snow melt lysimeter. These were assumed to be representative measurements of the SWE on the snow lysimeter at Risvollan. For all simulations the R^2 value was calculated from simulated and observed snow melt (R^2_{melt}) and from simulated and observed SWE (R^2_{swe}). The simulation was run from 1 Oct 1994 to 31 May 1995 with a temporal resolution of 1 hour. No updating of the SWE states in the GUHM was carried out during the simulation period.

$$\begin{aligned} 0.0001 &\leq z_0 &&\leq 0.02 \\ 0.01 &\leq W_{liq,max} &&\leq 0.04 \\ 0.0 &\leq T_{max} &&\leq 2.0 \end{aligned} \tag{7.1}$$

7.1.1 Results point simulations of SWE and snowmelt

Table 7.1 shows the best parameter set optimized for both SWE and snowmelt. Out of 9261 points in the parameter space, only 9 % had a R^2_{melt} value of

0.65 or better. For R^2_{swe} this value was 96 %. This indicates that calibrating on SWE does not give any guarantees that snow melt intensity is simulated correctly. It also implies that there exists a parameter space, where the GUHM snow routine performs satisfactory for multiple parameter combinations. Since only 9 % of the parameter space gave good results for R^2_{melt} it can be argued that the robustness of the snow routine is low, and the performance of the GUHM snow routine is dependent on calibration.

Table 7.1: Calibrated snow parameters for point simulation

Param	**Value**	**Unit**	**Param**	**Value**	**Unit**
PC_{rain}	1	-	$SWE_{liq,max}$	0.0145	(fraction)
PC_{snow}	1.1	-	K_{snow}	0.3	-
T_{min}	0.3	C	a_1	0.92	-
T_{max}	0.3	C	a_2	0.85	-
z_0	0.0001	m	a_3	0.46	-

Figure 7.1 (a) shows simulated and observed SWE from Oct 1994 to May 1995. The simulation was run with the parameters shown in Table 7.1. The R^2_{swe} value calculated for the 15 points of simulated and observed SWE showed a value of 0.97. Figure 7.1 (b) shows simulated and observed snow melt from 10 Apr 1995 to 8 May 1995. The parameter set produced a R^2_{melt} of 0.78, which is relatively good. Sand (1990) also simulated snow melt runoff from several snow lysimeters in Norway, using various degree-day and energy balance models. The results from the simulations using an energy balance agrees to a certain extent with the results found in this section, although Sand (1990) did not run whole seasons. Only shorter periods in the spring were simulated.

From Figure 7.1 it can be seen that some of the simulated snow melt peaks are little lower than the observed. This may be a result of the relatively small value of snow surface roughness set to 0.0001, which make the energy contribution from turbulent heat to be low. The results shown in Figure 7.1 (a) and (b) imply that both SWE and snow melt intensity can be simulated for whole seasons with short time resolution (1 hour). No updating of the SWE during the winter season in the model is necessary if the input data and model structure is of sufficient quality. This was also

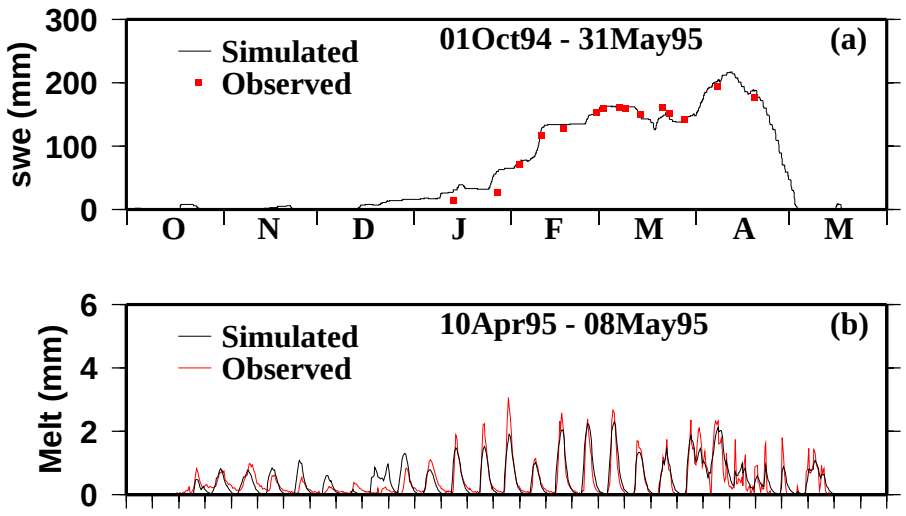

Fig. 7.1: Simulated and observed SWE and snowmelt intensity for lysimeter at Risvollan station

shown by Storck (2000).

Figure 7.2 (a) shows simulated snow temperature (T_s) and observed air temperature (T_a) for March and April 1995. When T_a is below freezing, T_s follows T_a with a lag. This lag is caused by the cold content in the snow. It can also be seen that T_s is never above zero degrees, which is an indication that the GUHM snow routine is working properly. Net long and short wave radiation are presented in Figure 7.2 (b). For most of the time the net short wave radiation is positive and net long wave radiation is negative. The reason for net long wave radiation being mostly negative has to do with differences in emissivity between the atmosphere and the snow surface. In Figure 7.2 (c) wind speed and relative humidity are shown, and in Figure 7.2 (d) latent and sensible heat fluxes are shown. When the wind speed is below 2 m/s the turbulent heat fluxes are almost zero. As soon as the wind speed approaches 2 m/s or above, the turbulent heat fluxes have a stronger influence on the snow packs energy balance, but even at wind speeds above 2 m/s latent and sensible heat are small compared to the energy contributed from solar radiation. In December to February the solar angle is relatively low at latitudes around 60 degrees. During these

periods there is a chance that it is the turbulent heat fluxes that dominates the snow packs energy balance, especially in periods with rainfall and high wind speed. During night conditions the long wave radiation may also play an important role, changing the cold content of the snow pack. Later in

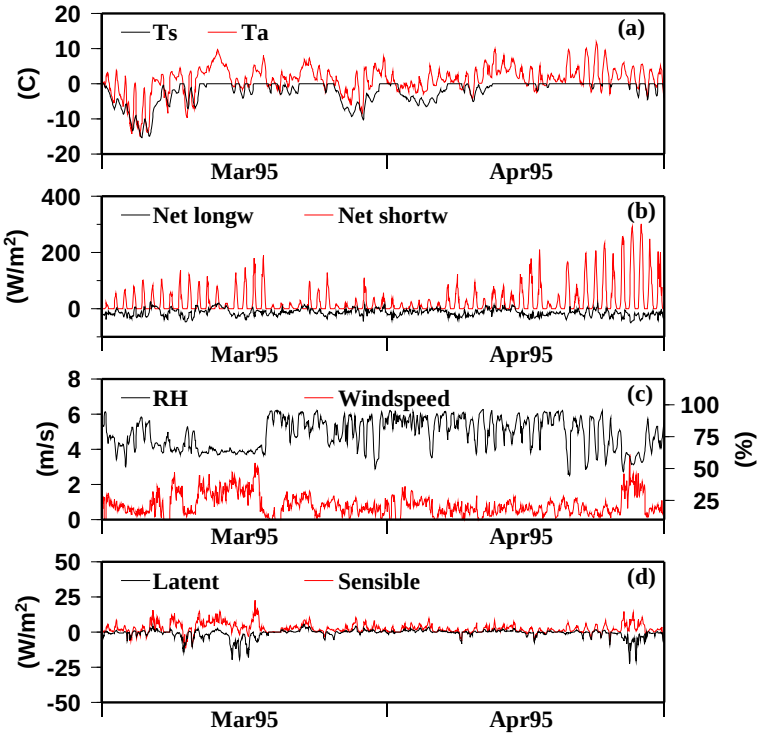

Fig. 7.2: Energy fluxes and meteorological data from March to April 1995

the spring when the sun angle in general is higher, solar radiation tend to dominate the available energy for melt. This can be seen in Figure 7.2, where the short wave radiation fluxes are large in April month. The energy fluxes shown in Figure 7.2 seems reasonable, which is a good indication that the GUHM snow routine is doing what was intended, namely, simulating snow accumulation and melt with an energy balance approach.

7.2 Application of GUHM to the Risvollan catchment

This section presents results from the application of the GUHM to the Risvollan catchment in Trondheim. All necessary input grids were prepared in a GIS using digital maps and a DEM, together with the pre-processing software described in earlier sections. The municipality of Trondheim provided the necessary geographical raw data. Model time step length was set to 1 hour for all simulations based on the recommendations given by Matheussen & Thorolfsson (1999) and Bengtsson & Singh (2000). No pipe flow simulations were done. The reason for this was that the time of concentration for the Risvollan catchment is around 20 minutes (Brandt & Torgersen 1994). The pipes are relatively steep and the transport time in the pipe network from the top to the outlet is around 5 to 10 minutes. The simulation time step in this research was set to 1 hour, which is much larger than the time of concentration and it was assumed that the simulated runoff would not be significantly influenced by use of pipe flow routing. The grid cell size was set to 2x2 metre to account for the large spatial variation in LCTs. The Risvollan catchment contained 49140 grid cells in the GUHM. Table 7.2 shows the number of cells and the areal coverage of each LCT. The dominating LCT is park with a total coverage of 64 % in the Risvollan catchment.

Table 7.2: Number of grid cells within each LCT and areal coverage (%)

LCT	**Grid cells**	**Area coverage (%)**
Road	6154	13
Deposit	2631	5
Wall	2656	5
Park	31339	64
Roof	6360	13
Sum	49140	100

Two time series of meteorological data, with 1 hour temporal resolution, were prepared, one calibration period (June1999 - June2002), and one validation dataset (June1998 - May1999 and July 2002 - June 2003). The

Table 7.3: Parameters in the albedo decay curves

Albedo parameters	**Urban**	**Rural**
a_1	0.85	0.92
a_2	0.75	0.85
a_3	0.50	0.46

Risvollan station is located in a depression at the downstream end of the catchment. Since the station was established in 1986, there has been severe vegetation growth around the station. Because of this it was decided to use wind speed and solar radiation data from Voll meteorological station instead of from the Risvollan station. It was assumed that these data better represented the average conditions in the Risvollan catchment. Wind speed and radiation data from Voll were not available for the period from Jun 1998 to Jan 1999, data from Risvollan was used instead for this period. The wind speed data from Voll were in average 2.4 m/s higher than at Risvollan. For the periods where wind speed data from Voll were missing, data from Risvollan corrected with 2.4 m/s was used as a substitute. The DEM in Figure 4.3 was generated in the following way. The municipality in Trondheim use a GIS to handle most of their maps of roads, buildings, sewer system, etc. The data are in the Norwegian SOSI format, which is a standard for description of digital geographical information, e.g. centre line of roads, elevation of roofs, terrain, etc, with x,y and z coordinates. All the data are in vector or point format. At first the data describing elevations of buildings, electricity masts, and other above ground objects, were filtered out. The remaining data then had only elevations of terrain, roads and parking spaces, i.e. ground elevations. The vector files were then converted into a grid with 0.5 metres in a GIS. This generated a grid with elevations only in some of the cells. An inverse square distance from the closest cells in North, South, East and West directions was used to interpolate in the blank cells. This resulted in DEM-terrain with a spatial resolution of 0.5 meters. The same method was used to generate a DEM using only data from the elevation of the buildings (DEM-buildings). Both DEM-terrain and DEM-buildings were resampled to a spatial resolution of 2 meters before the DEM-tb, shown in Figure 4.3 was generated as described earlier.

Calibration of the GUHM model was done in a two step procedure. First the snow routine was calibrated for the period June1999 - June2002, by comparing simulated and observed SCA and SWE. This was done by manually changing $W_{liq,max}$, T_{max}, T_{min}, PC_{snow} and PC_{rain}, which are global parameters affecting all grid cells. In GUHM, the snow surface roughness (z_0) is specified for each LCT, i.e. LCT park can have a different snow surface roughness than LCT road. For each LCT, the snow surface roughness was altered during calibration. Two albedo decay curves (urban and rural) were specified for the simulations. The parameters a_1, a_2 and a_3 are shown in Table 7.3. For LCT road and deposit the urban albedo curve was used. This curve drops the albedo to 0.5 within three days after a snowfall. LCT wall, roof and park used the urban albedo decay curve when liquid water was present in the snow and the rural in all other situations. After calibration of the snow routine the soil parameters were adjusted within reasonable values until simulated runoff satisfactorily matched the observed runoff. Because of the GUHMs relatively complex model structure and the fine spatial resolution that was used for Risvollan, the model computation time was long, which again limited the number of calibration runs that could be performed.

7.2.1 Results from application of GUHM to the Risvollan catchment

Table 7.4 presents the calibrated parameters in the snow routine of the GUHM. It can be seen that the snow surface roughness in LCT road and roof $Roadz_0$, $Roofz_0$ are relatively large (0.01 m). The snow surface roughness is a parameter that controls the turbulent heat fluxes, but can also be viewed as a parameter that takes on uncertainty in the other parameters as well as uncertainty in both model structure and input data. Storck (2000) used values of 0.007 and 0.2 metre for a shelter wood and beneath canopy, respectively. In LCT road, the influence from AA is strong. Snow is relocated to nearby areas after heavy snowfall, cars drive on the snow and anti-slippery or de-icing chemicals will lower albedo and increase melt, which can explain the relatively high z_0 value for LCT road. The modified heat flux Q_g for LCT roof (Q_{q-roof}) and wall (Q_{q-wall}) were calibrated to 35 and 15 W/m^2, respectively. Semádeni-Davies & Bengtsson (1998) estimated enhanced long wave radiation 4 m from a wall to be 9, 14 and

31 W/m^2 for wall temperatures of 3, 7 and 20 C, assuming an atmospheric emmisvity of 0.84 and ambient air temperature at 0 C. The Q_{g-wall} was set to 15 W/m^2 which somewhat corresponds with these values.

Table 7.4: Calibrated snow parameters

Param	**Value**	**Unit**	**Param**	**Value**	**Unit**
PC_{rain}	1	-	$Depositz_0$	0.007	m
PC_{snow}	1.04	-	$Parkz_0$	0.0012	m
T_{min}	1.52	C	SWE_{max}	12	mm
T_{max}	1.52	C	$SWE_{liq,max}$	0.025	(fraction)
$Roadz_0$	0.01	m	Q_{g-roof}	35	W/m^2
$Roofz_0$	0.01	m	Q_{g-wall}	15	W/m^2
$Wallz_0$	0.003	m	K_{snow}	0.3	-

Table 7.5 contain the values of the calibrated soil parameters (see also Fig. 3.2). It can be seen that LCT road and roof have very thin soil layers at only 2 mm. This forces rapid runoff response when snowmelt or rainfall starts. LCT deposit, wall and park were given field capacities (FC) of 100 mm. Common values for these parameters are between 75 and 300 mm (Killingtveit & Sœltun 1995). From Table 7.5 it can be seen that LCT road and roof have KUZ0 values of 0.95. This value forces rapid response from the linear reservoirs. In urban areas where the surfaces are impervious this effect is important. LZL and k_{GWR} were set to 20 mm and 0.005 for LCT park. These parameters force water to leave the catchment as groundwater recharge, not entering the pipe network. The initial conditions of SM, upper and lower linear reservoirs (Fig. 3.2), are shown in Table 7.5 as Isoil, Iup and Ilow.

Snow simulation results

Figure 7.3 shows simulated and observed SCA for three LCTs from March to April 2001. These are data from the calibration period. Simulated SCA was calculated as the number of grid cells with SWE larger than zero divided by the number of grid cells in the LCT (Tab. 7.2). In general, it can be seen that the snow is completely melted in the LCT road and roof

Table 7.5: Calibrated soil-runoff parameters

LCT	**FC** (mm)	**Beta**	**LP** (mm)	**KUZ0** (mm)	**KUZ1** (mm)	**UZ1** (mm)
Road	2	2.0	1	0.95	1.0	5
Deposit	100	0.5	40	0.50	0.2	15
Wall	100	1.0	40	0.15	0.2	15
Park	100	0.5	40	0.10	0.2	15
Roof	2	2.0	1	0.95	1.0	5
	UZ2 (mm)	q_{perc} (mm)	**KLZ** (mm)	**Isoil** (mm)	**Iup** (mm)	**Ilow** (mm)
Road	20	0.1	0.002	5	1	1
Deposit	30	0.5	0.002	70	5	5
Wall	30	0.5	0.002	70	5	5
Park	30	0.7	0.002	70	5	5
Roof	20	0.1	0.002	5	1	1

around 12th March, while LCT park has full snow cover until beginning of April 2001. Strong influence of AA in LCT road and roof compared to in LCT park explains these differences.

In Figure 7.3 (a) and (b) the simulated SCA matches the trends of the observed SCA, with some discrepancies. On March 31 2001, the observed SCA data show full snow cover in both LCT road and roof. The GUHM shows no snow cover for this date. In the GUHM, precipitation is split into snow and rain using T_{max} and T_{min} and in this application they were both set to 1.52 C (Table 7.4). If the high SCA for this date was caused by a snowfall during the previous days, and the air temperature was above this threshold, then the GUHM will treat precipitation as rain and not snow. This can be one explanation for the differences in simulated and observed SCA. In Figure 7.6 (a) and (b) it can be seen that SWE at the end of March 2001 is zero. This means that the agreement between the simulated and observed SCA at these low SWE values is very dependent on T_{max} and T_{min}. Another reason for the differences between simulated and observed SCA can be errors in the input data. If precipitation is not registered in one time step there will be no snow in the model, but the observed SCA

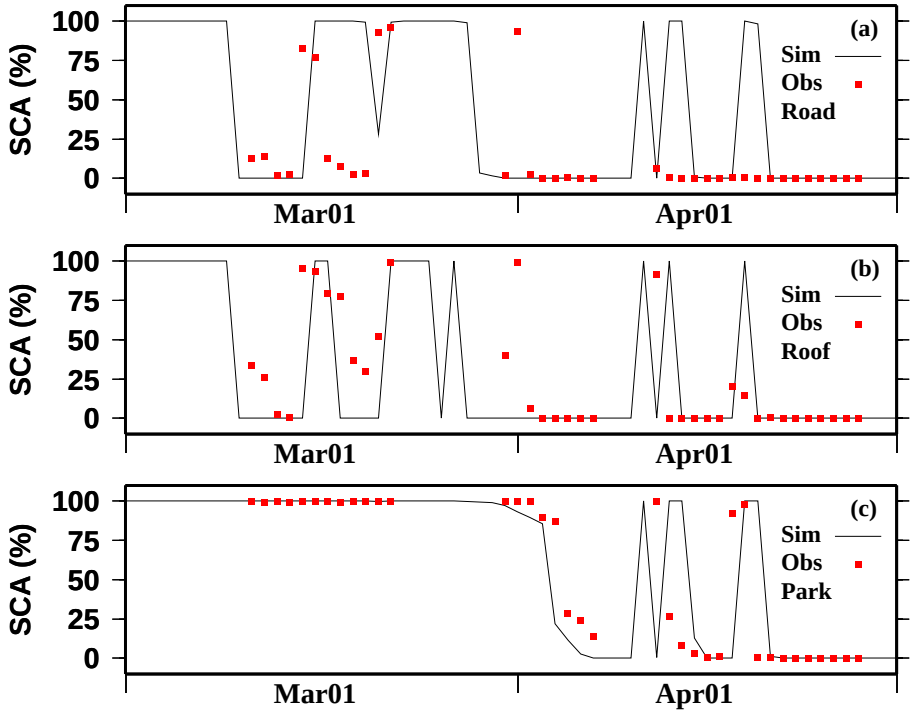

Fig. 7.3: Simulated and observed SCA spring 2001

will show snow cover. When there is almost zero SWE on the ground the models simulated SCA is extremely sensitive to such errors. Figure 7.3 (c) presents simulated and observed SCA for LCT park. There is a good match between the data, but in the beginning of April 2001 the simulated SCA has a more rapid decay than what was observed. Possible reasons for this will be explained later.

In Figure 7.4 simulated and observed SCA for the winter season 2001/ 2002 is presented. In general the simulated SCA from the GUHM seems to match the observed data fairly well. For both LCT road and roof, the observed data show that in Nov 2001 - Feb 2002 (Fig. 7.4 (a) and (b)) there are several mid-winter events, where all accumulated snow has melted. These trends are also simulated by the GUHM. At the end of March 2002 the observed data in LCT roof shows a more rapid decay than the simulated data. One reason for this can be that during the accumulation season snow

from roofs are wind transported to nearby areas, and will therefore become more rapidly snow free during melt situations. This effect is not modelled in the GUHM. Another explanation can be that the calibrated parameters $Roofz_0$ and Q_{g-roof} are set too low in the simulations. It should also be noted that the observed data are recorded for only a limited number of roofs in the Risvollan catchment and might not represent the catchment average. In LCT road, the observed data shows a slow decay in SCA at the end of March and beginning of April 2002 (Fig. 7.4 (a)). The results from

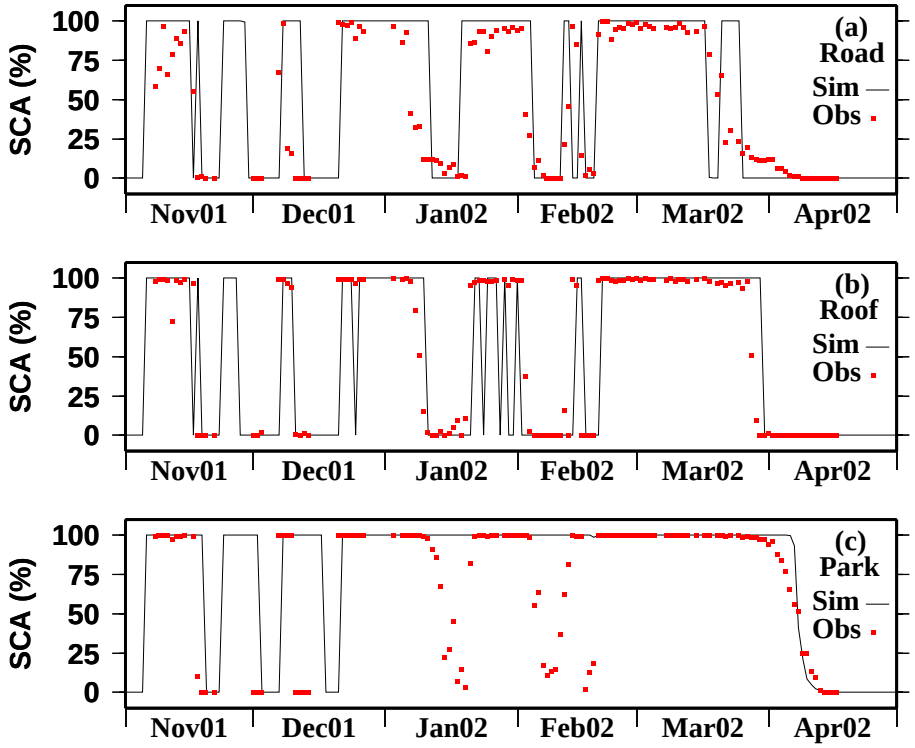

Fig. 7.4: Simulated and observed SCA 2001 2002

the GUHM have a more rapid decay, and all the snow is melted by the end of March 2002. One reason for this can be that some parts of the deposit areas, located next to roads, have been included in the LCT road when the observed data were analysed from the digital images in chapter 5. This noise is not present in the GUHM since there is a distinct difference between

snow in LCT road and deposit in the model. For LCT park there were two melt periods in Jan and Feb 2002, where the observed data show almost zero SCA (Fig. 7.4 (c)). This is not shown in the simulated results from the GUHM. There are several explanations for this difference in SCA. First of all the GUHM simulates no spatial variability in snow accumulation as a function of terrain and wind speed. Since only data from one precipitation gage was used, there is no variability in the accumulated snow pack right after snow fall. Within the GUHM, the spatial variability in SWE in LCT park, is forced by the spatial variability in available energy for melt, mainly controlled by shadow effects, slope and aspect. If only a thin snow pack, say below 30 mm has accumulated and melt starts, there is little chance that spatial variability in SCA and SWE will be shown in the GUHM. In Figure 7.6 (c) the SWE is almost zero in mid-February2002. Since there are no grid cells with zero SWE the SCA shows 100 % snow cover. The error in the SWE calculations need only to be a few mm and the simulated and observed SCA will not match. The snow surface roughness was calibrated to 0.0012 m. in LCT park. This might be too low since two mid-winter melt periods were not simulated correctly. There is a chance that the simulation results would have been better if more calibrations were carried out, but given the time limits of this project, this was not done. The main melt period in April 2002 seems to be simulated almost correctly but with a little more rapid melt than in the observed data (Fig. 7.4 (c)).

Figure 7.5 presents the simulated and observed SCA for the 2002/2003 validation season. The SCA in both LCT roof and road (Fig. 7.5 (a) and (b)), follows the observed SCA fairly well. In LCT park there are more differences between observed and simulated SCA. The observed SCA data show a gradually decay in SCA through the spring of 2003. During the winter 2002/2003 the snow pack was relatively shallow. Only one SWE survey was carried out in the basic snow courses (Fig. 6.1 course 1-3). The SWE on 9th Jan 2003 was only 54 mm in the LCT park. The variability in the SWE is mainly caused by spatial variability in accumulation patterns and not as an effect of spatial variability in melt energy. This can be one explanation why the GUHM simulated SCA does not match the observed SCA for the spring of 2003.

Figure 7.6 shows average simulated and observed SWE within four of the LCTs in the GUHM. The simulated results show a good agreement with the observed data. In the GUHM, snow is transported from LCT road to

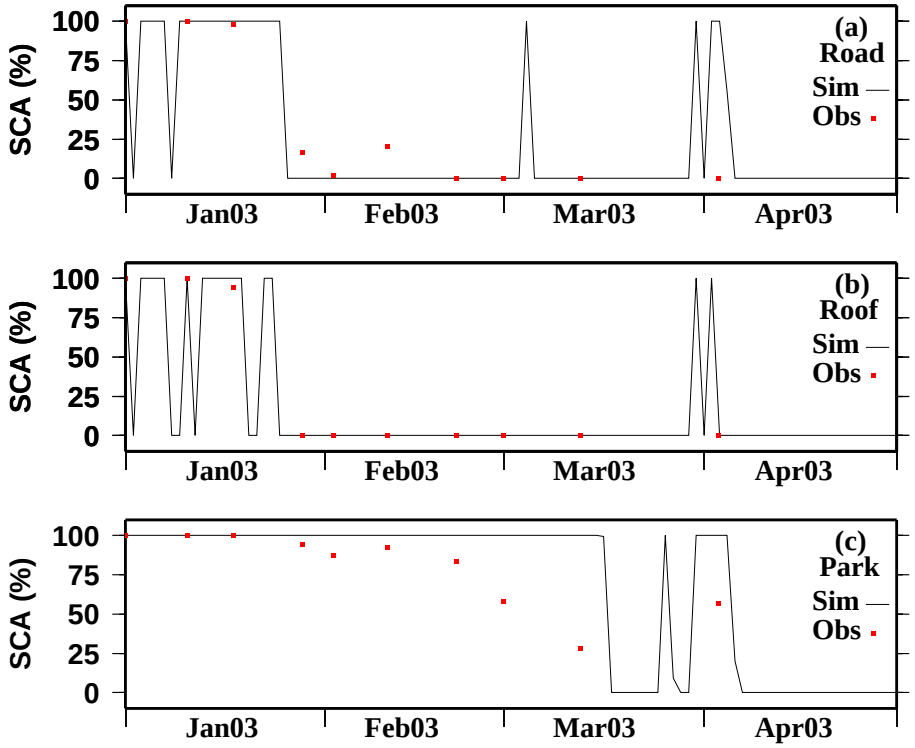

Fig. 7.5: Simulated and observed SCA spring 2003

LCT deposit when the SWE reaches a certain level. In this simulation the threshold (SWE_{max}) value was set to 12 mm. Figure 7.6 (a) shows SWE for LCT road and it can clearly be seen that the SWE has an upper limit of 12 mm. Figure 7.6 (d) shows SWE for LCT deposit. The maximum SWE for the winter season 2001/2002 is almost at 300 mm. This is a result of the relocation of SWE from LCT road to LCT deposit. SWE in LCT roof is shown in Figure 7.6 (b). The effect of high wind speed, strong turbulent heat exchange ($Roof z_0 = 0.01$), and increased heat from the underlying roof (Q_{g-roof}= 15 W/m^2), enhances the snow melt process and thus SWE is lower compared to SWE in LCT park. Figure 7.6 shows that the winter of 2000/2001 had relatively little snow fall compared to 1999/2000 and 2001/2002. The average simulated SWE in LCT park shows a strong correlation with the observed average SWE (Fig. 7.6 (c)). Figure

7.6 indicates that the snow routine in GUHM is able to simulate both the accumulation and melt season with satisfactory results.

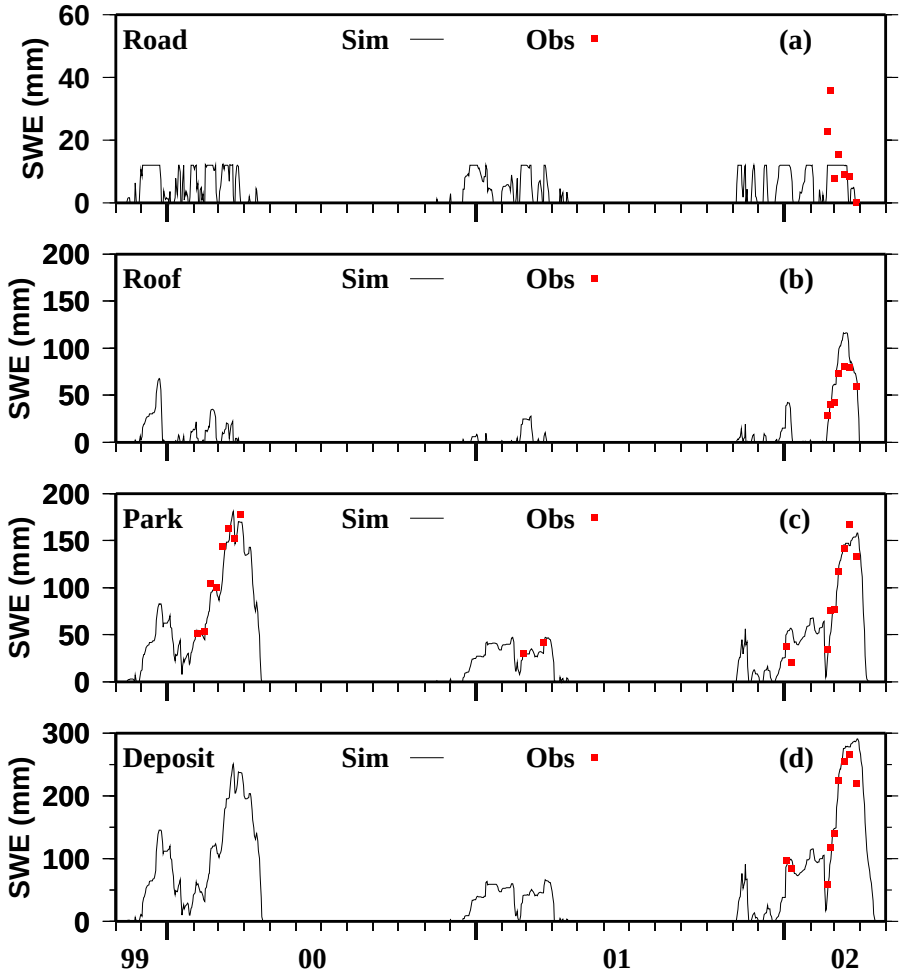

Fig. 7.6: Simulated and observed SWE from Nov 1999 to Apr 2002

Chapter 5 documented how a SCA map of the Risvollan catchment could be generated from aerial photos. Figure 7.7 (a) and (b) presents simulated and observed snow cover for 9th Jan 2002 (at noon), where (b) is generated from aerial photos and (a) is from the GUHM. At this date the roads and roofs are free for snow, which can be seen from both the simulation and the aerial photo generated snow cover map. In Figure 7.7 (a), the black colour indicates SWE lower than 2 mm. The average SWE in LCT park seems to be around 50 mm, on 9th Jan 2002. Figure 7.7 (b) shows close to full snow cover in LCT park on this date, and corresponds well with the simulated data. Both the simulated and observed snow cover data from 9th Jan 2002 illustrate the extreme influence AA has on the snow distribution. The snow is removed or melted in the LCT road and roof. By studying Figure 7.7 (a) carefully, some white pixels next to roads can be seen. This is deposit grid cells with SWE values above 60 mm caused by snow clearing of roads.

Figure 7.7 (c) and (d) shows simulated and observed snow cover on 11th Jan 2002. Both plots show similar patterns. LCT road and roof are snow free. In Figure 7.7 (d), the LCT park has partial snow cover, which is not reflected in the simulated snow cover (Figure 7.7 (c)). The reasons for this were discussed in previous sections. Early in the accumulation season the GUHM shows little variability in the snow pack in LCT park. It can only be seen in the melt periods when spatial variability in available energy for melt is triggered by solar radiation and causes non-uniformity in the snow pack.

Figure 7.8 (a) and (b) presents snow cover on 14th March 2002. Only the main road is free of snow. The small black dots in Figure 7.8 (b) are snow free areas on the roofs of the buildings, caused by heat from domestic ventilation systems. Even when the air temperature is well below freezing this heat melts the snow around the air outlets. The snow cover on the roads is almost at zero in Figure 7.8 (a) indicating that the trends in the SWE are correct in the GUHM. On 14th March 2002 it can be seen that the SWE on roofs is around 80-100 mm and around 150 mm in LCT park. Full snow cover in LCT roof and park is also seen in Figure 7.8 (b).

Figure 7.8 (c) and (d) shows snow cover at the end of the melt season (5th April 2002). At this point the spatial variability in the snow packs energy balance has clearly enhanced the spatial variability in the SWE. The green, orange and white areas in Figure 7.8 (c) are all north facing areas.

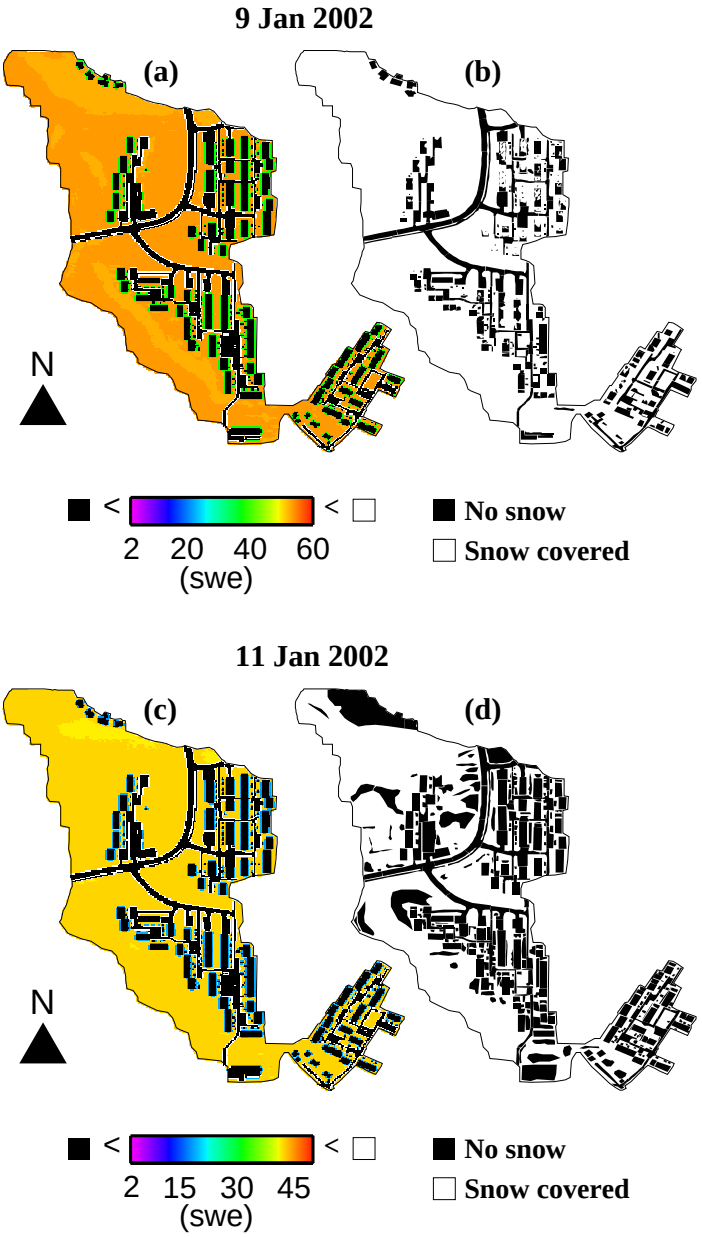

Fig. 7.7: Simulated (a,c) and observed (b,d) snow cover at 9th and 11th of Jan 2002. The observed data are estimated from aerial photos.

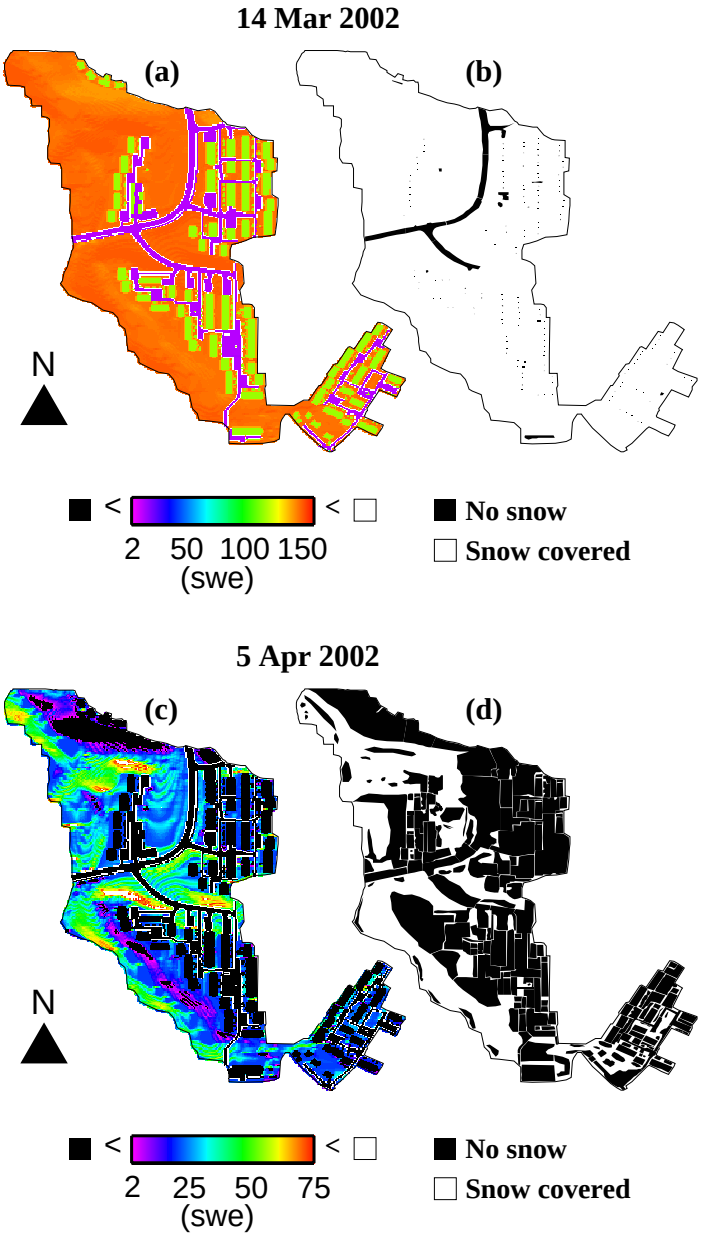

Fig. 7.8: Simulated (a,c) and observed (b,d) snow cover on 14th Mar and 5th Apr 2002. The observed data are estimated from aerial photos.

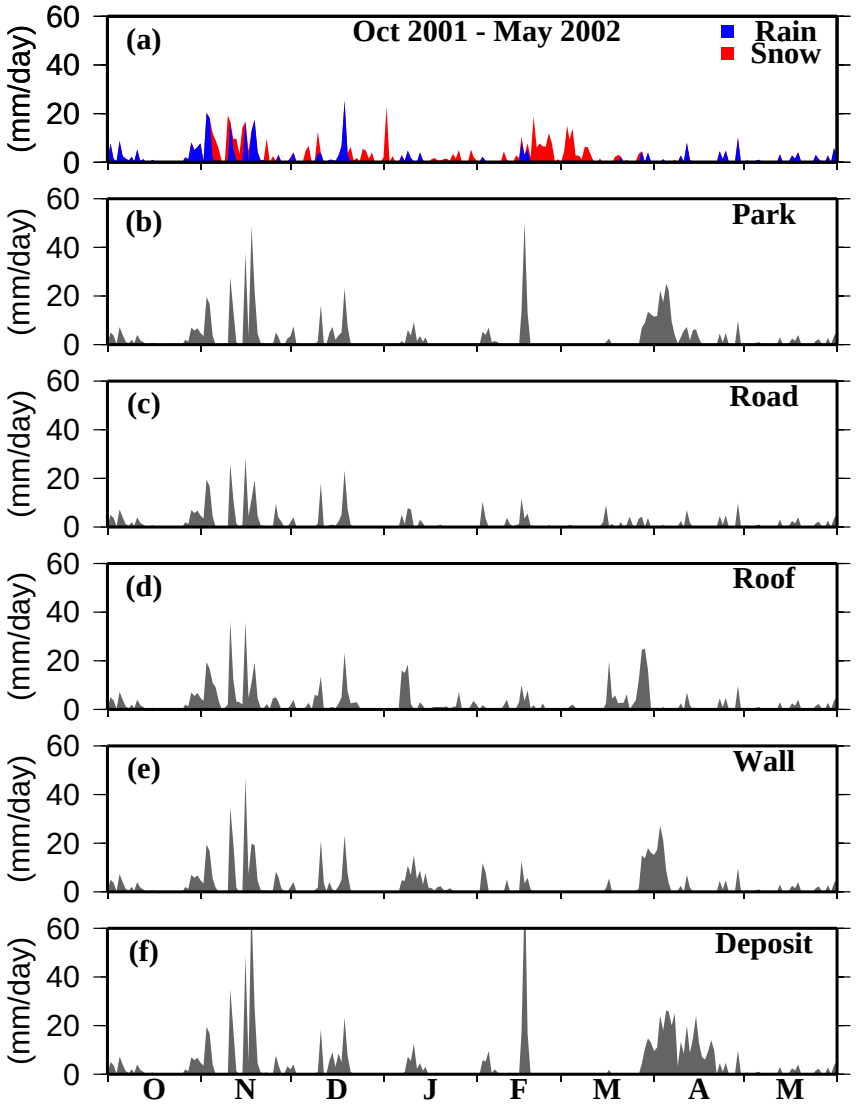

Fig. 7.9: Rain, snowfall and simulated effective precipitation (rain + melt) for five land cover types from Oct 2001 to May 2002

These grid cells have reduced incoming solar radiation contributing to melt due to location with respect to the sun. These areas corresponds well with the white areas in Figure 7.8 (d), indicating that the GUHM snow model is simulating the overall snow energy balance processes correctly. The black areas in Figure 7.8 (c) are snow free areas mostly consisting of roads, roofs, and south facing slopes. The melt is higher in these areas since both AA, slope, and aspect influence the available energy of the snow pack. The large variability in SWE shown in Figure 7.8 (c), is a good indication that the correction of short wave radiation to shadow effects, slope, and aspect, is working as intended in the GUHM.

Figure 7.9 presents rain plus melt for each of the five LCTs used in GUHM for the period Oct 2001 to May 2002. The data presented are generated in the following way. During snowmelt periods, when there is no precipitation, the data presented is an average snow melt rate for grid cells with snow cover. During rain or rain on snow events the data shows the average effective precipitation (rain plus melt) calculated as an average from all grid cells within the LCT. Figure 7.9 (a) displays the daily rain and snowfall. From Figure 7.9 (b) - (f), it can be seen that within LCT deposit the effective precipitation (rain + melt) has the highest intensities. The lowest ones are in LCT road. For LCT road it should be noted that the snow melt rates can be high because of the low albedo and the high snow surface roughness, but since there is little snow on these surfaces the effective precipitation fluxes are small. In March 2002 it can be seen that snow melt starts earlier in LCT roof and road compared to the other LCTs. This is a result of the high wind speeds, low albedo and large snow surface roughness. The modelling results show that AA force early melt in LCT road and roof. In LCT deposit the snow melt intensity is larger than in LCT park mainly as a result of AA (low albedo).

7.2.2 Results runoff simulations

Figure 7.10 presents simulated and observed runoff for the Risvollan catchment for the period from June 1999 to May 2002. The simulation was run with 1 hour time step and the period from June 1998 to May 1999 was used as a warm up period. For better interpretation of the results the time series in Figure 7.10 are plotted as 24 hour averages. The overall trends are good. The R^2 calculated for the simulated and observed runoff showed a

value of 0.72 for the three year period. The total volume of runoff was underestimated with 2 % by the GUHM. There are many possible reasons for this, e.g. bias in the evapotranspiration calculations, ground water recharge factors are calibrated wrongly, gage catch factors are wrongly adjusted, etc. More calibration could possibly have corrected these volume differences.

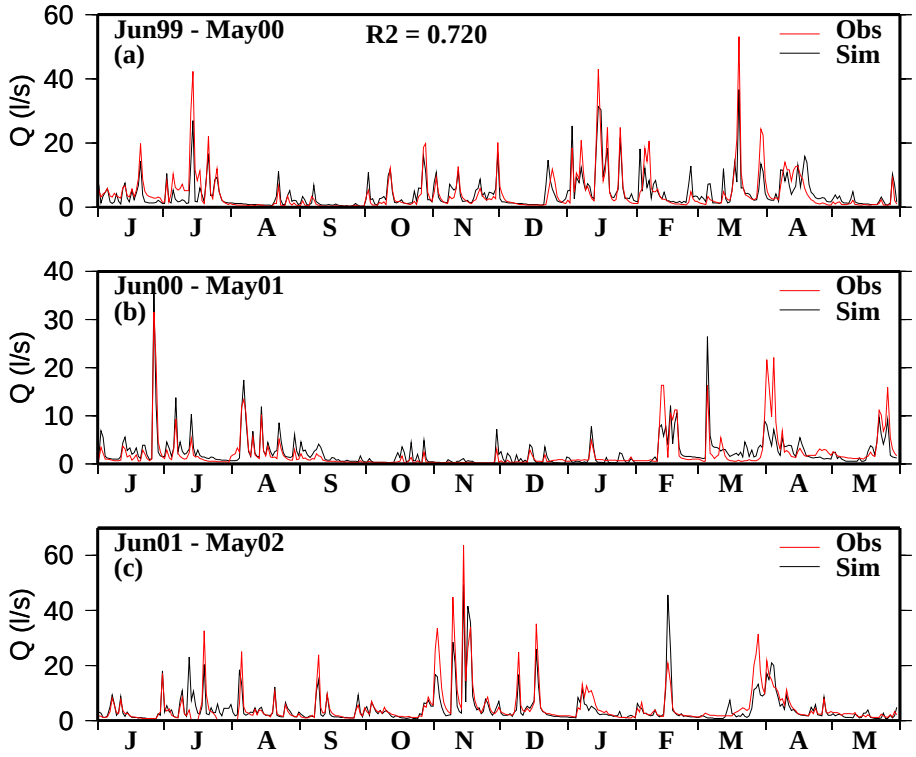

Fig. 7.10: Simulated and observed runoff for the calibration period, June 1999 to May 2002. The data are presented as daily averages.

For the summer periods there is a good match between the simulated and observed runoff, while in the winter months the differences are larger. In the beginning of April 2001 (Fig. 7.10 (b)), the observed data show daily runoff values around 20 l/s. The simulated flows for these days are near 8 l/s. The possible reason for this could be too early snow melt in the model, which would result in reduced runoff volumes later in the spring. Figure 7.3, end of March and beginning of April, shows that the snow pack

melts more rapidly in the model compared with the observed data which supports this explanation.

Another reason for the high flows seen in the observed data can be effects of frozen soils. If rain or snow melt reaches frozen soil the infiltration capacity is strongly reduced and the contributing area for runoff is large. The GUHM does not simulate such effects. In mid February 2002 (Fig 7.10 (c)) both the simulated and observed data shows a peak in runoff. The simulated runoff is about two times as high as the observed. If the soil moisture level in the LCT park is to high a larger area will contribute to runoff in the model than what is the case in the real world. In addition both snowmelt intensity and snow covered area contributing to runoff might be incorrect in the model.

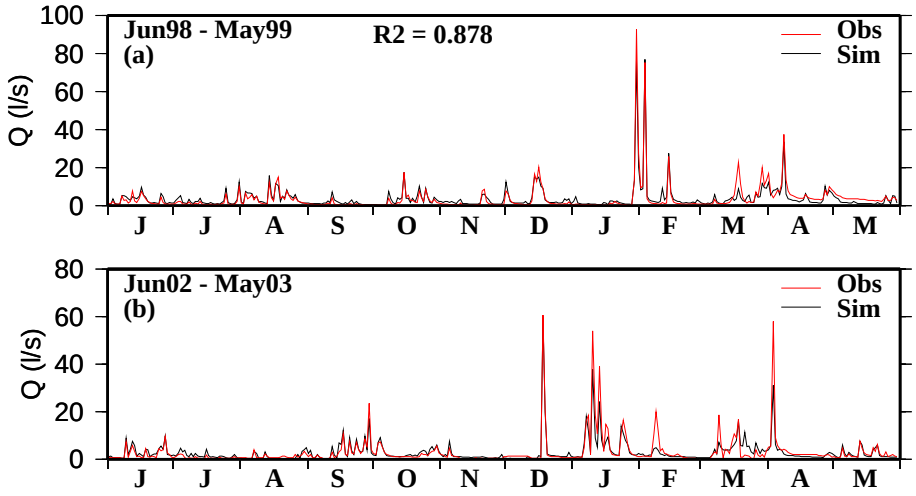

Fig. 7.11: Simulated and observed runoff for the validation periods 1998-1999 and 2002-2003. The data are presented as daily averages.

Figure 7.11 shows the runoff results from the validation periods June 1998 - May 1999 and June 2002 - May 2003. The plot is aggregated to a 24 hour time step. A comparison of the simulated and observed data gave a R^2 value of 0.88. From the results shown in Figure 7.11 (a) it can be seen that both dry and wet periods are simulated quite well by the model. During 2002-2003 (Fig 7.11 (b)) some of the peak flows are underestimated by the model and is clearly outside the uncertainty range of the observed data,

e.g. February 2003 (Fig 7.11). The runoff volumes in the period December to April 2003 seems to be in general lower than the observed data. One explanation to this can be that the precipitation gage correction factors have been set to low, or that the water sent to ground water recharge in LCT park is to high.

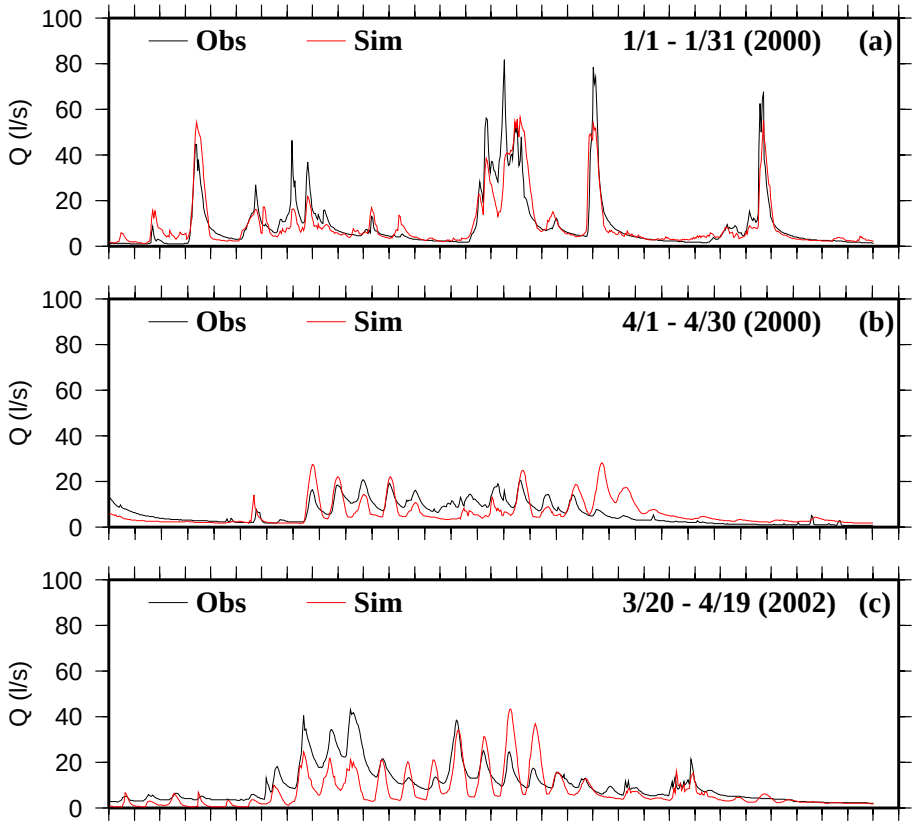

Fig. 7.12: Simulated and observed hourly runoff from the calibration period (2000-2002)

Three snowmelt periods from the calibration period are plotted with 1 hour time resolution in Figure 7.12. In (a) the results from January 2000 are presented. It can be seen that the difference between observed and simulated runoff is small, although some of the simulated peaks are little too low, compared with the observed. In Figure 7.12 (b) and (c) there are

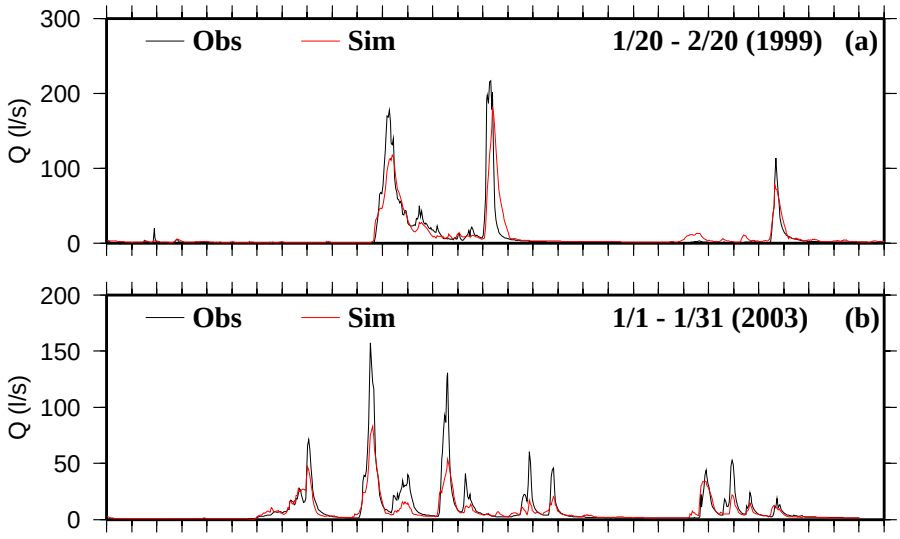

Fig. 7.13: Simulated and observed hourly runoff from the validation period (1999, 2003)

larger differences between the observed and simulated runoff data, but the diurnal trends are clearly shown. In Figure 7.12(b) it can be seen that the simulated runoff is larger than the observed at the end of the snowmelt season. The reason for this can be that there is still snow left in the model but not in the Risvollan catchment. Wrongly simulated SWE and SCA early in the accumulation season will affect the snow melt runoff later in the spring. In addition, the calibration parameters in the soil-runoff routine may not be correctly calibrated. The results shown in Figure 7.12 indicates that it is possible to simulate snowmelt runoff for whole seasons with high time resolution (1 hour).

The data shown in Figure 7.13 shows two melt periods, with 1 hour time resolution from the validation period. Both (a) and (b) show good agreement between simulated and observed runoff. Although in (b) the simulated runoff is underestimated during some periods. The diurnal cycles seem to be represented satisfactorily.

In Figure 7.14 specific runoff (l/sha) for the five LCTs in the GUHM is plotted for the period from Oct 2001 to May 2002. The highest rates are seen in LCT deposit (Fig. 7.14). The reason for this can be explained

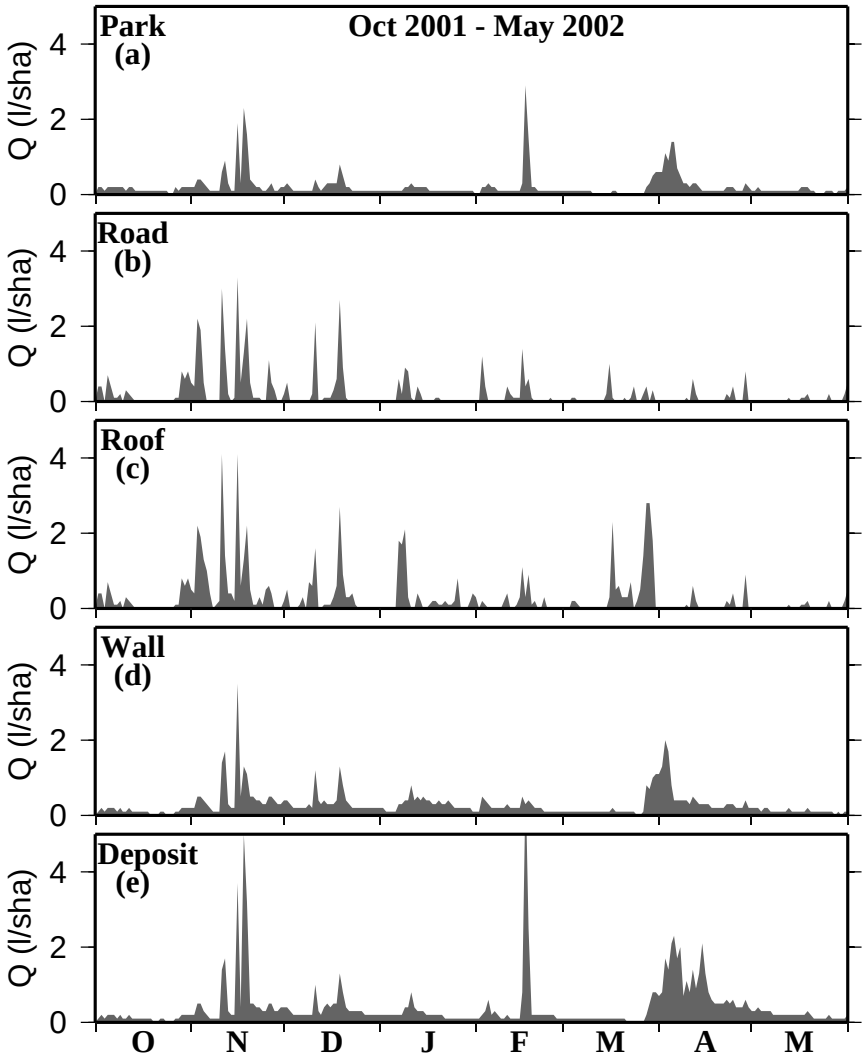

Fig. 7.14: Specific runoff Oct 2001 - May 2002

by AA which is strong in this LCT. Deposit areas receive snow from roads and have low albedo, which causes the specific runoff to be large from these surface types. It can also be seen that the runoff starts earlier in LCT road, and roof (Fig. 7.14 (b) and (c), March 2002) compared to LCT park where the main runoff period starts in late March/early April. In LCT road (Fig. 7.14 (b)), the specific runoff during spring melt is considerably lower than in the other LCTs. One explanation for this can be that all the snow has been removed to LCT deposit and there is no snow left contributing to snowmelt runoff. From Figure 7.14 it can be concluded that AA in various forms alter the specific runoff within the different parts of an urban catchment. Snow clearing of snow and locally low albedos, etc causes the specific runoff to be increased in some parts and decreased in others.

7.3 Discussion

According to Refsgaard & Storm (1996), differences between recorded data and simulated model output arise basically from four sources of uncertainty. These are (1) random or systematic errors in the input data i.e. precipitation. (2) Random or systematic errors in recorded data used for comparison of the simulated output. (3) Errors due to non-optimal parameter values (calibration) and (4) errors due to an incomplete or biased model structure. The objective of the calibration process is therefore to reduce error source 3 until it becomes insignificant compared to the error sources 1 and 2. If this is achieved during calibration, the only way to further improve the performance of the model is to change the model structure or reduce the uncertainty in the input data or the recorded data used for calibration.

In this work the GUHM was applied to the Risvollan catchment to test its performance in an urban cold climate. The model was tested for a total of five years, where three of them were used as a calibration period and two for validation. Three datasets (SWE, SCA and runoff) observed in the field were used to check the performance of the developed model.

Chapter 5 and 6 documented uncertainty in the estimates of SCA and SWE. Chapter 4 debated uncertainty in the observations of runoff discharge at Risvollan. A visual inspection of Figure 7.3, 7.4 and 7.5 reveal that simulated SCA, in LCT road, roof and park, in general followed the same trends as the observed data. In some periods the simulated SCA was definitely

outside the uncertainty range of the observed data. The same patterns were seen for simulated SWE and runoff. The main trends were good, but for some periods the simulated data showed poor correlation with the observed. It is therefore a challenge to decide if the modelling results could have been improved with better input data, by further calibration, improved GUHM model structure, or that the uncertainty in the recorded output should be reduced.

Precipitation and temperature data from only one meteorological station was used in this research. The Risvollan catchment is relatively small (20 ha) where uniform precipitation could be assumed. However, since the precipitation records from the nearby Voll meteorological station showed such a large difference in annual precipitation, the chance of having spatial distribution in precipitation patterns within the Risvollan catchment cannot be excluded. Killingtveit (1998) investigated spatial patterns in precipitation for Trondheim city and found correlation between annual precipitation and elevation above sea level. In Risvollan there is only a relatively small elevation range in the catchment (83 metre to 143 metre above sea level) which could indicate small spatial variability in precipitation. It has not been possible to assess the magnitude of the uncertainty in the meteorological input data used in this research, but the strong correlation of the data from Voll and Risvollan (Fig. 4.5 in chapter 4) is an indication that there are no extreme systematic or random errors in the input data. It should be noted that besides the input time series of meteorological data, other input data such as land cover maps, DEM, etc are also possible sources of input data errors.

There are several hydrological processes that influence the snow distribution and melt in the urban environment, which are not incorporated in the GUHM snow routine, e.g. non-uniformly distributed precipitation, snow drift from rooftops, better methods for calculating turbulent heat fluxes, etc., but even if such methods were implemented there is no guaranty that this would improve the modelling results. It is also clear that the parameters found by calibration has uncertainty related to them and if a larger portion of the parameter space in the GUHM was tested the uncertainty in the calibration parameters could have been assessed. A more optimal parameter set could also have been found through such investigations.

Observed catchment runoff can only to a minor extent be used to quan-

tify the performance of urban snowmelt models (Semádeni-Davies 2000). The reason for this is that runoff from a catchment is dependent not only on the snow covered area and melt intensity but the land surface cover, soil conditions and evapotranspiration. If a model performs poorly when comparing simulated and observed runoff it is difficult to identify if the errors are in the snow or in the soil-runoff routine of a model. The comparisons of simulated and observed runoff presented in this work should therefore be looked upon as an indicator of the snowmelt routines performance.

Refsgaard & Storm (1996) defined four sources of uncertainty in the simulated results of a hydrological model. Within hydrological modelling the term state variables can be used on for example SWE or soil moisture levels in a model. In the first time step initial values of these states must be set. Depending on the model structure, and the chosen point in the parameter space, the initial conditions will influence the results for a certain time in the simulation, and could be viewed as a fifth source of uncertainty. The results for the 1998-1999 (Fig. 7.11 (a)) season was run with no initialization period. Even though the results were good, they might have been influenced by the initial conditions in the soil moisture levels and in the linear reservoirs in the soil-runoff routine. In both the calibration period and the validation period the initial conditions of SWE in the snow routine in the GUHM was set to zero, implying that the snow simulations were not influenced by the uncertainty in the initial state. Valeo & Ho (2003) carried out snow melt simulations for the spring snowmelt period only. It was not debated how much the uncertainty of the initial values of SWE influenced the simulations. In this work all the simulations started in summer time and the initial conditions in the snow routine are therefore guaranteed to be correct.

In chapter 2 it was argued that the low albedos typically found nearby roads can influence snow melt rates in the urban environment. During snow melt conditions in late spring (March-April), when the sun angle is relatively high, the albedo formulation in an urban hydrological model will therefore strongly influence snow melt rates. In this work no validation of the albedo formulation was carried out, which introduces uncertainty in the simulation results. Winther (1993*a*) studied short and long term variability of snow albedo at a mountain shallow snow pack outside Trondheim city. A correlation between snow age and surface albedo was documented, and could maybe have been used in this research, but due to little influence from

AA in the snow pack studied, the albedo formulations proposed might not be used in urban areas. The results from Winther (1993*a*) also showed that when the SWE became lower than 50 mm the albedo dropped rapidly to values around 0.3 and 0.4. An explanation to this can be that shallow snow packs are transparent and short wave radiation will be absorbed by the ground below the snow. This can also happen in urban snow packs and are not taken into consideration in the GUHM.

In this work the GUHM model was calibrated against observations of SWE, SCA and runoff. None of the literature cited in chapter 2 showed similar testing of both the snow and runoff data in urban cold climates. It has been demonstrated that when observations of SWE and SCA are available it makes it easier to understand the results. Such data also makes it possible to identify if the modelling errors are caused by errors in the snow or in the soil-runoff routine of a model.

7.4 Conclusions

The GUHM snow routine was tested against point data from the snowmelt lysimeter at Risvollan station for the period Oct 1994 to May 1995. Both simulated SWE and snow melt intensity agreed well with the observed data ($R^2_{swe} = 0.97$, $R^2_{melt} = 0.78$). The results from the point simulations showed that the GUHM snow routine was capable of simulating snow accumulation and melt for whole winter seasons with short time steps (1 hour) without updating the SWE states during the winter season.

The GUHM was applied and calibrated for the Risvollan catchment for a three year period. Two winter seasons were used as validation period. The results showed that the GUHM was able to simulate snow accumulation and melt for whole seasons with short time resolution (1 hour) for an urban catchment. Comparison between observed and simulated SWE and SCA showed that the overall trends were captured by the model, however for some shorter periods the simulated SWE, SCA, and runoff, were outside the uncertainty range of the observed data. This can be explained to be a result of simplified model structure in GUHM, and that the modelling results could have been further improved by calibration.

The runoff simulations matched the observed data quite well. For the calibration period the R^2 value was calculated to 0.72 between simulated

and observed runoff. This value was 0.88 for the validation period. For some periods in the spring a discrepancy between simulated and observed data was seen, but the results demonstrated that the GUHM was capable of simulating effects of AA on urban snow distribution, and melt. From the results presented in this and in chapter 3 it can be concluded that objective 2 set in chapter 1 has been achieved. An urban hydrological model specially designed for urban snowmelt calculations has been developed and proved to produce good results.

Chapter 8

Effects of AA on snow distribution and melt

In this chapter the GUHM was used to quantify the effects of AA on snow distribution and melt in the Risvollan catchment. This was carried out by running the GUHM for six different land use scenarios, with varying degree of impervious surface cover (buildings and roads). Simulated runoff was also used as an indicator to quantify effects of AA on urban snow packs.

8.1 Land use scenarios

The purpose of the analysis was to study the effect of AA on snow distribution and melt in the Risvollan catchment by use of the GUHM. It was decided to use the calibrated parameter set from chapter 7 (Tab. 7.4 and 7.5), to run six different land use scenarios and then investigate changes in SWE, SCA and runoff as a result of varying degree of land use. The time period from June 1998 to June 2003 was used as the simulation period. The six land use scenarios are shown in Figure 8.1 (a) to (f), where Figure 8.1 (b) is the current land use situation in the Risvollan catchment with an impervious surface cover (ISC) of 26 %. The various land use scenarios will be referred to as ISC0, ISC26, ISC28, etc, shown in Figure 8.1 as (a), (b), (c), etc, through the rest of this thesis. In scenario ISC0 all buildings and roads were removed. The building elevations were replaced with the elevation of nearby terrain and all grid cells were set to LCT park.

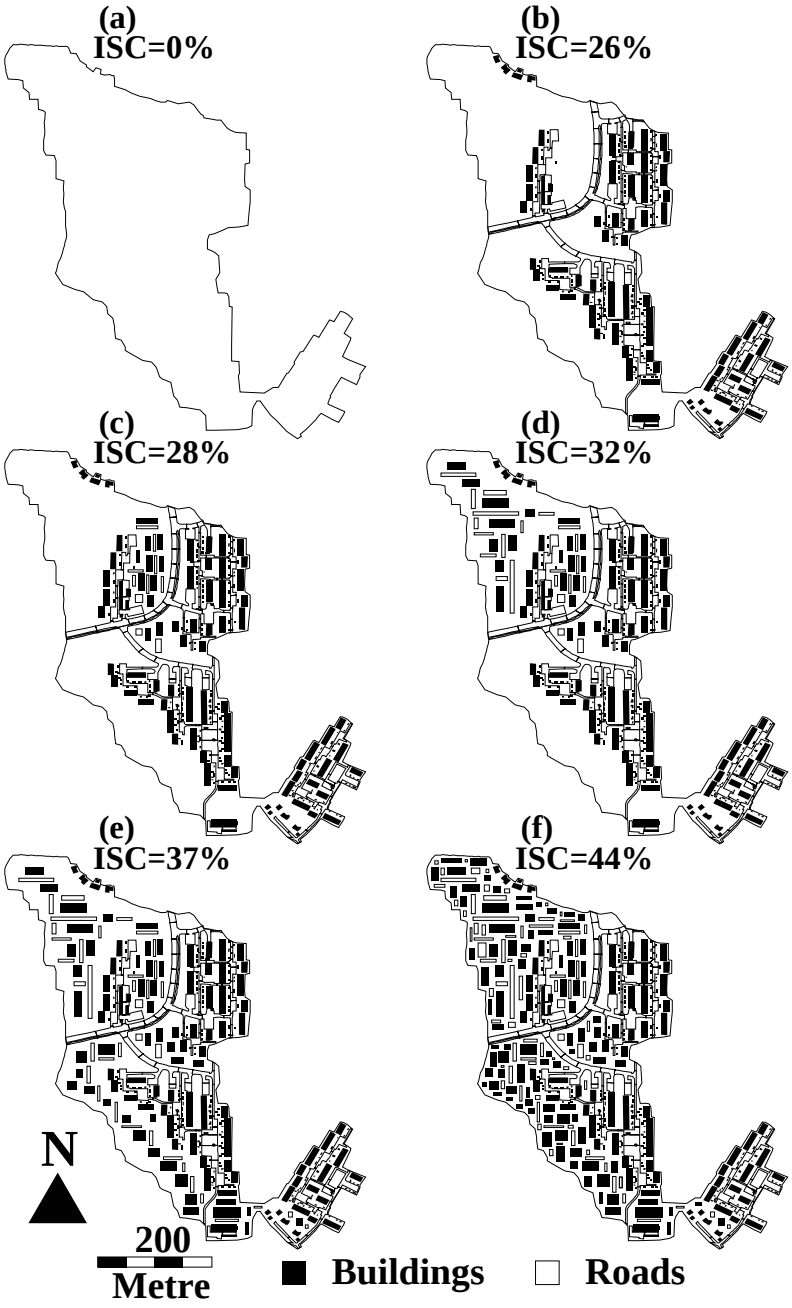

Fig. 8.1: Six land use scenarios for Risvollan catchment

In scenario ISC28 to ISC44 new buildings with roof elevations of six metre above the terrain (assuming two floor levels) were drawn into the LCT park areas of the Risvollan catchment. New roads were also drawn into the current park areas and given the elevation of the original terrain. This was carried out in a GIS. After this new input data (DEMs, slope, aspect, α_{shadow}, etc) for the five new input scenarios were prepared. Scenario ISC26 was the exact same model and input data as used in chapter 7.

Table 8.1: Area coverage of each land cover type (%) for six different land use scenarios

LCT	**ISC0**	**ISC26**	**ISC28**	**ISC32**	**ISC37**	**ISC44**
Road	0	13	13	15	16	18
Deposit	0	5	6	7	8	9
Wall	0	5	6	7	9	12
Park	100	64	60	53	46	34
Roof	0	13	15	17	21	26
SUM	100	100	100	100	100	100

Table 8.2: Parameters used to quantify degree of AA for the six different land use scenarios

	ISC0	**ISC26**	**ISC28**	**ISC32**	**ISC37**	**ISC44**
Pop	0	1500	1731	2263	3656	7312
PD	0	7653	8830	11548	18654	37307
LCR (%)	0	13	15	17	21	26
ISC (%)	0	26	28	32	37	44
FAR (%)	0	26	30	34	42	52

Table 8.1 presents the area coverage of each LCT (%) for the six land use scenarios, where ISC44 is the most developed scenario with an ISC of 44 %. In Table 8.2 the parameters Pop, PD, LCR, ISC, FAR (see also Tab. 1.1) are presented for the six land use scenarios shown in Figure 8.1. The population was calculated from the increase in building surface coverage of the catchment. In later sections, changes in SCA, SWE and catchment runoff due to various degree of land use will be quantified as a function of

the ISC parameter shown in Table 8.2.

8.2 Results

Figure 8.2 presents simulated SCA for the time period Oktober to April for the seasons from 1998 to 2002 for the land use scenarios ISC0, ISC26 and ISC44. The SCA data are scaled according to the areal coverage of each LCT. It can be seen that the simulated SCA is quite different between the three scenarios. In the ISC26 case the SCA tend to rapidly be reduced to first around 87 % and then down to 74 % when melt starts. For the ISC44 scenario the SCA is reduced to around 74 % and later to below 50 % when melt starts. This is not seen in the ISC0 scenario. The reason for the differences in SCA between the three scenarios can be explained by AAs. The snow on roads is relocated to nearby areas, have in general a low albedo, and the roads therefore become snow free rapidly when melt starts. Due to high wind speeds, exposure to solar radiation and heat from the roofs themselves, the snow on roofs disappears more rapidly than in park areas. Figure 8.2 indicates that the more developed an urban area is, the faster the SCA will be reduced during melt situations. This is why the SCA in the ISC44 scenario shows such a rapid decay compared to the ISC0, and to a certain extent the ISC26 scenario.

Figure 8.3 presents simulated time series of SWE for three of the six land use scenarios. The data are calculated as an area scaled average SWE from the five LCTs used in GUHM. From Figure 8.3 it can be seen that the SWE in the ISC0 case is in general higher than in the ISC26 and ISC44 case. The reason for this is that in the ISC26 and ISC44 cases more of the surface is covered with LCTs where the snow melt intensity is higher and starts earlier than in areas covered with e.g. LCT park. In LCT road, roof, deposit, and wall the available energy for melt is larger than for LCT park due to lower albedos, higher wind speeds, heat from walls and roof surfaces, etc. When the areal surface cover of the LCTs roads, roofs, deposit and wall, increase in a catchment, the earlier the snow melt will start and therefore the SWE is in general lower compared to in an untouched area.

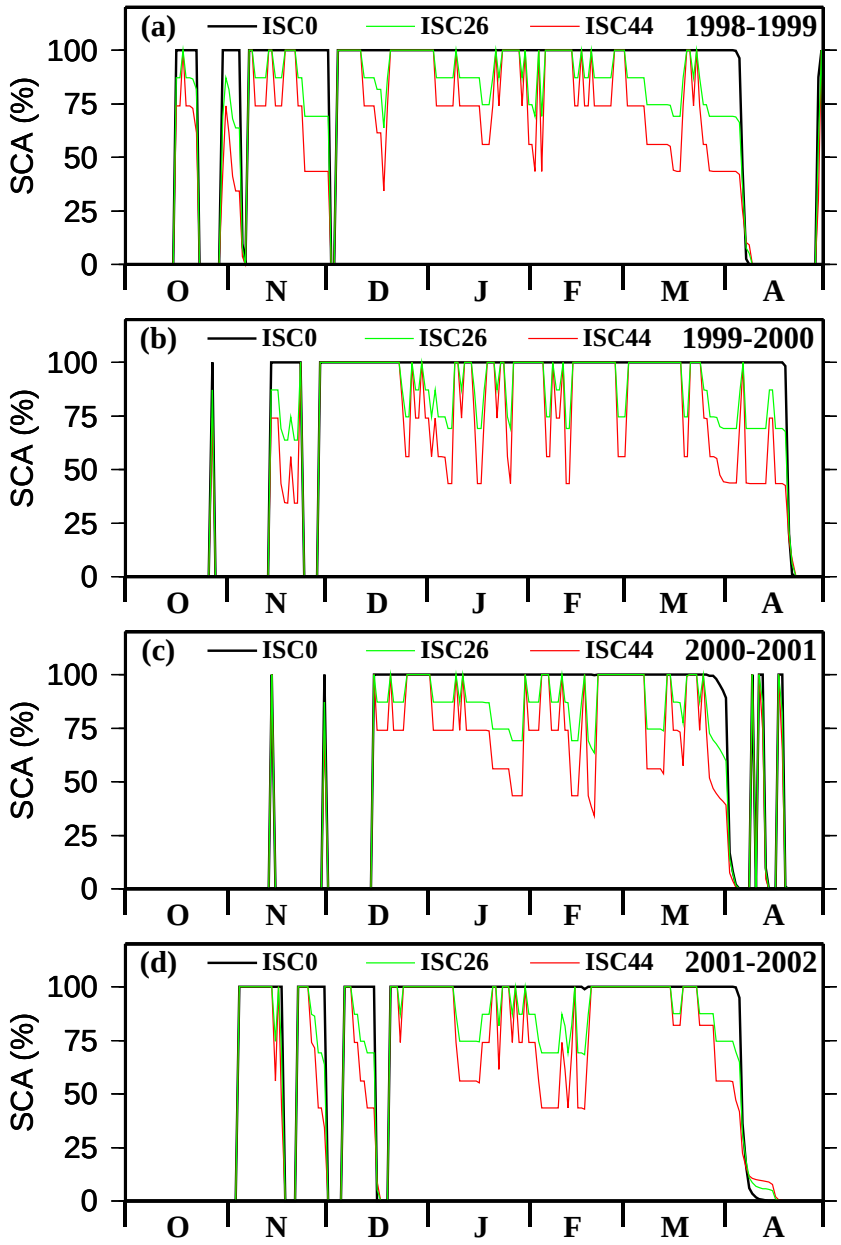

Fig. 8.2: Simulated area scaled SCA for land use scenario ISC0, ISC26 and ISC44

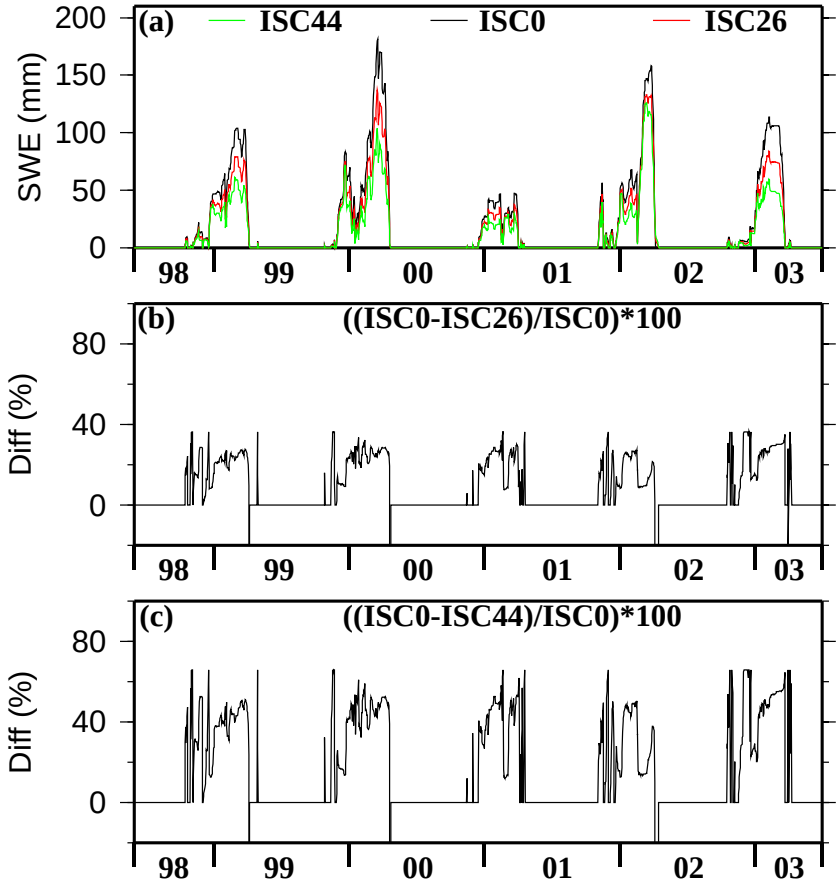

Fig. 8.3: Simulated area scaled SWE for land use scenario ISC0, ISC26 and ISC44

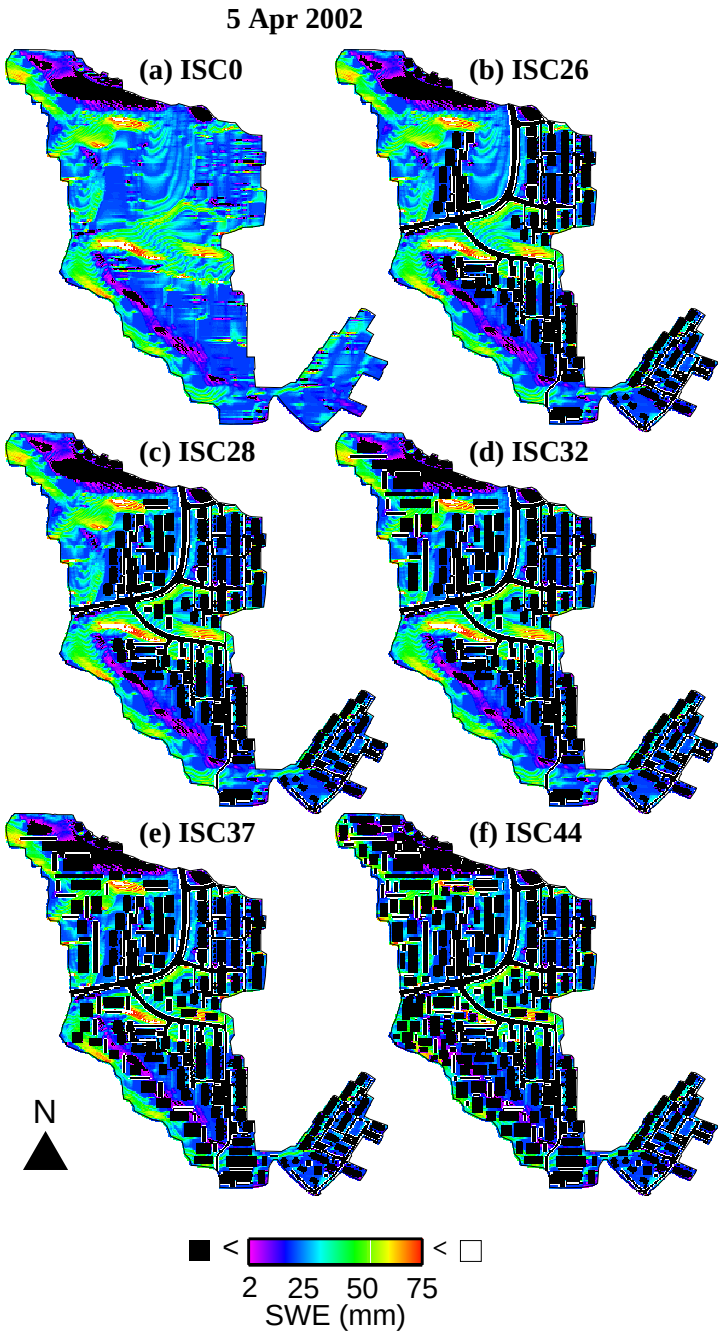

Fig. 8.4: Spatial plot of SWE (5th Apr 2002) for six land use scenarios

The differences (%) in SWE between the ISC0, ISC26 and ISC44 scenarios are presented in Figure 8.3 (b) and (c). The data are calculated as the SWE in the ISC0 minus the ISC26 (ISC44) scenario divided by ISC0 and multiplied by a hundred. This is when the SWE in the ISC0 scenario is above zero. For a large portion of the winter season the ISC26 and ISC44 scenarios had about 35 % and 50 % lower SWE than the ISC0 scenario. These findings indicate that the SWE in general is lowered in catchments influenced by AA. One plausible reason for this is that snow packs located in LCT road, roof, wall, and deposit receive more energy than snow located in LCT park. The negative values in Figure 8.3 (b) and (c) are from the late melt period, when SWE in LCT deposit makes the SWE in the ISC26 and ISC44 scenario larger than in the ISC0 scenario.

Figure 8.4 (a) to (f) shows a spatial plot of simulated SWE on 5th April 2002 (at noon) for all the six land use scenarios. A visual inspection of the figure reveals how AA influence both SWE and SCA in the Risvollan catchment. In Figure 8.4 (b) to (f) the SWE is considerably lowered in LCT road and roof, which is not the case in the ISC0 scenario (Fig. 8.4 (a)), since no effects of AA are simulated. All plots in Figure 8.4 shows a relatively large variability in SWE. The variability in SWE shown in Figure 8.4 (a) is only a result of spatial variability in available energy for melt caused by spatial differences in slope, aspect and shadow effects. As mentioned in previous sections variability in SWE as a function of terrain and wind speed is not accounted for in the GUHM, although such processes would generate variability in the SWE during the accumulations season in a catchment. For the five scenarios with developed land use (ISC26, ISC28,..ISC44) the variability in SWE is further enhanced by influence of AA. Roads are cleared for snow and dumped into snow piles, which can be seen as the white areas next to roads in Figure 8.4 (b) to (f). The white areas represent SWE values above 75 mm and are mostly located in grid cells of LCT deposit. In the plots shown in Figure 8.4 (b) to (f) there is a tendency that increased surface coverage of roads and buildings decreases SWE and therefore SCA for a catchment during melt periods. The reason for this has to do with snow clearing procedures, which influence the snow distribution, and that the snow in LCTs road, roof, deposit, and wall are exposed to snow melt energy not available for LCT park. An increase in these LCTs will therefore force the snow melt to start earlier in the season and have a higher intensity compared to in LCT park. The SWE and SCA

are therefore lowered more rapidly as a result of AA. This was also seen in Figure 7.9 where the intensities from rain and snow melt water were greater and started earlier in the winter season in the LCTs most heavily influenced by AA (deposit, road, roof, wall).

Figure 8.5 presents the snow distribution, sorted SWE data versus area, for the six land use scenarios for the 5th of April 2002. There is a clear tendency that AA causes a shift in the snow distribution. In the ISC0 scenario the largest SWE value is around 80 mm and only about 6 % of the area is snow free. In all the other scenarios around 10 % of the area is covered with grid cells having SWE values above 150 mm. This can be explained by road snow clearing. The snow free areas are also larger in all the five scenarios with presence of buildings and roads. In the ISC44 scenario the snow covered area is around 40 %. Based on the simulation results it can be concluded that AA changes the snow distribution in urbanized catchments due to snow clearing procedures and increased melt rates.

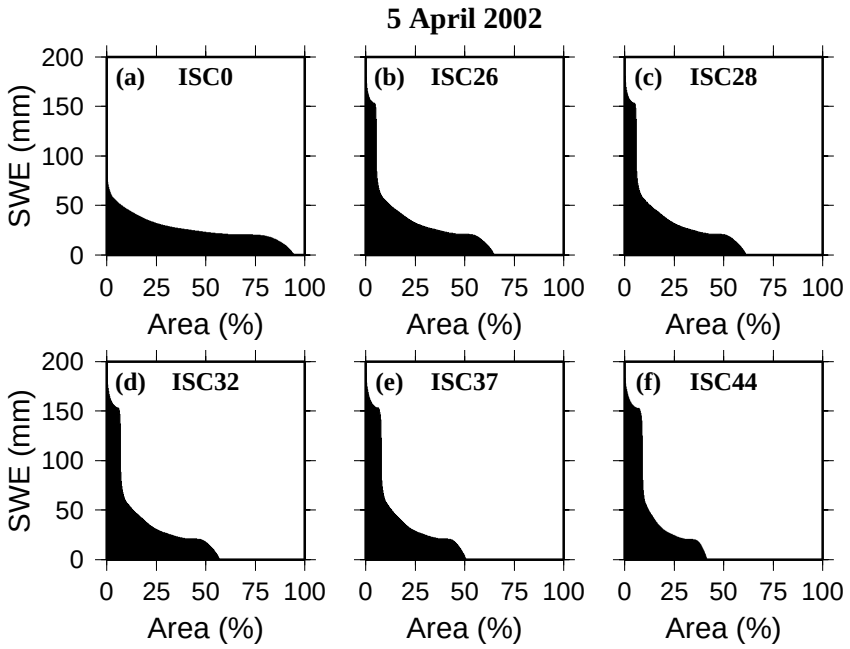

Fig. 8.5: Snow distribution 5th April 2002 for six land use scenarios

Figure 8.6 presents two types of data as a function of ISC (Tab. 8.2). The triangles indicated as AvgSWEmax represent average maximum seasonal SWE. The circles represent average SCA values calculated from the simulated SWE data in February, March and April (AvgSCA). Both the AvgSCA and AvgSWEmax data are calculated from the time period from 1998 to 2003. When land use (AA) increase the AvgSWEmax and AvgSCA are in general lowered. Early and rapid melt lowers SWE and therefore SCA. As mentioned earlier this is related to the increased energy availability for the snow packs in LCTs road, deposit, roof and wall (low albedo, roof heat conduction, etc). It can be seen that the AvgSWEmax is about 35

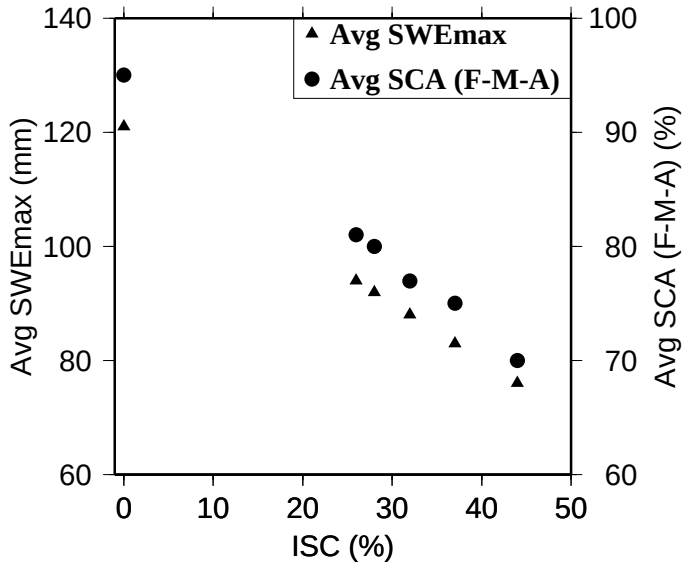

Fig. 8.6: Average maximum seasonal SWE and average SCA for February, March and April expressed as a function of impervious surface coverage (1998-2003)

% lower in the ISC44 case compared to the ISC0 data, while the AvgSWEmax in the ISC26 scenario is around 22 % lower than in the ISC0 scenario. The AvgSCA is at 70 % in the ISC44 data compared to the ISC0 scenario at 95 %. There seems to be a linear relations ship between ISC and lowering of AvgSWEmax and AvgSCA. The scenarios ISC28, ISC32 and ISC37 are placed on the line between the ISC0 and ISC44 scenario. The reason

for this is that the chosen point in the parameter space, found by calibration, is sensitive to an increase in LCTs such as roads and buildings. The simulation results indicate that AA lowers SWE and SCA in a developed catchment compared to in an untouched one.

Figure 8.7 presents simulated runoff, aggregated to daily averages, for the time period from June 1998 to May 2003. Red colour shows the time series from the ISC0 scenario and the black and green lines shows the ISC26 and ISC44 scenario, respectively. The overall trend is that peak and volume runoff seems to increase as a result of AA. The ISC0 scenario has in general the lowest runoff values, although there are seasonal differences (the discussion section presents more on this). In the summer period runoff peaks are in general increased as a result of AA. Both the ISC26 and ISC44 runoff data shows higher peak values from June to October compared to the ISC0 data. During low flow periods (dry weather) the base flow seems to have been lowered in the ISC26 and ISC44 cases compared to the ISC0 case. One explanation to this is that the ISC26 and ISC44 scenarios have larger coverage of impervious surfaces resulting in increased peak flows and lowered base flows. Similar effects of urbanization on catchment runoff was also reported by Kang et al. (1998) and Beighley & Moglen (2002), and others.

During the winter months, November to April, the situation is somewhat more complicated since SCA and snow melt intensity in combination with soil moisture levels has strong influence on the catchment runoff. In the period from December to early March the runoff in the ISC26 and ISC44 scenarios is in general higher than in the ISC0 scenario due to earlier and more intense snow melt caused by AA. Increased impervious surface cover and early melt forced by the extra snow melt energy available in LCT roads, roofs, wall and deposit results in a time shift in the runoff from late spring (April) to mid winter (Jan to March). This is especially seen in the winter seasons 1999/2000 and 2001/2002 (Fig. 8.7 (b) and (d)).

Later in the melt season, e.g. April 2000 and in April 2002 (Fig. 8.7 (b) and (d)), the runoff from the ISC0 case is around 10 % to 30 % larger compared to the ISC26 and ISC44 scenarios, respectively. In the ISC26 and ISC44 case, melt starts early since the snow packs in the LCT road, roof, wall and deposit receives more energy compared to LCT park. This forces more of the snow to melt earlier in the season. At the end of the spring there will therefore be little snow left contributing to snow melt runoff and

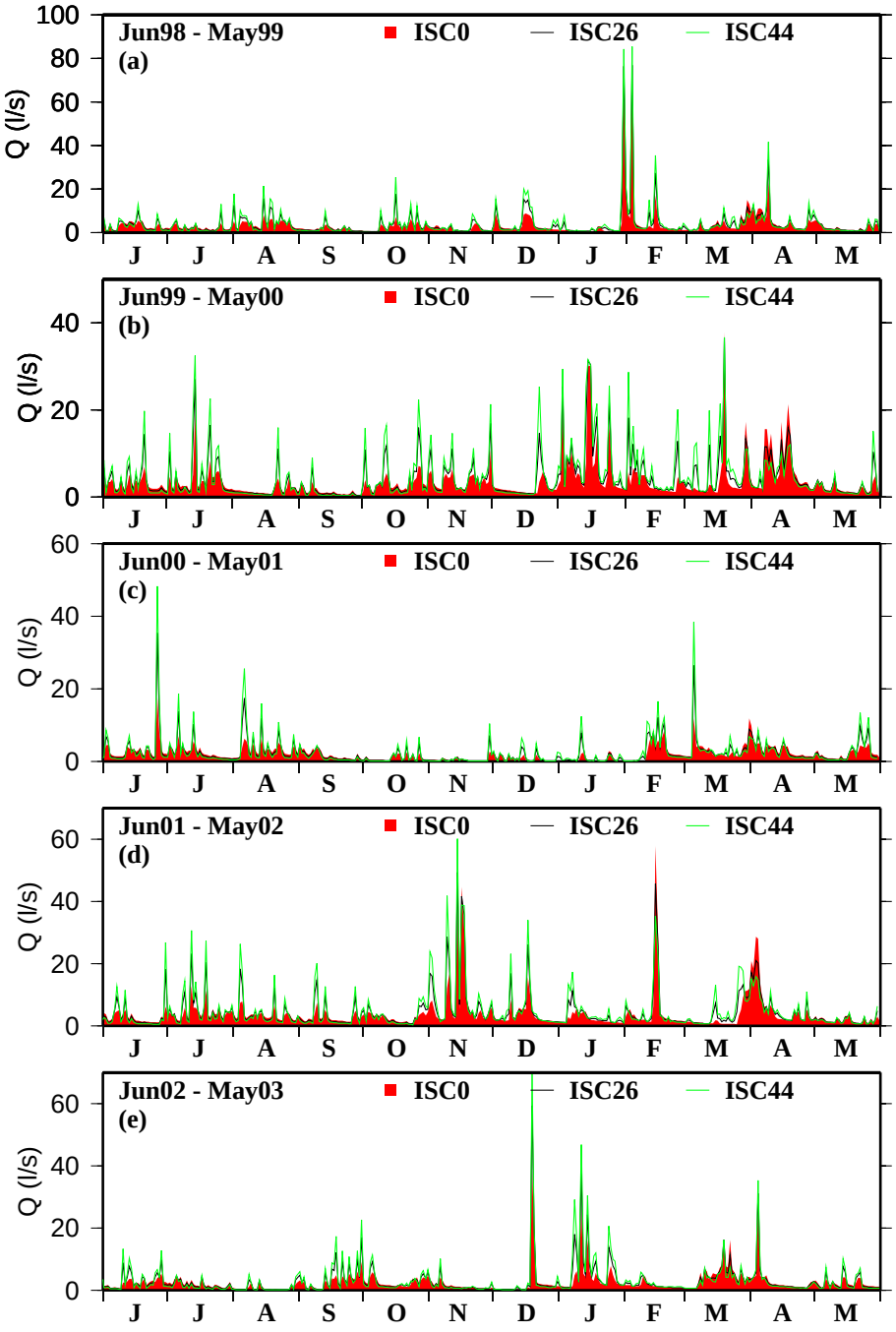

Fig. 8.7: Simulated runoff (1998-2003) at Risvollan for three land use scenarios

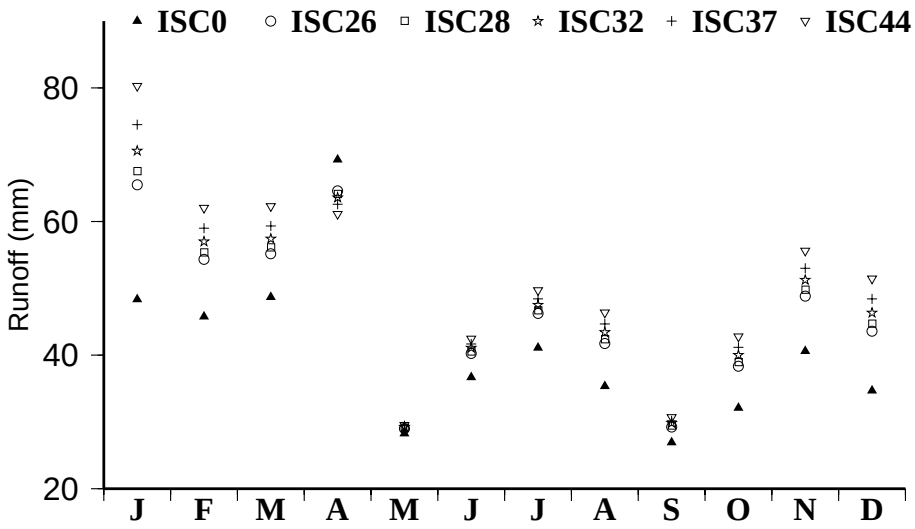

Fig. 8.8: Simulated monthly runoff for six land use scenarios in Risvollan catchment

the runoff from the ISC0 scenario is therefore larger than the ISC26 and ISC44 scenarios for April 2000 and 2002, since there is still snow available for runoff. From Figure 7.4 (a) and (b), it can be seen that the roads and roofs are snow free at the end of March 2002, while park areas have almost full snow cover. During melt situations only, the reduced SCA will therefore lower the contributing runoff area, which explains the differences seen in runoff during April 2000 and 2002. The discussion section will present more details on this.

Figure 8.8 shows simulated average runoff in mm for each month of the year calculated from the period from June 1998 to June 2003 for the six land use scenarios. The overall trend indicates that runoff has increased with enhanced land use. It can also be seen that when the degree of urbanisation increases there is a time shift in the runoff in the winter time. For the months January, February, and March the runoff volumes have increased as a result of increasing AA. The two main reasons for this are enhanced and early snow melt caused by AA and more impervious surface cover. In April the ISC0 scenario has the largest runoff volume, due to delayed snow melt compared to the other five scenarios. This is because in the ISC0 scenario more snow melts in April compared to in the other scenarios. Figure 8.8

also shows that the runoff in May month in general has not increased as a result of AA. This might be explained by the soil moisture levels. During the winter time there is relatively low ET and the soil moisture levels in GUHM are therefore filled rapidly when melt starts. If the soil moisture levels are in general high in May the runoff contributing area will also be high and therefore not so dependent on ISC. So even the ISC has increased, runoff will more or less stay the same.

Annual runoff ratio can be calculated as the volume of runoff in mm divided by the annual average precipitation. Figure 8.9 presents simulated annual runoff ratio as a function of ISC for the Risvollan catchment. The data are based on the time period from June 1998 to June 2003. It can be seen that the runoff ratio increases almost linearly with the increase in ISC. The ISC44 scenario shows the largest runoff ratio with a value of 69 %. The runoff ratio for the ISC0 scenario is only at 55 %. These results are not surprising since the increase in ISC will in general increase the runoff volumes (Kang et al. 1998, Weng 2001).

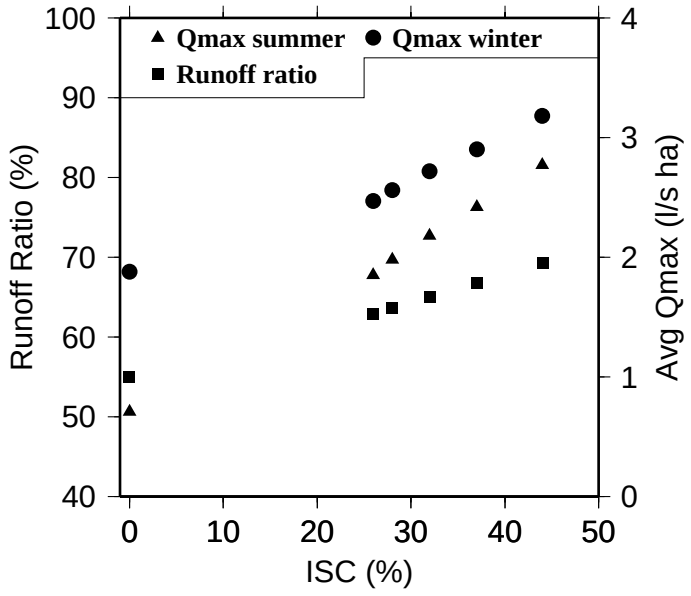

Fig. 8.9: Simulated annual runoff ratio and average monthly maximum peak runoff as a function of impervious surface coverage

Figure 8.9 also shows average monthly maximum peak flows calculated from the hourly time series. The black circles are for the months of November to April and the black triangles are for the summer period (May to October). For both the summer situations and the winter situations the runoff peaks increase with increased ISC. The runoff peaks for the winter season is in general higher than in the summer situations. For the ISC value of 44 % the runoff peaks in the winter period are in general around 40 % higher than for the runoff values at an ISC value of 0 %. For the summer period this difference is at 57 %, implying that the winter peak runoff values are less sensitive to the increase in ISC than in the summer time. The reason for this might be that in the winter time runoff is produced from a larger portion of the catchment than in the summer time, due to soil saturation. From the results showed in Figure 8.9 it can be concluded that the annual runoff ratio and average monthly peak flows, both in summer and winter time, is increased as a result of AA.

8.3 Discussion

Buttle & Xu (1988) found that the SCA was about 20 % lower in a suburban catchment, prior to two spring melt periods, than in a nearby rural catchment in Canada. Bengtsson & Westerström (1992) reported that most impervious surfaces in the city of Luleå in Sweden were usually free from snow when significant runoff began in spring. Buttle (1986) reported that snow that falls on roofs often melt relatively quickly compared to other surfaces (park), due to exposure to solar radiation and heat flux from the roofs themselves. These results agree to a certain extent with the results found in this chapter. It was shown that during melt periods, the SCA was rapidly reduced to values between 50 % and 74 % in the Risvollan catchment depending on the ISC (Fig. 8.2). It is clear that when surface types like roofs and roads increase in a catchment the SCA will rapidly be reduced as a result of increase in AA. This was shown in Figure 8.2.

McMurter (1976) reported that the end of winter SWE of a rural and construction area, in Canada, was four and three times larger than in a nearby urban area, respectively. Buttle (1986) and Bengtsson & Westerström (1992) reported similar findings showing that the snow melts faster and disappear more rapidly in built up areas compared to rural ones. Fig-

ure 8.3 showed that the SWE within the Risvollan catchment was lowered rapidly as a result of AA, which corresponds to the results found by McMurter (1976), Buttle (1986) and Bengtsson & Westerström (1992). In chapter 6 it was shown that the SWE within LCT road, deposit, roof, and wall was about 36 % lower than in LCT park (13th March 2002), and supports the simulation results presented in this chapter. The reason for the lowered SWE in urbanized catchments is that the snow packs are exposed to energy not available in rural areas. This theory was also reported by Todhunter et al. (1992). Since this energy is available more of the snow will melt in an early stage of the season and therefore the SWE will in general be lower compared to in untouched areas.

Steinecke (1999) compared climate data from the city centre and a sparsely built-up non-urban outskirt in the city of Reykjavik (Iceland), and found that the city centre had only 0.2 C higher air temperatures than the outskirt, indicating a weak UHI effect. The anthropogenic average heat release was estimated to 35 W/m^2. The population density (PD) of Reykjavik was reported to be 2684 P/km^2 by Steinecke (1999). In Risvollan the current level of development is at 26 % ISC, with an estimated PD of 7653 P/km^2 (Tab 8.2), which is larger than the PD for Reykjavik. Despite this it is not likely that the average air temperature in Risvollan has increased as a result of AA, since the data presented in Figure 4.5 showed that the air temperature at Risvollan was in general lower than at Voll climate station, even though Voll is located in a more open site, not influenced by buildings. One could ask what level of urbanization that Risvollan had to be developed too before the UHI started to show. The answer to this question is not known but it is clear that increasing AA will eventually end up producing an UHI effect, since the total energy transfer to an urban catchment, due to e.g. indoor heating of houses, will rise and eventually lead to increased outdoor air temperature. In the ISC44 scenario ISC was set to 44 %. If this level of urbanization leads to increase in air temperature it is likely that this will influence snowmelt runoff, since an increase in air temperature will enhance turbulent heat transfer to the snow packs. In such a scenario more of the snow fall will hit building walls directly and there is a chance for instantaneous melt or evaporation of the snow. These effects are not simulated by the GUHM and introduce uncertainty in the simulation results. If it is assumed that an increase in AA, say above ISC of 44 %, in Risvollan leads to a localized UHI effect, then snow melt will start

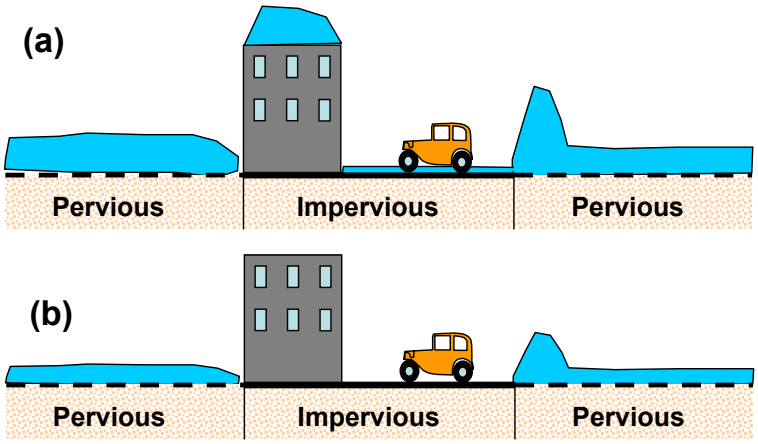

Fig. 8.10: Runoff situations in urbanized catchments

even earlier in the season and an even stronger time shift, from spring to mid-winter, in snow melt runoff will be seen. Ichinose et al. (1999) reported anthropogenic heat fluxes for central Tokyo of 400 W/m^2 in daytime with maximum values up to 1590 W/m^2. Such large energy fluxes will naturally have strong influence on the snow packs energy balance and lead to earlier start and more intense melt in such environments.

Taylor (1977) studied impact of suburban development on runoff response on a small urban catchment (0.7 km^2, 38 % ISC) and found that urban direct runoff volumes exceeded volumes found in a nearby rural catchment (1.14 km^2) by a factor of 7.5 for spring snowmelt and rain-on-snow events. Taylor (1982) also reported an increase in rapid runoff response during spring as a result of urbanization from 7 % to 30 % ISC for a 0.97 km^2 catchment in Canada. Buttle (1990) studied the same catchment as Taylor (1977) and found similar results showing that runoff had increased during spring snowmelt as a result of urbanization. It was also pointed out that when assessing effects of urbanization on snowmelt generated runoff a distinction between snowmelt only and rain-on-snow events should be made. In addition to this it could also be interesting to make a distinction between the runoff events happening early in the melt season when the impervious surfaces have snow cover and the later situations, when only the park/garden and snow deposit areas have snow in them.

Figure 8.10 illustrate two different runoff situations. Figure (a) shows a situation where all parts of a catchment contains snow. The roads are cleared for snow but there is still some ice/snow left. The roofs are also covered with snow. This situation is typical right after major snow falls in a catchment like Risvollan. When snowmelt starts in situation (a) it has been shown that the snow melt intensity is enhanced in the surfaces most influenced by AA. The roofs and roads will therefore become snow free before the park and garden areas. This was also shown in chapter 5 and 6. Compared to a catchment where there are no houses or roads the snowmelt will be more intense and the runoff production will be larger, independently of soil moisture levels and possible rainfall. So for the case shown in Figure 8.10 (a), the runoff will be enhanced by AA, and are concurrent results with the findings reported by Taylor (1977) and Buttle (1990), who reported an increase in runoff during snow melt events for urbanized catchments.

The situation shown in Figure 8.10 (b) illustrates the runoff situation later in the melt season when roads and roofs are free from snow. Only the deposit and park areas contain snow. Bengtsson & Westerström (1992) commented that the infiltration capacity of most soils in urban areas is so heavily reduced during spring snow melt conditions that melt-induced runoff from grassed and gravelled surfaces are similar to those from impervious surfaces. This view was also shared by Semádeni-Davies (1999*a*) who commented that soils could have lowered infiltration capacity due to freezing. Thus, in situation (b) shown in Figure 8.10 (b), if the infiltration capacity in the pervious surface types is low, the runoff is controlled only by SCA and snow melt intensity during snow melt events with no rainfall. Since AA has lowered the SCA, the runoff in the situations will therefore be lower compared to in an untouched catchment where the SCA would be larger. Figure 8.7 presented simulated runoff for three of the six land use scenarios, ISC0, ISC26 and ISC44. The runoff in April 2000 and April 2002 (Fig. 8.7 (b) and (d)), from the ISC0 scenario was lower than in both the ISC26 and ISC44 scenario. The reason for this can be explained by the situation illustrated in Figure 8.10 (b) and are somewhat contradicting to the results found by Taylor (1977), who reported that snow melt runoff, in general had increased as a result of urbanization. The viewpoints presented by Taylor (1977) can only be true for snow melt events happening early in the melt season when the SCA is high in all surface covers.

During rain-on-snow events, occurring in situations like the one shown

in Figure 8.10 (b), the effects of AA on runoff will be dependent on the infiltration capacity of the pervious surface types. If some of the snow melt is allowed to infiltrate in the pervious surface types it is likely that the runoff in developed catchments will have a higher runoff compared to in an untouched area. The reason for this is the presence of impervious surface covers. On the contrary, if the infiltration capacity in the pervious surface types is close to zero, the effects of AA will be lowered runoff because of lower SCA. This can also explain why the runoff in April 2000 and 2002 from the ISC0 scenario was larger compared with the ISC26 and ISC44 scenarios.

As pointed out in earlier sections there is uncertainty related to the results from the simulations. The methodology used in this research, was to first calibrate the GUHM for the current situation (ISC26) and afterwards simulate snow melt and runoff for five other land use scenarios. The results showed that SCA and SWE were reduced in all the five scenarios with ISC equal to or above 26 % compared to when Risvollan was simulated as an area consisting mainly of sparsely vegetated park areas (ISC0). In chapter 7 it was shown that there existed several points in the parameter space that all gave good results for the simulation of SWE and snow melt intensity for the data from the lysimeter at Risvollan. There is no reason to believe that this is not the case for the application of the GUHM to the Risvollan catchment. One can therefore question if the difference in SCA and SWE between the six scenarios are sensitive to the chosen point in the parameter space, found by the calibration. In LCT road and roof the snow surface roughness ($roadz_0$ and $roofz_0$) were calibrated to 0.01 m, which is large compared to the snow surface roughness in LCT park (0.0012 m). It is likely that these parameters could have been higher or lower and the calibration results in the ISC26 case would still have been good. Thus, the difference in SCA and SWE between the six scenarios is sensitive to the calibration of the model. In addition to this the simulation results will also be dependent on the model structure. As mentioned earlier neither snow drift or effects of frozen soils are simulated in the GUHM, and therefore the results have uncertainties related to them. Because of this the results from the analysis of AA influence on snow distribution and melt using only the GUHM should be viewed as additional evidence to the results found in chapter 5 and 6. In those chapters evidence of AAs influence on SWE and SCA in the urban environment was found by field observations.

8.4 Conclusions

The GUHM was used to simulate snow accumulation, melt and runoff for six different land use scenarios for the Risvollan catchment. The six scenarios (ISC0, ISC26,..,ISC44), had varying degree of impervious surface cover (buildings and roads), ranging from 0 to 44 %.

SCA was shown to rapidly be lowered to between 50 % and 74 % during melt situations depending on the degree of AA compared to the scenario (ISC0) where Risvollan was simulated as an catchment containing only park areas. This difference was attributed to clearing of snow from roads to nearby areas, and high snow melt rates on roads, roofs, snow deposits and areas nearby building walls. The average SCA for February, March and April was around 35 % lower for the scenario with highest cover of impervious surfaces (44 %), compared to the scenario simulated with no influence of AA.

It was shown that for a large part of the winter season the ISC0 scenario had about 35 % and 50 % larger SWE than in the ISC26 and ISC44 scenarios, respectively. This was explained by the extra energy available in urbanized areas compared to rural ones, which enhances snow melt and therefore lowers SWE.

The major effect of AA on snow distribution and melt in the Risvollan catchment was shown to be early and enhanced melt as a result of increase in the snow pack energy availability, due to urbanization. More runoff will be produced in January to March compared to in April because of early melt in the urbanized parts.

The simulation results showed a linear relationship between coverage of impervious surfaces and catchment runoff. Both runoff ratio and peak flow values was shown to grow with increasing degree of impervious surface coverage. The simulated annual runoff ratio for the Risvollan catchment was shown to increase from 55 % to 69 % when the ISC was increased from 0 to 44 %.

Chapter 9

Summary and conclusions

9.1 Summary

In urban cold climates snow melt runoff influence both flood frequencies and CSO discharge in urban storm water systems. Despite this, current design practices in Norway assume that it is rainfall runoff mechanisms that generate the highest annual peak flows in urban drainage systems. Although numerous and comprehensive studies of rural snow hydrology have been carried out the effort put into studying urban snow processes are limited.

In this work focus was put on studying the effects of AA on snow distribution and melt in the urban environment. More specifically this was how the presence and operation of roads and buildings influence snow melt rates and snow distribution in the cities.

A literature review on urban snow hydrology was presented in chapter 2. Several authors reported that albedo of urban snow packs will be more rapidly lowered compared to snow located in more untouched terrain. The low albedos, typically found in piled snow or snow packs nearby roads, increases snow melt intensity. It was also argued that the net radiation balance of urban snow packs can be altered by the presence of buildings. It was also debated that the natural variability of urban snow packs is further enhanced by AA, where snow clearing of roads was an important process to consider in such a context.

Several urban snow melt models were presented through the cited literature. Examples of degree-day based and more complex energy balance

based snow melt simulations, carried out for urban areas were cited. The various models had only to a limited degree been tested against catchment representative observations of SWE and SCA data. Runoff was most often used as an indicator of the snow melt models performances. Only a few researchers reported results where an urban snow melt model had been tested for whole seasons and run with a temporal resolution of 1 hour or less. It was argued that this should be done to avoid problems with initialization and long term memory in the models. It was debated that an urban hydrological model should try to model as many as possible of the AA influencing snow distribution and melt in the urban environment.

One of the objectives in this work was to develop an urban hydrological model specially designed to deal with urban snow melt calculations. Chapter 3 presented the gridded urban hydrological model (GUHM). The principal idea of the GUHM was to subdivide and urban catchment into equal area orthogonal grid cells. For each grid cell meteorological data were used to calculate a time series of SWE, rain and snow melt, etc, carried out in the snow melt routine using an energy balance approach. A soil-runoff routine used the output from the snow routine to calculate runoff from each cell. Catchment runoff was calculated as the sum of runoff from all cells. Currently, GUHM has no pipe flow module, but can be coupled with existing public domain or proprietary models if desired. In GUHM, each grid cell could be one out of five possible LCTs road, roof, deposit, wall, and park. All LCTs used the same snow and soil-runoff routine but for LCT, wall, road, roof and deposit, changes were made in the snow routine depending on the dominating AA. Grid cells of type roof represented building rooftops. In this LCT, wind speed was corrected following a logarithmic wind profile adjusted for the difference between instrument height above ground and the height of the building rooftops. Inside heating of buildings contributes to an increased heat flux into the snow through heat conduction. In GUHM the user must specify the magnitude of this flux named Q_{g-roof}. Snow clearing procedures was also accounted for in the GUHM. To model this effect the LCT road was only allowed to accumulate SWE up to a user specified threshold level, before it was relocated to the nearest grid cell of LCT deposit. All LCTs used user specified albedo decay curves that expresses albedo as a function of time since last snow fall. Grid cells of LCT wall were located adjacent to the roof grid cells. In the snowmelt simulations the snow pack in these cells were given an extra user specified

energy input, to account for effects of increased long wave radiation from surrounding buildings, and lowered effective albedo as a result of multiple reflections between snow pack and building walls. Grid cells of LCT park represented park/garden areas. No specific changes in the snow routine were done for these cells. The GUHM needs a time series of air temperature, precipitation, shortwave radiation, relative humidity and wind speed to run.

The Risvollan urban catchment was used as the study area in this work and was presented in chapter 4. It is located about 4 km southeast of Trondheim city (Norway) and is a 20 ha residential area. It consists of 26 % impervious surfaces (13 % roofs and 13 % paved areas) and 74 % grass lawn and park areas. At the downstream end of the catchment, Risvollan hydrological and meteorological station is situated. Data from Risvollan and the nearby Voll meteorological station was used in this research.

In chapter 5 a technique for observing time series of SCA for an urban catchment was presented. The purpose of the SCA observations was to a) identify differences in SCA between three land cover types (road, roof and park), and b) use the observed time series of SCA to calibrate and validate the GUHM. The method was based on image processing and ANN technology and was verified against SCA estimated from aerial photos. It was shown that SCA on roads and roofs were in general more rapidly lowered than in park areas of the Risvollan catchment. This was explained by snow clearing of snow from roads to nearby areas, and strong snow melt on roofs and roads. A time series of SCA for the three winter periods (2000-2003) was observed for the Risvollan urban catchment.

Chapter 6 presented results from field observations of SWE in the Risvollan catchment. The purpose of collecting the SWE data was to identify differences in mean aerial SWE within four land cover types (road, roof, deposit, park) and use these data during calibration and validation of the GUHM. Observations were carried out in 9 different snow courses in the Risvollan catchment during 2000 - 2003. It was shown that the LCT deposit and road had the highest and lowest SWE values, respectively. For the 2001 to 2002 winter season it was shown that the areal mean SWE was 36 % and 45 % lower in the LCTs mostly influenced by AA at the middle and end of the winter season, compared to in the LCT park. This was attributed to the extra energy availability, due to lower albedos, roof heat conduction, etc. in LCT road, deposit and roof.

The field observations showed that SWE and SCA are more rapidly lowered in the LCTs most heavily influenced by AA. The LCTs road and roofs become more rapidly snow free compared to LCT park. This was explained to be an effect of snow clearing procedures, snow drift from roofs to nearby areas, locally low albedo, in addition to heat release from the roofs themselves.

In chapter 7, the GUHM snow routine was tested against point data from the snowmelt lysimeter at Risvollan station for the period from Oct 1994 to May 1995. Observations of SWE and snowmelt intensity were used to calibrate the GUHM snow routine. Both simulated SWE and snow melt intensity matched the observed data ($R^2_{swe} = 0.97$, $R^2_{melt} = 0.78$) quite well. The results from the point simulations showed that the GUHM snow routine was capable of simulating snow accumulation and melt for whole seasons with short time steps (1 hour) without updating the SWE states during the winter season.

The GUHM was also applied and calibrated for the Risvollan catchment for a three year period. Two winter seasons were used as validation period. The results showed that the GUHM was able to simulate snow accumulation, melt and spatial variation in SWE and SCA, for whole seasons with short time resolution, with satisfactory results. Comparison between observed and simulated SWE and SCA showed that the overall trends were captured by GUHM but for some shorter periods the simulated signals were outside the uncertainty range of the observed data (SWE, SCA). This was explained to be a result of too few calibration runs and limitations in the GUHM model structure. For example snowdrift from rooftops into nearby areas was not taken into consideration. The runoff simulations matched the observed data quite well. The R^2 value for the calibration period (June 1999 to May 2002) was 0.72 and 0.88 for the validation period (June 1998 to May 1999 and June 2002 to May 2003). This was based on an aggregated time series from 1 hour to 24 hours. For some periods in the spring a discrepancy between simulated and observed runoff data was seen. The plausible reasons for this was attributed to the calibration of both the snow melt and soil-runoff routine in the GUHM, which could have been improved.

Chapter 8 presented results where the GUHM was used to quantify the effects of AA on snow distribution and melt in the Risvollan catchment. This was carried out by running the GUHM for six different land use scenarios (ISC0, ISC26,..,ISC44), with varying degree of impervious surfaces

(buildings and roads). Simulated runoff was also used as an indicator to quantify effects of AA on urban snow packs.

SCA was shown to rapidly be lowered to between 50 % and 74 % during melt situations depending on the degree of AA compared to the scenario (ISC0) where Risvollan was simulated as an untouched rural catchment. This difference was attributed to clearing of snow from roads to nearby areas, and high snow melt rates on roads, roofs, snow deposits and areas nearby building walls. The average SCA for February, March and April was around 35 % lower for the scenario with highest cover of impervious surfaces (44 %), compared to the scenario simulated with no influence of AA. It was shown that for a large part of the winter season the ISC0 scenario had about 35 % and 50 % larger SWE than in the ISC26 and ISC44 scenarios, respectively. This was explained by the extra energy available in urbanized areas compared to rural ones, which enhances snow melt and therefore lowers SWE.

The overall effect of AA on snow distribution and melt in the Risvollan catchment was shown to be early and enhanced melt as a result of increase in the snow pack energy availability, due to urbanization. More runoff will be produced in January to March compared to in April because of early melt in the urbanized parts.

The simulation results showed a linear relationship between coverage of impervious surfaces and catchment runoff. Both annual runoff ratio and peak flow values was shown to grow with increasing degree of impervious surface coverage. The simulated annual runoff ratio for the Risvollan catchment was shown to increase from 55 % to 69 % when the ISC was increased from 0 to 44 %.

9.2 Main conclusions

A new gridded urban hydrological model (GUHM), specially designed to deal with urban snow melt calculations, was developed as part of this research. The snow model structure include processes such as snow clearing of roads, locally low albedos, roof heat conduction, modified wind speeds on rooftops in addition to effects of slope, aspect and shadowing from buildings and terrain. The model can be used as an all year surface hydrology model in urban cold climates to simulate rain and snow melt runoff with

short time resolution (<1h).

A method for observing SCA for an urban catchment was developed. A digital camera mounted on a tall building recorded time series of images, which was later analysed with a feed forward ANN to generate a time series of SCA for the Risvollan catchment. Snow water equivalent was measured in 9 different snow courses in the Risvollan catchment during the period from 2000 to 2003 and included measurements within four different LCTs (road, roof, deposit and park).

The field observations in the Risvollan catchment showed that SCA and SWE are more rapidly lowered in the LCTs most heavily influenced by AA compared to the untouched park areas. The explanation for this was attributed to snow clearing of roads, snow drift of snow from rooftops to nearby terrain and high melt rates in the LCTs road, roofs and deposit. The high melt rates was explained to be a result of low albedos on roads and deposits, rooftop snow packs exposure to wind and solar radiation, in addition to heat release from the roof themselves.

The GUHM was applied to the Risvollan catchment for the period June 1998 to June 2003. The model was calibrated for the period June 1999 to May 2002 and the simulated SCA, SWE and runoff was compared with observed data. The modelling time step was set to 1 hour and the grid cell resolution was 2x2 metre. The results showed that the model was capable of reproducing the SCA, SWE and runoff with satisfactory results for both the calibration and validation period.

The GUHM was used to quantify effects of AA on snow distribution and melt for six different land use scenarios in the Risvollan catchment for the period June 1998 to June 2003. The modelling results showed that when the area coverage of buildings and roads increase, the SCA and SWE will be more rapidly lowered during melt periods. Because of this more runoff will be produced in the early winter season (Jan-March) compared to if the catchment had been covered with only park areas. Since urbanization increase the impervious surface cover in a catchment the peak and volume runoff will also increase.

Chapter 10

Future work

This research investigated effects of AA on snow distribution and melt in the urban environment. SWE and SCA were observed in the field and documented several forms of AA that influences the urban snow pack, e.g. snow clearing, increased melt intensity in various LCTs, etc.

Several questions remain unanswered and should be addressed in future work. It was argued that random sampling, for the purpose of avoiding bias, of observed SWE in the urban environment, was difficult to carry out. This is clearly a problem that must be solved if the uncertainties in the observations are to be correctly assessed and maybe lowered. One possible solution could be to sample many more points in each LCT than was conducted in this work. Afterwards, random selection of a small number of samples can be drawn from the collected data, and uncertainty in just taking a few samples can be assessed.

Remote sensing (space and air borne) technologies is clearly a field which should be used more within studies of urban snowmelt processes. Although it was argued that the spatial and temporal resolution is still too course, low repeat cycles when the spatial resolution is high and vica versa, there are indications that the resolution of these data is constantly being improved. For example Norman et al. (2003) showed an example of how surface energy fluxes, especially ET, could be estimated with remote sensing technology at 10 meter spatial resolution. In the future, it should be investigated if SWE and SCA can be remotely sensed in urban areas at the appropriate spatial resolution, say 1 to 5 metres. Such data can be used to better understand the spatial and temporal distribution of urban

snow packs and be used for calibration and validation purposes of urban hydrological models.

Future research with the digital-camera-ANN technology could benefit, if a more robust camera was used. Better heating and communication software could insure a higher capture rate of images throughout the winter season. It should also be tested if the methodology could be used to detect SCA for other LCTs such as, areas piled with snow and areas close to building walls.

Further investigations on urban wind fields and how to calculate the turbulent heat fluxes should be carried out. In addition it should be investigated how the buildings influence the accumulation patterns (snow drift) and how these effects can be included in an urban hydrological model.

The GUHM did not take into account possible effects of frozen soils on peak runoff. This process might also influence the flood frequency in urbanized catchments as well as in rural ones and is a field that deserves attention.

In the future GUHM can be calibrated even better for the Risvollan catchment. A comprehensive residual study of the results can also be carried out to try to further explain why or why not the GUHM was working as it did. The uncertainties in the modelling results from the GUHM could possibly also be assessed through a sensitivity analysis of the parameter space in GUHM.

References

Anderson, E. A. (1976), 'A point energy and mass balance model of a snow cover', NOAA Technical Report NWS 19. Office of Hydrology, National Weather Service, Silver Spring, Md, U.S. Department of commerce, National Oceanic and Atmospheric Administration.

Arnfield, A. J. (2003), 'Review two decades of urban climate research: a review of turbulence, exchange of energy and water, and the urban heat island', *International Journal of Climatology* **23**, 1–26.

Bales, R. C. & Harrington, R. F. (1995), 'Resent progress in snow hydrology', *Reviews of Geophysics, Supplemental* pp. 153–161. U.S. National report to international unioun of geodesy and geophysics 1991-1994.

Bang, B., Nielsen, A., Sundsbø, P. A. & Wiik, T. (1994), 'Computer simulation of wind speed, wind pressure and snow accumulation around buildings (snow-sim)', *Energy and Buildings* **21**(Issue 3), 235–243.

Bartosova, A. & Novotny, V. (1999), 'Model of spring runoff quantity and quality for urban watersheds', *Journal of Water Science and Technology* **39**(12), 249–256.

Beighley, R. E. & Moglen, G. E. (2002), 'Trend assessment in rainfall-runoff behavior in urbanizing watersheds', *Journal of Hydrologic Engineering* **7**(1), 27–34.

Bengtsson, L. & Semádeni-Davies, A. (2000), Theoretical background, Technical Report 40, UNESCO, IRTCUD, Paris. Chapter 1 in: Ur-

ban Drainage in Specific Climates. Vol II. Urban Drainage in cold climates, IHP-V Technical Documents in Hydrology. Chief Editor: C. Maksimovic.

Bengtsson, L. & Singh, V. P. (2000), 'Model sophistication in relation to scales in snowmelt runoff modeling', *Nordic Hydrology* **31**(4/5), 267–286.

Bengtsson, L. & Westerström, G. (1992), 'Urban snowmelt and runoff in northern Sweden', *Hydrological Sciences Journal* **37**(3,6/1992), 263–275.

Bengtsson, L. (1981), Snowmelt-generated runoff in urban areas. Second International Conf. on Urban Storm Drainage, Urbana, Illinois, USA June 14-19, pp 444-451.

Bengtsson, L. (1984), Modelling snowmelt induced runoff with short time resolution. Third International Conference on urban storm drainage, Göteborg, Sweden June 4-8, pp 305-314.

Bergström, S. & Forsman, A. (1973), 'Development of a conceptual deterministic rainfall-runoff model', *Nordic Hydrology* (4), 147–170.

Bergström, S. (1976), 'Development and application of a conceptual runoff model for Scandinavian catchments.'. Department of Water Resources Engineering. Lund Institute of technology.

Beven, K. (1993), 'Prophecy, reality and uncertainty in distributed hydrological modelling', *Advances in Water Resources* **16**, 41–51.

Brandt, J. & Torgersen, G. (1994), 'Snowmelt in urban areas. in Norwegian: Snøsmelting i urbane strøk.'. Report from project work spring 1994, Prosjekt oppgave i VAR teknikk våren 1994. Institutt for vassbygging, NTH.

Bras, R. L. (1990), *Hydrology - an introduction to hydrologic science*, Addison-Wesley publishing company, Massachutes Institute of Technology. ISBN 0-201-05922-3.

Bruland, O. & Killingtveit, A. (2002), 'An energy balance based HBV-model with application to an Arctic watershed on Svalbard, Spitsbergen', *Nordic Hydrology* **33**(2-3), 123–144.

Brunvold, E. (2000), 'Simulation of urban snowmelt runoff using SWMM. Analysis of the floods March 31, 1997 in the Risvollan and Fredlybekken catchments.'. MSc report. In Norwegian. Norwegian University of Science and Technology, Department of hydraulic and environmental engineering. Trondheim, Norway, Ref no. D1-2000-29.

Buttle, J. M., Sami, K. & Xu, F. (1990), Resolution of data limitations facing snowmelt runoff modelling in suburban areas. Proceedings of the International Conference on Urban Drainage Under Wintry Conditions, Narvik, Norway.

Buttle, J. M. & Xu, F. (1988), 'Snowmelt runoff in suburban environments', *Nordic Hydrology* **19**, 19–40.

Buttle, J. M. (1986), Snow accumulation patterns and snowmelt runoff in a suburban environment. Proc. Eastern Snow Conference.

Buttle, J. M. (1990), 'Effects of suburbanization upon snowmelt runoff', *Hydrological Sciences* **35**(3, 6/1990), 285–302.

Byggforsk (1998), 'U-verdier for eldre konstruksjoner før og etter isolering'. Technical report in Norwegian, Heat transmission (U-values) for older buildings before and after insulation, Utbedring og ombygging. Bygninskonstruksjoner. Byggforskserien Byggforvaltning 720.012.

Chow, V. T., Maidment, D. R. & Mays, L. W. (1988), *Applied Hydrology*, 1 edn, McGraw-Hill Inc. ISBN 0-07-010810-2.

Conway, H., Gades, A. & Raymond, C. F. (1996), 'Albedo of dirty snow during conditions of melt', *Water Resources Research* **32**(No. 6), 1713–1718.

Dalsbø, G. A. (2003), 'Personal communication'. Norwegian Meteorological Institute.

Davies, R. E., Mckenzie, J. C. & Jordan, R. (1995), 'Distributed snow process modelling: an image processing approach', *Hydrological Processes* **9**, 865–875.

DeVries, J. J. & Hromadka, T. V. (1992), *Computer models for surface water*, McGraw Hill Inc. Chapter 21 in Handbook of Hydrology, ISBN 0-07-039732-5.

DHI (2000), 'MOUSE version 2000, short introduction and tutorial', Manual published by Danish Hydraulic Institute(DHI). Dated 25-march-2000, see also http://www.dhisoftware.com/mouse/.

Dozier, J. (1987), 'Resent research in snow hydrology', *Reviews of Geophysics* **25**(No. 2), 153–161. U.S. National report to international unioun of geodesy and geophysics 1983-1986.

Fily, M., Dedieu, J. P. & Surdyka, S. (1995), 'A SAR image study of a snow-covered area in the French alps', *Remote Sensing Environment* **51**, 253–262.

Gallant, S. I. (1993), *Neural network learning and expert systems*, The MIT Press. Massachutes Institute of Technology, Textbook, ISBN 0-262-07145-2, 365 p.

Govindaraju, R. S. (2000*a*), 'Artificial neural networks in hydrology. II: Hydrologic applications', *J. of Hydrologic Engineering* **5**(2). Paper no 19091.

Govindaraju, R. S. (2000*b*), 'Artificial neural networks in hydrology. I: Preliminary concepts', *J. of Hydrologic Engineering* **5**(2). Paper no 19090.

Granger, R. J., Pomeroy, J. W. & Parviainen, J. (2002), 'Boundary-layer integration approach to advection of sensible heat to a patchy snow cover', *Hydrological Processes* **16**, 3559–3569.

Gray, D. M. & Male, D. H., eds (1982), *Handbook of Snow, Principles Processes Management and Use*, Pergamon Press Canada Ltd. ISBN 0-08-025375-X.

Gray, D. M. & Prowse, T. D. (1992), *Snow and floating ice. Handbook of hydrology Ch. 7*, McGraw Hill Inc. ISBN 0-07-039732-5.

Gustafsson, L. G. (1995), 'Utveckling och tillämpning av en konceptuell avrinningsmodell för urban hydrologi'. Report Series A:25 Department of Hydraulics. Chalmers University of Technology. Göteborg, Sweden. In Swedish, summary in English. ISSN 0348-105.

Hall, D. K., Solberg, R. & Riggs, G. A. (2002), Validation of satellite snow cover maps in North America and Norway, *in* 'Proceedings of the 59th Eastern Snow Conf.'. 5-7 June, Stowe, VT, USA.

Hanssen, S. O., Thue, J. V., Wangensteen, I., Gjerstad, F., Novakovic, V. & Sjøvold, O. (1992), *ENØK I BYGNINGER*, Universitetsforlaget AS. Textbook on energy economics of buildings, in Norwegian. ISBN 82-00-40909-0.

Hernebring, C., Gustafsson, L. G. & Westerström, G. (1994), Modelling of flow components in sewer systems influenced by snow melt processes using the MouseNam concept, *in* S. Lyngfelt & G. Svensson, eds, 'Proceedings of the International User-Group Meeting on Computer Aided Analysis and Operation in Sewage Transport and Treatment Technology. IUGM-1994'. Chalmers University of Technology, Meddelande nr 95. Göteborg, Sweden.

Hernebring, C., Marklund, S. & Gustafsson, L. G. (1997), 'Modelling of flow components in sewer systems influenced by snow melt processes using the MouseNam concept', 2nd DHI Software User Conference, Helsingør, Denmark.

Hernebring, C. (1996), Snowmelt induced runoff in sewer systems, snösmältningspåverkan på avloppssystem inom urbana områdan., Technical Report Forsk Publ 1996-07, VAV-VA, Sweden. In Swedish, abstract in English, ISSN 1102-5638.

Hillel, D. (1987), 'Modelling in soil physics: a critical review', *Soil Science Society of America* pp. 35–42. in: Boersma, L.I: (ed.): Future developments in soil science research. 1936-1986 Golden Anniversary contributions, Madison, Wis.

Ho, C. L. I. & Valeo, C. (2003), 'Observations of urban snow processes', *Hydrological Processes* . Article IN PRESS, manuscript received from

Caterina Valeo, Email: valeo@geomatics.ucalgary.ca, University of Calgary. Canada, 1 Oct 2003.

Huber, W. C. & Dickinson, R. E. (1992), 'Storm Water Management Model, SWMM. version 4, users manual'. EPA/600/3-88/001a, NTIS PB88-236641/AS.

Ichinose, T., Shimodozono, K. & Hanaki, K. (1999), 'Impact of anthropogenic heat on urban climate in Tokyo', *Atmospheric Environment* **33**, 3897–3909.

Iqbal, M. (1983), *An Introduction to Solar Radiation*, Academic Press, Toronto. 390 pages, ISBN: 0-12-373750-8, 0-12-373752-4.

Islam, S. & Kothari, R. (2000), 'Artificial neural networks in remote sensing of hydrologic processes', *Journal of hydrologic engineering* **5**(2). Paper no. 19089.

ISO1438 (1980), 'Water flow measurement in open channels using weirs and venturi flumes - part 1: Thin-plate weirs.', Ref. No. ISO 1438/1-1980(E). First edition - 1980-04-15.

Jordan, R. (1991), 'A one dimensional temperature model for a snow cover. technical documentation for SNTHERM.89', Special Report 91-16. U.S: Army Corps of Engineers, Cold Regions Research & Engineering Laboratory.

Kang, I. S., Park, J. I. & Singh, V. P. (1998), 'Effect of urbanization on runoff characteristics of the On-Cheon Stream watershed in Pusan, Korea', *Hydrological Processes* **12**, 351–363.

Kidder, S. Q. & Wu, H. T. (1987), 'A multispectral study of the St. Louis area under snow-covered conditions using NOAA-7 AVHRR data', *Remote sensing of the environment* **22**, 159–172.

Killingtveit, Å., Rinde, T., Markhus, E., Bostrøm, T., Furuberg, T., Sœgrov, S. & Milina, J. (1994), Application of a semi-distributed urban hydrology model, *in* 'Nordic Hydrologic Conference', Nordic Association for Hydrology. NHP-Report No. 34, ISBN 87-89813-13-8, ISSN 0900-0267, 2-4 Aug Tórshavn Faroe Island.

Killingtveit, Å. & Sœltun, N. R. (1995), *Hydrology*, Vol. 7 of *Hydropower development*. Norwegian Institute of technology, Division of Hydraulic Engineering, ISBN 82-7598-026-7.

Killingtveit, Å. (1998), 'Analysis of precipitation patterns in Trondheim. final report. (In Norwegian) analyse av nedbørfordeling i Trondheim, sluttrapport.'. Institutt for vassbygging, IVB-rapport B1-1998-2.

Lei, J. H. (1996), Uncertainty analysis of urban rainfall - runoff modelling, PhD thesis, The Norwegian University of Science and Technology. Department of Hydraulic and Environmental Engineering. August, Trondheim, Norway, ISBN 82-7119-966-8.

Lillesand, T. M. & Kiefer, R. W. (1987), *Remote sensing and image interpretation*, John Wiley & Sons Inc, New York. Second edition, ISBN 0-471-85462-X, 721 p.

Liston, G. E. (1995), 'Local advection of momentum, heat and moisture during the melt of patchy snow covers', *J. Appl. Meteorol.* **17**, 1833–1842.

Maksimovic, C. & Thorolfsson, S. T. (1990), Effect of regional climate conditions on rainfall-runoff process in urban catchments: the case of snowy surfaces, *in* 'International symposium on regionalisation in hydrology'. Ljublana, Yugoslavia, 23-26 April.

Maksimovic, C. (2000), General overview of urban drainage principles and practice, Technical Report 40, UNESCO, IRTCUD, Paris. Chapter 0 in: Urban Drainage in Specific Climates. Vol II. Urban Drainage in cold climates, IHP-V Technical Documents in Hydrology.

Marchand, W. D., Bruland, O. & Killingtveit, Å. (2001), 'Improved measurements and analysis of spatial snow cover by combining a ground based radar system with a differential global positioning system receiver.', *Nordic Hydrology* **32**(3), 181–194.

Marchand, W. & Killingtveit, Å. (2003), 'Statistical properties of spatial snow cover in mountainous catchments in norway', *Nordic Hydrology* . Accepted for publication. Article is part of Ph.D. thesis published

at NTNU, Department of hydraulic and environmental engineering, ISBN 82-471-5616-4, .

Marsalek, J., Oberts, G., Exall, K. & Viklander, M. (2003), 'Review of operation of urban drainage systems in cold weather: Water quality considerations', *Water Science and Technology* **48**(9), 11–20.

Marsalek, J. (1991), Urban drainage in cold climate: Problems, solutions and research needs, *in* C. Maksimovic, ed., 'New technologies in urban drainage UDT 91', ELSEVIER APPLIED SCIENCE London and New York. Dubrovnik, Yugoslavia 17-21 June.

Marsh, P. (1999), 'Snowcover formation and melt: recent advances and future prospects', *Hydrological Processes* (13), 2117–2134.

Matheussen, B. V., Kirschbaum, R. L., Goodman, I. A., ODonnell, G. M. & Lettenmaier, D. P. (2000), 'Effects of land cover change on streamflow in the interior columbia river basin (usa and canada)', *Hydrological Processes* **14**, 867–885.

Matheussen, B. V. & Thorolfsson, S. T. (1999), Simulation errors due to insufficient temporal resolution in urban snowmelt models, *in* I. Joliffe & J. Ball, eds, 'The 8th International Conference on Urban Storm Drainage (8ICUSD)', Vol. 4. pp 2107-2114, 30 August - 3 September, Sydney, Australia, ISBN 0 85825 718 1.

Matheussen, B. V. (1996), 'Studier av snøsmelting og vinteravrenning i Risvollan forskningsfelt. Studies of snow melt and winter runoff in Risvollan research catchment.', Master Thesis in Norwegian. Hovedoppgave i overvannsteknologi, NTNU, Institutt for vassbygging. D1-1996-25.

McMurter, D. G. (1976), Ground snow distribution and spring runoff in a partially urbanized basin, *in* 'Eastern Snow Conference'. (33), pp 163-177.

Melloh, R. A., Hardy, J. P., Davis, R. E. & Robinson, P. B. (2001), 'Spectral albedo/reflectance of littered forest snow during the melt season', *Hydrological Processes* **15**, 3409–3422.

Melloh, R. A. (1999), 'A synopsis and comparison of selected snowmelt algorithms', CRREL REPORT 99-8. US Army Corps of Engineers, Cold Regions Research and Engineering Laboratory, http://www.crrel.usace.army.mil/, pp 1-17.

Michalsky, J. (1988*a*), 'The astronomical almanac's algorithm for approximate solar position (1950-2050).', *Solar Energy* **40**(3), 227–235.

Michalsky, J. (1988*b*), 'Errata: The atronomical almanac's algorithm for approximate solar position (1950-2050)', *Solar Energy* **41**(1), 113.

Milina, J., Sœgrov, S., Selseth, I., Schilling, W. & Markhus, E. (1999), Effect of urbanization on storm water runoff, *in* '8th International Conference on Urban Storm Drainage 8ICUSD', Vol. 4. 30 Aug - 3 Sept, Sydney, Australia, ISBN 0 85825 718 1, pp 1616-1624.

Mosevoll, G., Wedum, K. & Sœgrov, S. (1991), Håndbok i vannføringsmålinger i vann- og avløpsanlegg., Technical report, SINTEF Norsk hydroteknisk laboratorium. Tech. report in Norwegian. Handbook in discharge measurements within storm/sewer systems.Report nr STF60A91046.

Nilssen, O. & Bjørgum, F. (2001), 'Presentation in Norwegian: Problems and challenges in storm water runoff for the city of Trondheim.', National meeting: Storm water technology in Norway. - New challenges. Fagmøte Norsk Hydrologiråd, NORVAR. Gardermoen, Oct.

Noilhan, J. (1981), 'A model for the net total radiation flux at the surfaces of a building', *Building and Environment* **16**(4), 259–266.

Norman, J. M., Anderson, M. C., Kustas, W. P., French, A. N. & Mecikalski, J. (2003), 'Remote sensing of surface energy fluxes at 10^1-m pixel resolution', *Water Resources Research* **39**(8), SWC 9, 1–17.

NS-EN752-4 (1998), 'NS-EN 752-4, Drain and sewer systems outside buildings. Part 4: Hydraulic design and environmental considerations'. Norsk standard, 1. utgave, Engelsk versjon.

Oberts, G. L. (1990), Design considerations for management of urban runoff in wintry conditions, *in* 'Proc. Int. Conf. on Urban Hydrology under Wintry Conditions'. Narvik, Norway, March 19-21.

Oberts, G. L. (1994), 'Influence of snowmelt dynamics on stormwater runoff quality', *Watershed Protection Techniques* **1**(2), 16–22.

Oberts, G. L. (2003), Cold Climate BMPs: solving the management puzzle, *in* '1st International Conference on Urban Drainage and Highway Runoff in Cold Climate'. 25-27 March, Riksgr̊ansen, Sweden.

Oke, T. R. (1988), 'The urban energy balance', *Progress in physical geography* **12**, 471–508.

Oveland, T. A. (1995), 'PINE as an urban hydrologic simulation tool. PINE som urbanhydrologisk simuleringsverktøy'. MSc report. In Norwegian. The Norwegian Institute of Technology, Department of hydraulic and environmental engineering. Trondheim, Norway, Ref no. D1-1995-18.

Pomeroy, J. W. & Gray, D. M. (1995), *Snowcover. Accumulation, relocation and management*. National Hydrology Research Institute Science Report No. 7, NRHI 11 Innovation Boulevard, Saskatoon, Saskatchewan, Canada S7N 3H5, ISBN 0-660-15816-7.

Refsgaard, J. C. & Storm, B. (1996), *Distributed Hydrological Modelling, Ch 3, Construction, Calibration and Validation of Hydrological Models*, Vol. 22, Kluwer Academic Publishers. Water Science and Technology Library, ISBN 0-7923-4042-6.

Refsgaard, J. C. (1996), *Distributed Hydrological Modelling, Ch 2, Terminology, modelling protocol and classification of hydrological model codes*, Vol. 22, Kluwer Academic Publishers. Water Science and Technology Library, ISBN 0-7923-4042-6.

Rinde, T. (1998), A flexible hydrological modelling system developed using an object orientated methodology, PhD thesis, Norwegian University of Science and Technology, Department of hydraulic and environmental engineering. IVB-rapport B2-1998-3, Trondheim, Norway.

Risholt, L. P. (2000), Pollution based real time control of urban drainage systems, PhD thesis, Norwegian University of Science and Technology, NTNU. Department of hydraulic and environmental engineering. Trondheim, Norway. ISBN 82-7984-062-1, ISSN 0802-3271.

RReDC (2000), 'Solar radiation resource information,solar position and intensity, solar codes & algorithms, NREL's SOLPOS, february 2000', Website: http://rredc.nrel.gov/solar/codesandalgorithms/solpos/ and http://www.nrel.gov/. C code distributed on the internet. Renewable Resource Data Center (RReDC) Department of Energy's Office of Energy Efficiency and Renewable Energy. Electric and Hydrogen Systems Center. National Renewable Energy Laboratory (NREL) 1617 Cole Blvd, Golden, CO, USA.

Ruffieux, D. (1995), 'Winter surface energy budget in Denver Colorado', *Atmospheric Environment* **9**(No 13), pp. 1579–1587.

Sætern, A. I. (2002), 'Tiltaksanalyse vha urbanhydrologisk modell. studieområde: Fredlybekken feltet i Trondheim', Master Thesis in Norwegian. Hovedoppgave i overvannsteknologi, NTNU, Institutt for vassbygging. D1-2002-06.

Sand, K. (1990), Modeling snowmelt runoff processes in temperate and arctic environments, PhD thesis, NTH, The University of Trondheim, The Norwegian Institute of technology, Division of hydraulic and sanitary engineering. IVB-Rapport B-2-1990-1, ISBN 82-7119-219-1.

Schilling, W., Lei, J., König, A., Milina, J., Selseth, I. & Sægrov, S. (1998), Integrated model of the trondheim hvringen wastewater system- phase 2., Technical Report nr, SINTEF Civil and environmental engineering, N-7034 Trondheim. Technical report, ISBN 82-14-00328-8.

Schmugge, T. J., Kustas, W. P., Ritchie, J. C., Jackson, T. J. & Rango, A. (2002), 'Remote sensing in hydrology', *Advances in water resources* **25**, 1367–1385.

Semádeni-Davies, A. & Bengtsson, L. (1998), 'Snowmelt sensitivity to radiation in the urban environment', *Hydrological Sciences Journal* **43**(1), 67–89.

Semádeni-Davies, A. & Bengtsson, L. (2000), Snow and snowmelt, Technical Report 40, UNESCO, IRTCUD, Paris. Chapter 2 in: Urban Drainage in Specific Climates. Vol II. Urban Drainage in cold climates, IHP-V Technical Documents in Hydrology.

Semádeni-Davies, A. F. & Matheussen, B. V. (2003), Progress in urban snow hydrology (1990-2003): fom Narvik to Riksgrånsen, *in* '1st International Conference on Urban Drainage and Highway Runoff in Cold Climate', IWA, IAHR, AIRH, Luleå University of Technology. 25-27 March, Riksgränsen Sweden.

Semádeni-Davies, A. F. (1999*a*), Urban Snowmelt Processes, Modelling and Observation, PhD thesis, Lund Institute of Technology, Lund University, Sweden, Department of Water Resources Engineering. ISSN 1101-9824.

Semádeni-Davies, A., Lundberg, A. & Bengtsson, L. (2001), 'Radiation balance of urban snow: a water management perspective', *Cold Regions Science and Technology* **33**, 59–76.

Semádeni-Davies, A. (1998), 'Modelling snowmelt induced waste water inflows', *Nordic Hydrology* **29**(4/5), 285–302.

Semádeni-Davies, A. (1999*b*), 'Snow heterogeneity in Luleå, Sweden', *Urban Water* **1**, 39–47.

Semádeni-Davies, A. (2000), 'Representation of snow in urban drainage models', *Journal of Hydrologic Engineering* **5**(4), 363–370. Paper no. 19154.

Shuttleworth, W. J. (1993), *Evaporation*, McGraw-Hill. Chapter 4 in Handbook of hydrology, ISBN 0-07-039732-5.

Simpson, J. J. & McIntire, T. J. (2001), 'A recurrent neural network classifier for improved retrievals of areal extent of snow cover', *IEEE Transactions on geoscience and remote sensing* **39**(10), 2135–2147.

Skartveit, A. & Olseth, J. A. (1987), 'A model for the diffuse fraction of hourly global radiation.', *Solar Energy* **38**, 271–274.

Steinecke, K. (1999), 'Urban climatological studies in the Reykjavik subarctic environment, Iceland', *Atmospheric Environment* **33**, 4157–4162.

Storck, P., Bowling, L., Wetherbee, P. & Lettenmaier, D. P. (1998), 'Application of a GIS-based distributed hydrology model for prediction of

forest harvest effects on peak stream flow in the Pacific Northwest', *Hydrological Processes* **12**, 889–904.

Storck, P. (2000), Trees, snow and flooding: An investigation of forest canopy effects on snow accumulation and melt at the plot and watershed scales in the Pacific Northwest., PhD thesis, University of Washington, Department of Civil Engineering Environmental Engineering and Science. Water Resources Series, Technical Report No. 161, March, Seattle, 98195 Washington, USA.

Sundin, E. (1998), Snow deposit melt and atmospheric icing, PhD thesis, Luleå University of Technology. Doctoral thesis, Department of Environmental Engineering. Division of water Resources Engineering, SE-97187 Luleå, Sweden, 1998:37, ISSN 1402-1544.

Tait, A. B., Hall, D. K., Foster, J. L. & Armstrong, R. L. (2000), 'Utilizing multiple datasets for snow-cover mapping', *Remote Sensing Environment* **72**, 111–126.

Tappeiner, U., Tappeiner, G., Aschenwald, J., Tasser, E. & Ostendorf, B. (2001), 'GIS-Based modelling of spatial pattern of snow cover duration in an alpine area', *Ecological Modelling* **138**, 265–275.

Tarboton, D. G. & Luce, C. H. (1996), 'Utah Energy Balance Snow Accumulation and Melt Model (UEB), computer model technical description and users guide.'. Utah Water Research Laboratory, Utah State University, USDA Forest Service, Intermountain Research Station.

Taylor, C. H. (1977), 'Seasonal variations in the impact of suburban development on runoff responce: Peterborough, Ontario', *Water Resources Research* **13**(2), 464–468.

Taylor, C. H. (1982), 'The effect on storm runoff response of seasonal variations in contributing zones in small watersheds', *Nordic Hydrology* **13**, 165–182.

Thordarson, S. (2002), Wind flow studies for drifting snow on roads, PhD thesis, Norwegian University of Science and Technology. PhD Thesis. Department of road and railway engineering, NTNU, Trondheim, Norway, ISBN 82-471-5481-1, ISSN 0809-103X.

Thorolfsson, S. T. & Brandt, J. (1996), The influence of snowmelt on urban runoff in Norway., *in* '7th International Conference on Urban Storm Drainage', Vol. 1, Hannover, Germany. ISBN 3-00-00868-8.

Thorolfsson, S. T. & Høgeli, S. (1994), Risvollan - Trondheim urbanhydrologiske forskningsfelt. del 1 dokumentasjon av målestasjonen, Technical report, The Norwegian Institute of Technology, NTH. In Norwegian, report nr B1-1994-3.

Thorolfsson, S. T. & Killingtveit, Å. (1991), The use of conceptual hydrological models for modelling urban runoff from precipitation and snowmelt, *in* C. Maksimovic, ed., 'New technologies in urban drainage, UDT91', IRTCUD, Elsevier Applied Science, London and New York. Dubrovnik, Yugoslavia.

Thorolfsson, S. T., Matheussen, B. V., Frisvold, H., Nilsen, O., Kristiansen, V. & Pedersen-Øverleir, A. (2003), Urban hydrological data collection in cold climate. Experiences at Risvollan, Trondheim, Norway., *in* '1st international conference on urban drainage and highway runoff in cold climate', IWA, IAHR, Luleå university of technology. 25-27 March, Riksgrȁnsen Sweden.

Thorolfsson, S. T. & Sand, K. (1991), Urban snowmelt research in Norway: Measurements and modelling approach, *in* C. Maksimovic, ed., 'New technologies in urban drainage, UDT91', IRTCUD, Elsevier Applied Science, London and New York. Dubrovnik, Yugoslavia.

Todhunter, P. E., Xu, F. & Buttle, J. M. (1992), 'A model of net radiation over suburban snowpacks', *Atmospheric Environment* **26B**(No 1), 17–27.

TokyoMap (2004), 'Mid-tokyo-maps', http://www.mid-tokyo.com. Information found on the internett. The website referenced several sources: Toritsu koen/shizenkoen gaido (Guide to City Parks), Tokyo Parks Association; Koen chousho (Park record) 2000, Tokyo Bureau of Construction; Tokyo to no koen to rokuchi" (Parks and green space in Tokyo) 2000, Tokyo Bureau of Construction; Community District Needs 1990, New York City Department of City Planning; Koen chousho" (Park record), 2000, Bureau of GeneralAffairs; Sanborn:

Manhattan Land Book of the City of New York 1992-93; Tokyo no tochi riyou (Land use in Tokyo) the 23 ward area, 1996, Tokyo Metropolitan Government; City planning references 1997, New York City Department of City Planning, Mori Building Co., Ltd. Copyright (c) 2001 Mori Building Co., Ltd.

Trondheim (2002), 'Statistics of Trondheim 2001, In Norwegian, Trondheimsstatistikken'. Trondheim kommune, Plan og Bygningsenheten, Juni 2002.

Tsuchiya, M., Tomabechi, T., Hongo, T. & Ueda, H. (2002), 'Wind effects on snow drift on stepped flat roofs', *Journal of wind engineering and industrial aerodynamics* **90**, 1881–1892.

Turpin, O., Ferguson, R. & Johansson, B. (1999), 'Use of remote sensing to test and update simulated snow cover in hydrological models', *Hydrological processes* **13**, 2067–2077.

Valeo, C. & Ho, C. L. I. (2003), 'Modelling urban winter runoff', *Journal of hydrology* . Article IN PRESS, manuscript received from Caterina Valeo, Email: valeo@geomatics.ucalgary.ca, University of Calgary. Canada, 1 Oct 2003.

Vignola, F. & McDaniels, D. K. (1988), 'Direct beam radiation: projection onto tilted surfaces', *Solar Energy* **40**(3), 237–247.

Viklander, M. (1999), 'Substances in urban snow. A comparison of the contamination of snow in different parts of the city of Luleå, Sweden', *Water, Air and Soil Pollution* **114**, 377–394.

Walpole, R. E., Myers, R. H. & Myers, S. L. (1998), *Probability and statistics for engineers and scientists*, 6 edn, Prentice Hall International Inc. ISBN 0-13-095246, 739 p.

Weng, Q. (2001), 'Modeling urban growth effects on surface runoff with the integration of remote sensing and GIS', *Environmental Management* **28**(6), 737–748.

Westerström, G. (1984), Snowmelt runoff from Porsön residential area, Luleå, Sweden, *in* 'Proceedings of the Third International Confer-

ence on Urban Storm Drainage'. Volume 1: Analysis and Design of Stormwater Systems.

Westerström, G. (1986), An urban snowmelt runoff case study, *in* 'Proceedings of International Symposium on comparison of urban drainage with real catchment data'. Dubrovnik, Yugoslavia, April.

Winstral, A. & Marks, D. (2002), 'Simulating wind fields and snow redistribution using terrain-based parameters to model snow accumulation and melt over semi-arid mountain catchment', *Hydrological Processes* **16**, 3585–3603.

Winther, J. G. (1993*a*), 'Short- and long term variability of snow albedo', *Nordic Hydrology* **24**, 199–212.

Winther, J. G. (1993*b*), Snow and glacier ice characteristics measured using landsat TM data, PhD thesis, Universitetet i Trondheim, Norge tekniske høgskole, institutt for vassbygging, Trondheim. Ph.D. thesis. Doktoringeniøravhandling 1993:89, NTH, Institutt for vassbygging. IVB-rapport B-2-1993-5, ISBN 82-7119-552-2, ISSN 0802-3271.

Xu, F. & Buttle, J. M. (1987), Patterns of net radiation over urban snow packs, *in* 'Proc. Eastern Snow Conference', Vol. Vol 43.

Zhu, H. I. & Schilling, W. (1994), Simulation errors due to insufficient rainfall resolution. Annual Combined Sewer Overflow. Int. Workshop on Rainfall. St. Moritz. 30.11 - 4.12.

Zimmerman, J. C. (1981), 'Sun-pointing programs and their accuracy'. SAND81-0761, Experimental Systems Operation Division 4721, Sandia National Laboratories, Albuquerque, NM., USA.